A MODIFIED MIXTURE THEORY FRAMEWORK FOR THE MELTING OF PURE PCM AND PCM/METAL FOAM COMPOSITE

KAI JIAO

PhD

The Hong Kong Polytechnic University

2022

The Hong Kong Polytechnic University

The Department of Building Environment and Energy Engineering

A modified mixture theory framework for the melting of pure PCM and PCM/metal foam composite

Kai Jiao

A thesis submitted in partial fulfilment of the requirements for the degree of Doctor of Philosophy

July 2022

CERTIFICATE OF ORIGINALITY

I hereby declare that this thesis is my own work and that, to the best of my knowledge and belief, it reproduces no material previously published or written, nor material that has been accepted for the award of any other degree or diploma, except where due acknowledgement has been made in the text.

(Signed)

Kai Jiao (Name of student)

Abstract

Since it was proposed in 1960, the mixture theory has been widely utilized to decouple the interactions between constituents in both homogeneous and heterogeneous mixtures in a macroscopic scale.

In this thesis, a modified mixture theory framework is developed to analyze the phase change problems of phase change materials (PCMs) and their composites. Mixture theory based mathematical models are established for one-dimensional pure PCMs and PCM/metal foam composites, and two-dimensional melting of pure PCMs. Volume change due to the density variation during the phase change of PCMs is considered. For the one-dimensional model, the local thermal non-equilibrium effect is considered, and the velocity correlated to the density change during paraffin melting is introduced. A new constituential heat flux term is presented to explain the heat supply from different constituents, and a new interpretation for internal energy supply term is introduced. The governing equations are numerically solved by using a finite difference method. Temperature field, mushy

zone evolution, and velocity profile at the boundary are predicted. Experiments are conducted to validate the numerical analysis. It is shown that the numerical results obtained by the mixture theory model have a satisfying agreement with the real situation. For the two-dimensional model, we propose that the three regions can be modeled individually and then coupled using an enthalpy method. Like the one-dimensional mixture model, in the two-dimensional model we assume that the velocity field in the mushy zone is solely dependent on the density variation and the flow in the liquid region can not penetrate the boundary of the mushy zone.

We also revise the energy equation to a more general form for different mixture structures. Both local thermal equilibrium and local thermal non-equilibrium situations are considered. The different mixture structures are considered by proposing an effective volumetric fraction for each constituent of the mixture. A new expression for the effective thermal conductivity is provided for mixtures with local thermal equilibrium model, while for the local thermal non-equilibrium situations, a new energy equation set is given together with our interpretations of heat flux terms and local thermal interaction terms. Moreover, it is shown that the expression of the effective thermal conductivity under the local thermal equilibrium conditions can be obtained by assuming the temperatures of the constituents are the same in the local thermal non-equilibrium model. By comparing the numerical results, it is shown that the mixture model can provide satisfying predictions for the real situations for different types of mixture structures and for both local thermal

equilibrium and local thermal non-equilibrium. With this revised heat equation, the scope of the previously proposed mixture theory framework is extended. On one hand, it can be used to predict the heat transfer behavior of multi-constituent materials with different structures including soil, tissues, nanoparticle-embedded materials, etc.; on the other hand, it can also be used to develop optimized structures for heat transfer enhancement.

Publications arising from the thesis

Journal papers

Jiao, **Kai**, Lin Lu, Tao Wen, and Qiuwang Wang (2022c). "A modified mixture theory for one-dimensional melting of pure PCM and PCM/metal foam composite: Numerical analysis and experiment validation". In: *International Journal of Heat and Mass Transfer* 186, p. 122461.

Jiao, **Kai**, Lin Lu, Tao Wen, and Qiuwang Wang (2022e). "Development of mixture theory based heat conduction equations for different mixture structures". Manuscript submitted for publication.

Jiao, **Kai**, Lin Lu, Tao Wen, and Qiuwang Wang (2022a). "A 2-D mixture theory model for paraffin/copper foam melting in a cavity". Unpublished Manuscript.

Jiao, **Kai**, Lin Lu, Tao Wen, and Qiuwang Wang (2022b). "A comprehensive review of approximations of momentum equation for mixtures". Unpublished Manuscript.

Jiao, **Kai**, Lin Lu, Tao Wen, and Qiuwang Wang (2022d). “A novel natural convection model for paraffin melting in a cavity considering volume change”. Unpublished Manuscript.

Wen, Tao, Jielin Luo, **Kai Jiao**, and Lin Lu (2022). “Pool boiling heat transfer enhancement of aqueous solution with quaternary ammonium cationic surfactants on copper surface”. In: *International Journal of Heat and Mass Transfer* 190, p. 122761.

Wen, Tao, Guangya Zhu, **Kai Jiao**, and Lin Lu (2021). “Experimental study on the thermal and flow characteristics of ZnO/water nanofluid in mini-channels integrated with GA-optimized ANN prediction and CFD simulation”. In: *International Journal of Heat and Mass Transfer* 178, p. 121617.

Acknowledgements

First and foremost, I would like to give a deep and sincere gratitude to my chief supervisor, Prof. Lin Lu for her continuous guidance and invaluable support throughout my Ph.D. study. Her infectious enthusiasm in both research and life helps me to steel myself to finish my research.

I am extremely thankful to my two co-supervisors. I would like to express my gratitude to Prof. Qiuwang Wang who guided me to this research topic and offered invaluable vision in my research field. I am also grateful to Dr. Tao Wen for his generous help with my experiments and to my daily life.

Very special thanks to all the members of the Renewable Energy Research Group. Thanks to Prof. Hongxing Yang and Prof. Sunliang Cao for their priceless instructions in my confirmation. Thanks to my office members in ZN824 for the happy and memorable time we have been through together.

Further, I acknowledge the generous financial support from the NSFC/RGC Joint Research Scheme sponsored by the Research Grants Council of Hong Kong

and the National Natural Science Foundation of China.

Finally, I would like to thank my family for their unconditional and unequivocal love of the highest order.

Contents

List of Figures

List of Tables

Nomenclature

$\acute{\rho}^{\alpha}$	True density of constituent α (kg/m^3)
Δt	Time step (s)
Δx	Grid size (m)
$\hat{\rho}^{\alpha}$	Mass supply to constituent α (kg/m^3)$\cdot$s)
$\hat{\varepsilon}^{\alpha}$	Energy supply to constituent α from other constituents (W/m^3)
γ^{α}	External energy supply to constituent α (J/s)
$\mathbf{q}$	Heat flux vector of the mixture (W/m^2)
$\mathbf{q}^{\alpha}$	Constituential heat flux vector (W/m^2)
$\mathbf{T}$	Stress tensor of the mixture (N/m^2)
$\mathbf{T}^{\alpha}$	Constituential stress tensor (N/m^2)

$\mathbf{u}^\alpha$	Diffusion velocity of constituent α (m/s)
$\mathbf{v}^\alpha$	Velocity of constituent α (m/s)
ρ	Density of the mixture α (kg/m^3)
ρ^α	Apparent density of constituent α (kg/m^3)
Nu	Nusselt number
Re	Reynolds number
ε	Internal energy density of the mixture (J/kg)
ε^α	Internal energy density of constituent α (J/kg)
ε_I	Inner part of internal energy density of the mixture (J/kg)
φ^α	Volumetric fraction of constituent α
φ_e^α	Effective volumetric fraction of constituent α
A	Area of the interface of the constituents (m^2)
a_{Pm}	Specific surface area (1/m)
d_f	Fiber diameter of metal foam (m)
d_P	True density of constituent α (kg/m^3)
h	Local heat transfer coefficient W/(m^3·K)

k Thermal conductivity (W/(m·K))

k^{α} Thermal conductivity of constituent α (W/(m·K))

T Temperature/Temperature of the mixture (K)

t Time (s)

T^{α} Temperature of constituent α (K)

Cp Specific heat (J/(kg·K))

Cp^{α} Specific heat (J/(kg·K))

Subscripts

b Boundary

hm Harmonic mean

i $(i = 1, 2, 3)$ Indices of coordinates

l, j Grid number

m Mean

wm Weighted mean

Superscripts

α, β constituent α and β

l	Liquid
m	Metal foam
n	Time layer
ni	Nickel
pa	Paraffin
s	Solid

Chapter 1

Introduction

The development of modern society requires an increasing amount of energy, which leads to booming levels of greenhouse gas emissions. In 2016, global greenhouse gas emissions reached 31.2 per cent above the 1990 level, with an average annual increase of 0.9 per cent since 2010 (Change 2019). This results in a noticeable global temperature increase and serious climate change problems in recent years. Such that nowadays it is more urgent than ever to find and develop new technologies for effective use of energy. In building, over 50 per cent of building energy consumption is for cooling and heating purposes, which is mostly originated from fossil fuels burning. Although there exists several replaceable energy sources such as solar energy and industrial waste heat, they are not widely used in practice due to the gap between supply and demand. Therefore, research on latent thermal energy storage (LTES) systems, which correct the gap between demand

and supply, is becoming more and more popular.

As a modal energy storage medium, organic phase change materials (PCMs) such as paraffin wax and fatty acid have been studied for many years for their high latent heat and wide range of adjustable melting temperatures. However, the intrinsic problems of PCMs, such as low thermal consuctivities, greatly expel them from practical usage. In order to solve this problem, many experimental studies have been using extra additives with high thermal conductivity to promote the heat transfer of PCMs, including metal foams (Fiedler et al. 2008; Dukhan and Bodke 2010), nano-particles (Zeng et al. 2007; Al-Jethelah et al. 2018), and carbon materials (B.-r. Li et al. 2019; Kumaresan et al. 2012). Although some of the endeavors have acquired noticeable improvements to the heat transfer performance of PCMs, the extra additives also introduce more complexity into mathematical model development and numerical calculation. In view of the difficulties in the mathematical modeling of PCMs and PCM composites, in this thesis, we focus on the development of a new mixture model that is able to interpret the interactions between liquid PCM, solid PCM, and extra additives.

Usually, three physical models and their associated numerical approaches are widely used to analyze PCMs and their composites: molecular dynamics (MD) simulation, lattice-Boltzmann method (LBM), and continuum approach. MD is a molecular scale method based on Newton's equations of motion. Since thermodynamical processes are analyzed in molecular-scale, MD simulation is suitable for

numerically computing thermophysical properties of pure PCMs and PCM composites (M. Zhang et al. 2020). However, for macroscopic problems of large dimension, the computational cost of MD is expensive and unpleasant (Erastova 2012). LBM is a mesoscale method usually used for solving phase change problems involving a complex geometry such as metal foams (Chen et al. 2014). Both MD simulation and LBM are able to investigate the thermal mechanism of PCMs/PCM composites in a microscopic view, but many models of them are not validated against enough macroscopic experimental results (R. Huang and H. Wu 2015). Continuum physics on the other hand is a statistical physics assuming materials are continuous. Although it would lose accuracy for microscopic problems for the fact that real materials are composed of discrete particles, numerical methods based on continuum physics are computational friendly and have good agreements with experimental results for macroscopic phase change problems. Nevertheless, classical continuum physics is limited in dealing with problems involving multiple constituents since physical properties are not the same for different constituent, for example the PCM/metal foam composite. Also, the local thermal equilibrium may vanish due to the property differences. To overcome the drawbacks of classical continuum mechanics in dealing with phase change problems, the continuum mixture theory was introduced by Bennon and Incropera (1987). The mixture theory is a branch of continuum physics and it was firstly presented by Truesdell and Toupin (1960). Different from the classical continuum physics which treats a

mixture as a continuous body or several continuous parts connected by jump conditions, the mixture theory decouples the mixture by constructing balance equations for individual constituents and studies the interactions between them. Over the years the mixture theory idea has been employed to solve a bunch of phase change problems of PCMs and their composites (Mesalhy et al. 2005; Xia et al. 2016; Frusteri et al. 2006; Esapour et al. 2018). Nevertheless, one can find that the expressions for heat transfer terms can vary in different studies. For example, though both were analyzing PCM melting in a foam structure, Hu et al. (2019) and Li et al. (2012) were using two different ways to describe the energy conservation. This is because the mixture theory is merely a general framework, which needs to be deconstructed and simplified in terms of assumptions proposed by different researchers. As a result, the precise interpretation of mixture theory needs to be further investigated. Another problem in existing studies is that the velocity generated due to the density difference between solid PCM and liquid PCM is rarely discussed. This velocity vanishes mainly because of two reasons: first, the densities of solid PCM and liquid PCM are assumed to be equal for simplicity; second, the velocity is just ignored because its scale is little. However, the velocity driven by density change plays an interesting role in the heat transfer of PCMs and its influence on the phase change process can be various (Hassab et al. 2017; Sparrow and Broadbent 1982; Faden, König-Haagen, Franquet, et al. 2021).

Generally, there are two approaches to obtain the temperature profile of a mix-

ture with energy variations. The first is to assume that there is local thermal equilibrium for the constituents in a mixture so that one only need to estimate an effective thermal conductivity k_e based on the volumetric fraction and thermal conductivity of each constituent. Usually, the value of k_e is between the harmonic mean and the weighted mean of the thermal conductivities of all the constituents (Bart 1994; Carson et al. 2005; Donald A Nield, Bejan, et al. 2006). Sadly, a general expression of effective thermal conductivity k_e for different mixture structures is yet to be developed, and in order to obtain a relatively reliable k_e, researchers need to choose different expressions in terms of the structure of the mixture. For example, Abidi et al. (2021) used a Maxwell model to estimate the effective thermal conductivity of calcium chloride hexahydrate incorporated with nanoparticles. Nield (1991) proposed that k_e can be well estimated by a weighted geometric mean for a 2-constituent mixture while the difference between the thermal conductivities of the two materials is not huge. Another approach to predict the temperatures of a mixture is to consider the local thermal non-equilibrium effect. In this case, energy balance equations should be calculated respectively for each constituent. Following the classical equation given by Bories (1987), for a static two-constituent mixture (α and β), if there is no internal heat supply, the energy equation set is

given by

$$\begin{aligned} \varphi^{\alpha}\acute{\rho}^{\alpha}Cp^{\alpha}\frac{\partial T^{\alpha}}{\partial t} &= \varphi^{\alpha}\nabla\cdot(k^{\alpha}\nabla T^{\alpha}) + h(T^{\beta}-T^{\alpha}) \\ \varphi^{\beta}\acute{\rho}^{\beta}Cp^{\beta}\frac{\partial T^{\beta}}{\partial t} &= \varphi^{\beta}\nabla\cdot(k^{\beta}\nabla T^{\beta}) + h(T^{\alpha}-T^{\beta}) \end{aligned} \tag{1.1}$$

Eq. (1.1) implies that the rate of change of the thermal energy of an individual constituent equals the heat conduction from the surrounding same constituent plus the heat from local thermal interaction with the other constituent. However, this expression somehow violates the concept of the mixture theory. One of the key assumptions in the mixture theory is that a spatial point is simultaneously occupied by all constituents (Atkin and Craine 1976), such that constituent α should also receive the heat conduction from β. Moreover, the local heat transfer coefficient h is usually determined empirically or experimentally. This indirect manner could affect the credibility of this approach to some extent (Donald A Nield, Bejan, et al. 2006). Further, the coefficient h in most studies is highly correlated with the local Nusselt number, and a theoretical expression of h for pure conduction problems is yet to be developed.

1.1 Organization of the Thesis

The thesis is composed of 6 chapters including the current introduction chapter.

Chapter 2 gives an overview of the PCMs as well as their characteristics. Dif-

ferent heat transfer enhancement methods regarding the low thermal conductivities of PCMs are briefly introduced. Research gaps are discussed to highlight the problems that we want to solve in this thesis, and the research methods are briefly introduced.

Chapter 3 presents the mixture theory framework that consists of three parts: balance laws, entropy inequality, and jump conditions. Local forms of these equations and inequality for the whole mixture are also given. The approximations of the momentum equations are introduced in this chapter , including the Darcy's equation, the Brinkman's equation and their variations. It is proposed that the Darcy's equation is not rigorous to describe the flow model in the mushy zone where mass interactions exist from the view of the mixture theory. We should notice that though the mixture theory framework is presented from the aspect of PCMs, in this chapter no extra assumptions are made such that the equations and inequality are also valid for other mixtures.

In Chapter 4, we build the mathematical model for one-dimensional melting of pure PCM and PCM composites. Each source term for an individual constituent is fully considered. A new expression for heat flux terms is defined including heat conduction terms between different constituents that have not been presented before. A new expression for the internal energy supply terms is also given. By analyzing the governing equations, it is suggested that the nonlinearity of one-dimensional melting problems only comes from the phase change itself, and the

addition of metal foam does not introduce extra complexity. Three different problems: pure PCM melting, PCM melting in a copper foam, and PCM melting in a nickel foam, are numerically solved using a finite difference method based on the modified mixture theory model. The PCM used in this thesis is paraffin wax with three phase change processes. Considering the densities of liquid paraffin and solid paraffin are different, the velocity profile is obtained by the balance of mass. It is shown that this velocity, which is rarely considered by researchers, has a noticeable influence on the precise prediction of temperature profile. The absence of local thermal equilibrium is considered in this model. The result shows that the temperature difference between metal foam and paraffin is trivial except near the heating side at the beginning of the melting process. Experiments are designed to validate the numerical results. It is shown that the numerical calculation based on the modified mixture theory model well predicts the phase change process by comparing the temperature profile. Based on the findings in the one-dimension problem, we also give the mixture model for the two-dimensional pure paraffin melting with a new proposed flow model that avoids the usage of Darcy's equation in the mushy zone where mass interactions exist.

In Chapter 5, we propose a new heat conduction model base on the energy equations of the mixture theory, which is valid for both local thermal equilibrium and local thermal non-equilibrium situations. Mixture structures are considered in the model by introducing the effective volumetric fraction which is defined as

the volumetric fraction that is continuous along the heat flow direction. For the local thermal equilibrium situations, we give a new expression for the effective thermal conductivity of the mixture. For the local thermal non-equilibrium situations, revised definitions of heat flux terms and local thermal interactions terms are proposed to illustrate the heat transfers between each constituent. Four mixture structures are evaluated in this research, which can serve as analogies to different materials such as porous materials and nanoparticle-embedded materials, and the related heat transfer problems are solved by two methods: 1. using the classical heat equation and analyzing every constituent individually, which represents the real situations; 2. treating the mixture as a whole and applying our revised mixture model. By comparing the numerical results by the two methods, it is shown that the mixture theory can provide satisfying predictions to the real situations for both local thermal equilibrium and local thermal non-equilibrium situations even if the mixture structures do not strictly follow the assumptions of the mixture theory.

Finally, the thesis is concluded in Chapter 6 and the recommendations for future work are also given.

Chapter 2

Literature Review

According to the medium of heat storage, there are three types of TES systems: latent heat, sensible heat and reversible thermochemical reaction. Among all the traditional and advanced techniques, TES systems using phase change materials is a promising way due to their high energy density and the isothermal nature of the storage process. However, PCMs usually suffer some drawbacks such as leakage problems and low thermal conductivities, which greatly restricts their practical applications in real situations. In this chapter, we give an overview of the types of PCMs and their characteristics. Different heat transfer enhancement methods regarding the low thermal conductivities of PCMs are briefly introduced.

2.1 PCMs for Thermal Energy Storage

For thermal energy storage (TES) systems with PCMS, phase change is involved during the heat absorption and release processes, and thus latent heat storage systems usually possess a higher energy density than that of sensible ones. Moreover, PCMs hold a stable temperature range during phase change, such that latent heat storage has incomparable advantages as a thermal energy storage method (Tian and Zhao 2011). It is not hard to find out that the capacity of the TES systems is based on the chosen materials, therefore the study of PCMs is a key issue for energy storage.

2.1.1 Requirements for PCM Characteristics

One has to make sure the TES system has a high energy capacity, and more importantly, the system is steady and sustainable. Abhat (1983) indicates that a TES system should as least possess three following features: (1) a heat storage substance that undergoes a solid-to-liquid phase transition within the desired operating temperature range and wherein the bulk of the heat added is stored as the latent heat of fusion; (2) a containment for the storage substance; (3) a heat exchanging surface for transferring heat from the heat source to the heat storage substance and from the latter to the heat sink, e.g. from the solar collector to the heat storage substance to the load loop. As a result, although there are numerous phase change

materials, few can be used in TES systems. Atul Sharma et al. (2009) listed the requirements of material properties for PCMs that can be used for energy storage: suitable phase-transition temperature; high latent heat of transition; good heat transfer; favorable phase equilibrium; high density; small volume change during phase change; low vapor pressure; no supercooling; sufficient crystallization rate; long-term chemical stability; compatibility with materials of construction; no toxicity; no fire hazard; abundant, available, and cost effective. However, no material can meet all these requirements. However, all PCMs have one to several defects, such as supercooling, phase separation, leakage problems, and low thermal conductivity. The details of different types of PCMs are introduced in the following section.

2.1.2 Classification of PCMs

There are different criteria to classify PCMs. For example, according to the state of PCMs before and after phase change, they can be classified into solid–solid PCMs, solid–liquid PCMs, solid–gas PCMs and liquid–gas PCMs. In this literature review, PCMs are classified based on their chemical nature (Lin et al. 2018): organic phase change materials, inorganic phase change materials, and eutectic phase change materials. Table 2.1 shows several potential candidates for PCMs that can be used in TES systems along with their melting temperature T_m and latent

heat L.

Table 2.1: Name and physical properties of some PCM candidates.

PCM	T_m (°C)	L (kJ/kg)
$KF{\cdot}4H_2O$ (Khudhair and Farid 2004)	18.5 - 19	231
$CaCl_2 \cdot 6H_2O$ (Khudhair and Farid 2004)	29.7	171
Butyl stearate (Khudhair and Farid 2004)	18 - 23	140
Dodecanol (Khudhair and Farid 2004)	17.5 - 23.3	9.9151
Propyl palmitate (Khudhair and Farid 2004)	16 - 19	186
Dimethyl-sulfoxide (Zalba et al. 2003)	16.5	85.7
Paraffin C_{18} (Zalba et al. 2003)	28	244
Parffin wax C_{14} (Zalba et al. 2003)	64	173.6
Erythritol C_{14} (Zalba et al. 2003)	118	339.8
Propyl palmiate C_{14} (Zalba et al. 2003)	10	186
Capric acid (Farid et al. 2004)	32	152.7
Caprylic acid (Farid et al. 2004)	16	148.5
Naphthalene (Farid et al. 2004)	80	147.7

Organic PCM can be further divided into paraffins and non-paraffins. Pure Paraffin is also known as alkane, which has a general chemical formula C_nH_{2n+2}. The melting point of the alkanes increases with the increasing number of carbon atoms, which is indicated in Table 1. The wide range of melting point of paraffins makes them promising candidates for TES systems for different purposes. The solid paraffins usually have two allotropic modifications that are different in their physical properties and the crystal structure (Abhat 1983). The primary modification exists at higher temperature whereas the secondary modification exists at lower temperature. One modification can transfer to the other and the process is reversible. Paraffins as heat storage materials exhibit many advantages such as high heat of fusion, negligible supercooling, low vapor pressure in the melt, chemically

inert and stable, self nucleating, no phase segregation and commercial availability at reasonable cost. Non-paraffins are a large group of materials and they have very different properties, but most of them are fatty acids or fatty-acid-like materials. Although the cost is higher compared with paraffins, fatty acids have the advantages that paraffins process but the melting point is relatively lower. Therefore they are mostly used in low temperature TES systems. Also, the liquid fatty acids usually have a high surface tension, which makes the liquids retained in the pores of host materials and avoids leakage issues(Sarı and Karaipekli 2009). All organic PCMs have a common drawback: they all have low heat conductivities. Therefore some thermal conductivity enhancement methods should be applied before practical usage. It is worth mentioning that the risk of fire hazard has to be considered when using organic PCMs. Sittisart and Farid (2004) investigated the addition of fire retardants for this issue.

Inorganic PCM can be divided into salt hydrates and metallics, where the former is of most interest. Telkes (1952) first investigated salt hydrates as a phase change material back in the 1950s. Salt hydrate is an ionic compound in which a number of water molecules are attracted by the ions and therefore enclosed within its crystal lattice (Onder and Sarier 2015). Salt hydrates have a prospective future due to their high energy storage density and low cost. Moreover, they are usually inflammable and inodorous compared with organic PCMs. However, there are three main disadvantages: (1) some salt hydrates melt incongruently, which

means that they melt to a saturated aqueous phase and a solid phase that is generally a lower hydrate of the same salt. Because of density differences, the solid phase tends to build up at the bottom of the container. Thus salt hydrates are chemically unstable since this transferring is irreversible (Abhat 1983). (2) Salt hydrates have a tendency to supercool, which prevents the release of the stored latent heat. However, some researchers utilize this property as an opportunity for long-term storage of thermal energy while the supercooled liquid is kept at ambient temperature (Bjørnar Sandnes 2003; Sandnes and Rekstad 2006). (3) They are very corrosive to many metals that are always used for heat transfer enhancement, which limits the performance of the whole system (Noël et al. 2016). In order to overcome these drawbacks, encapsulation is an ideal solution. Although salt hydrates are difficult to encapsulate due to their hydrophilicity and tendency to alter their water content (Graham et al. 2016), there are studies that investigated the encapsulation of salt hydrates (J. Huang et al. 2013; Rabin et al. 1995).

All of the aforementioned PCMs share a crucial disadvantage: their thermal conductivities are very low that it highly affects their heat transfer performance. Therefore metallics are being developed as a media to store thermal energy in recent years. Metallics includes low melting metals and metal eutectics. Due to high thermal conductivity, no heat transfer enhancement method is required, which grants metallics the highest overall energy density. Compared with salt hydrates, metallics are more economical and stable (J. Yagi and Akiyama 1995).

Therefore metallics are innovative and prospective materials for high-temperature TES systems. On the other hand, metallics generally have containment problems and associated safety issues, and their liquid phase is highly corrosive to metal materials (Copus et al. 2019). Similar to salt hydrates, encapsulation is an ideal option to correct these disadvantages. However, two obstacles are to be overcome for encapsulation, chemical corrosion and phase change expansion (Fukahori et al. 2016).

An eutectic is a minimum melting composition of two or more components (they can be either organic or inorganic), each of which melts and freezes congruently. During crystallization, a mixture of the component crystals is formed (Rathod and Banerjee 2013). The idea of eutectics is to tailor PCMs with specific physical properties by using different materials. For instance, two kinds of fatty acids can be mixed together in order to decrease the phase change temperature. According to the components used, eutectic can be utilized in many areas such as building and high temperature thermal energy storage (Wang and Meng 2010; B.-r. Li et al. 2019; Sarı 2003).

2.2 Heat Transfer Enhancement Methods

Although metallics possess a high thermal conductivity, most of the applications of PCMs such as industrial waste heat recovery, comfort application in building,

electric peak-shaving, solar building power systems and temperature control systems are under a temperature condition lower than 500 ˚C (Lin et al. 2018). As a result, organic PCMs and salt hydrates are still the most frequent materials used in TES systems. Since the thermal conductivity of these materials is very disappointing, enhancement of heat transfer of PCMs is becoming a popular topic. There are two methods to improve the performance of PCMs in heat storage (T. Li et al. 2014): (1)enlarging heat exchange area by refining the structure of heat exchangers or encapsulation; (2)enhancing thermal conductivity by adding fillers or forcing convection of liquid phase. The purpose of this section is to review the heat transfer enhancement methods that are commonly used.

2.2.1 Encapsulation

For most applications, PCMs must be encapsulated for several considerations (Lane 1983; Tomohiro Akiyama and J.-I. Yagi 2000). First, most PCMs undergo a stable form to mobile form change from discharged state to charged state. Therefore they have to be encapsulated in a container to maintain the structural stability of TES systems. Second, some PCMs are encapsulated to protect them from the outside environment, which is especially significant for chemical unstable or corrosive materials. Third, encapsulation usually provides a larger contact surface for heat exchange purposes. Last, encapsulated materials are much more portable for han-

dling and shipment.

Three representative encapsulation methods are tank-heat exchangers, macroencapsulation and microencapsulation. Tank-heat exchangers for PCMs are similar to other existing tanks used in thermal industry. They are cost-effective and have a large capacity. In order to enhance the heat transfer rate, many researchers are focusing on developing novel structures to enlarge the contact surface. Mahdi et al. (2018) studied a novel fin configuration in triplex-tube storage. The result showed that this new structure enhances natrual convection and enlarges the heat transfer surface. Compared with conventional fin configuration and pure PCM dispersed with Al_2O_3 nanoparticles, the melting time was shortened by 14 and 2.2 times respectively. Lu et al. (2018) proposed a water storage tank structure containing 2 types of PCMs that can be used in solar hot water systems. The results indicated that the phase change heat storage tank containing two different melting points PCMs can shorten the heat storage time to a certain extent.

Macroencapsulation includes a certain amount of PCM in a discrete unit. The volume of PCM per unit may range from a few grams to pounds (Lane 1983). The flexible size and portable character make macroencapsulation the most common type of PCM encapsulation. The encapsulation materials can be plastic or metal. If the capsule is rigid enough, the encapsulation can also add mechanical stability to a system. For example, in buildings, PCM encapsulated in wallboards or bricks is often used for passive temperature management. Vicente et al. (2014)

tested the performance of macrocapsulated PCM in horizontally hollowed clay brick. The PCM macrocapsules increased the heat storage capacity of the tested wall specimens. The result shows a maximum 80 percent high thermal fluctuation reduction compared with bricks without PCM. If good heat transfer is important to the system, the better option is to chose containers with metal walls, which also provide a higher mechanical stability. It is however necessary to select a suitable metal which is not corroded by the PCM. This selection should also consider the metal properties and potential restrictions for shaping and welding may exist (Mehling and Cabeza 2008). Cui et al. (2017) developed a PCM macroencapsulation method using hollow steel balls(HSB). This PCM-HSB composite has a high thermal conductivity and avoids leakage problems. By applying it to the building, the results showed that the room temperature was reduced by a range of 3-6 percent.

Microencapsulation is the encapsulation of solid or liquid particles of 1 μm to 1000 μm diameter with a solid shell. Restricted by the size, heat transfer inside microencapsulation is dominated by heat conduction, which decreases the heat transfer rate (Regin et al. 2008). On the other hand, the small encapsulation renders a larger contact surface to volume ratio so that the overall heat transfer is increased. Cycling stability is also increased since phase separation is restricted to microscopic distances. Moreover, it is easy to integrate microcapsules with other materials (Mehling and Cabeza 2008). However, the high cost deters

the massive application of microencapsulation. Although there are studies investigating more economical methods of microencapsulation for commercialization (Hawlader et al. 2003), it is promising and affordable for space technology to some extent (Rathore and Shukla 2019).

2.2.2 Adding Additives with High Thermal Conductivity

Besides enlarging heat exchange area by encapsulation, enhancing thermal conductivity is another method to improve the performance of PCMs. The most used technique is to add additives with high thermal conductivity. The potential additives include porous graphite matrix, porous metallic matrix, metallic particles, microencapsulated materials, carbon fibers, carbon nanotubes, et al.

Porous matrices are popular additives and a lot of studies have been conducted. Despite the disadvantage of reducing thermal capacity, porous matrices exhibit reliable performance. Among all porous matrices, metallic porous foams may be the most promising material because they are chemically stable against most organic PCMs and much cheaper than graphene. Fiedler et al. (2008) conducted an experiment to test the performance of different types of foam additives. The results showed that copper foams increase the heat conductivity by 80 percent and give a better performance compared with other metals. It is noticeable that the bigger fraction of metal(lower porosity) renders a higher heat conductivity.

However, low porosity does not grant better performance since natural convection within the liquid PCM plays a big role in the overall heat transfer. The existence of additives restricts the natural convection and slows down the rapid temperature change of the liquid PCM. Therefore the porosity should be selected carefully to achieve the maximum performance.

Nano-additives are another sort of filler to enhance the heat conductivity of PCM. There are three types of nano-additives:organic nanomaterials, Inorganic nanomaterials, and Hybrid nanomaterials (H Al-Kayiem et al. 2013). Among these nanomaterials, organic nanomaterials are commonly used as nano-additives to improve the performance of heat transfer. Organic nanomaterials include fullerenes, carbon nanotubes (CNT), single-walled carbon nanotubes (SWCNT), multi-walled carbon nanotubes (MWCNT), graphite and nanofibers. Most of them are carbon-based nanomaterials. S Shaikh et al. (2008) explored the enhancement of heat conduction of different carbon-based materials. A 13 percent heat conduction enhancement was observed for paraffin with 1 percent single wall carbon nanotubes. Like porous matrices, nano-additives also constrain natural convection. Li et al. (2014) conducted experiments and tested MWCNT, graphite, graphene with stearic acid. A higher thermal conductivity is observed for all nano-additives. They also found that the phase change enthalpy decreases. Moreover, the effect of natural convection decreases. Under this combination effect, the results indicated that for MWCNT and graphene, charging time is decreased and discharging time

is increased when the mass ratio is less than 5 percent, but for graphite it is always increasing. However, this feature is not always a disadvantage. Zou et al. (2018) tested the performance of graphene and carbon nanotubes as additives for PCM. The results showed that the graphene-MWCNT composite with a ratio of 3/7 has the highest thermal conductivity. Moreover, they addressed that the holdback in natural convection restrains a rapid temperature rise in liquid PCM which is good for the thermal management system used for lithium-ion power battery.

2.2.3 Employing Multiple PCMs

Employing multiple PCMs is a special method to enhance heat transfer and has been reported as an attractive technique. The idea is to pack more than one PCMs of different melting temperatures. The heat transfer rate of the heat storage system during charging (melting) and discharging (solidification) is mainly driven by the difference between the temperature of the outer environment(mostly fluid flow or air) and the melting point of PCM. For a single PCM, this temperature difference would obviously decrease in the flow direction, which decreases heat transfer rate and causes poor performance of the system. However, if multiple PCMs of different melting temperatures are packed in the unit in the decreasing order of their melting points, then nearly a constant temperature difference can be maintained during the melting process, even though the temperature decreases in the flow di-

rection. This leads to almost a constant heat flux to the PCM. During discharging, if the flow direction is reversed, then the PCMs remain in the increasing order of their melting points. As a, nearly constant heat flux but from the PCM to outer flow is possible (Jegadheeswaran and Pohekar 2009).

2.2.4 Using Ultrasonic Technology

The ultrasound-influenced heat transfer was initially studied in the 1960s, however the application of that is still underdevelopment nowadays. It is assured that the ultrasound with a frequency between 20 and about 100 kHz improves the performance of heat transfer in liquid. This is because ultrasound can disrupt a fluid bulk to create cavitation or acoustic streaming, two phenomena with powerful macroscopic effects for heat transfer enhancement (Legay et al. 2011). The experiment conducted by Y.K. Oh et al. (2002) showed that ultrasonic vibrations accelerated the melting process of paraffins as much as 2.5 times compared with its natural process.

The combination of ultrasound and nano-additives for heat transfer enhancement is rarely studied. The idea of this combination is to make the nano-additives resonant by applying an ultrasonic wave whose frequency matches the natural frequency of the additives. This application is promising since carbon nanotubes are well studied as resonators (Gibson et al. 2007).

2.3 Research Gaps

2.3.1 Difficulties of PCMs in Practical Applications

There exist two major obstacles preventing the PCMs in their practical applications in TES systems. First, the thermal conductivities of PCMs that are suitable for applications for thermal energy storage or temperature regulation are disappointing. For example, the thermal conductivities of paraffin wax in our study is around 0.18 to 0.25 W/(m·K). Although the low conductivity could be an advantage for some special usages like temperature control, generally PCMs are mostly integrated with thermal energy storage systems where a high thermal conductivity is expected. As a result, using additives is one of the popular techniques to improve the heat transfer performance of PCMs. As aforementioned, metal matrices are shown to possess better performance than other carbon materials, but their cost is relatively high. Therefore, for big thermal energy storage systems, carbon materials are preferred. Nevertheless, the application of carbon materials has two drawbacks: (1) the thermal conductivity of PCM/carbon-material composites is still nonideal for practical usage;(2) because of the poor dispersion and density difference, carbon materials in liquid PCMs often have a separation problem. Consequently, thermal conductivity enhancement materials and techniques for PCMs should be further investigated. Second, the densities of PCMs can suffer a notable change during their phase change processes. Ukrainczyk et al. (2010) ex-

perimentally studied thermophysical properties of five different PCMs (paraffin), indicating a noticeable density change during their phase change process. And this deviation between densities of solid and liquid PCMs could lead to leakage problems.

2.3.2 Difficulties in Mathematical Modeling and Numerical Calculation

Numerical studies are always required to analyze the phase change problems of pure PCMs and their composites. Three numerical approaches and their associated physical models are widely used: molecular dynamics (MD) simulation, lattice-Boltzmann method (LBM), and continuum approach. MD is a molecular scale method based on Newton's equations of motion. Since thermodynamical processes are analyzed on a molecular-scale, MD simulation is suitable for numerically computing thermophysical properties of pure PCMs and PCM composites (M. Zhang et al. 2020). However, for macroscopic problems of large dimensions, the computational cost of MD is expensive and unpleasant (Erastova 2012). LBM is a mesoscale method usually used for solving phase change problems involving complex geometry such as metal foams (Chen et al. 2014). Both MD simulation and LBM are able to investigate the thermal mechanism of PCMs/PCM composites in a microscopic view, but many models of them are not validated against

enough macroscopic experimental results (R. Huang and H. Wu 2015). Continuum physics on the other hand is a statistical physics assuming materials are continuous. Although it would lose accuracy for microscopic problems for the fact that real materials are composed of discrete particles, numerical methods based on continuum physics are computational friendly and have good agreements with experimental results for macroscopic phase change problems. Nevertheless, classical continuum physics is limited in dealing with problems involving multiple constituents since physical properties are not always continuous across the interface of two constituents, for example, the mush region existed in the phase change process of paraffin where solid phase and liquid phase coexist, and PCM/nanoparticle composites. To overcome this drawback, mixture approaches are introduced by researchers for phase change problems, which allows studying interaction of multiple constituents and making local thermal non-equilibrium assumptions (P. Zhang et al. 2015; Srivatsa et al. 2014). These studies model phase change problems of PCM or PCM composites as Stephan problems in a porous medium which was proposed by Voller (1985) base on the Darcy's equation. However, this kind of formulation has its own restrictions. First, the incompressible assumption on PCMs generates errors in describing multiple-constituent phase change problems that have a varying porosity, for example the heat transfer in mushy zone of some PCMs. Researchers always use an averaging density (W. Li et al. 2012) to assure the incompressibility or just make physically non-rigorous assumptions

(Faden, König-Haagen, and Brüggemann 2019). However, the density variation of the PCMs could play an important role in the precise prediction of the phase change problems. For one dimensional problems, the density variation between the solid PCM and liquid PCM could evoke a velocity that can serve as a negative feedback for the whole heat transfer process. And for two-dimensional problems the velocity driven by the density variation between the solid PCM and the liquid PCM can serve an important role, while is shown in Chpter 4. Second, the formulation cannot cover the influence from deformations and motions of constituents, and non-Darcian effects (Verma and Dewan 2017). Therefore, using averaging or effective physical properties is still the choice for many phase change problems involving deformable or movable additives like carbon nanotubes and nanoparticles (Bennon and Incropera 1988; Alshaer et al. 2015; B. Li and Zhai 2017; Mahdavi et al. 2018). Third, the Darcy's equation is derived based on a assumption of no mass interaction, however this is not true for melting PCMs, and as a result the basic form of the Darcy's equation is not rigid for the phase change problems of PCMs

2.4 Research Objectives and Methodologies

In this research, we would like to focus on the mathematical modeling of PCMs and PCM composites in their phase change processes based on a mixture theory

framework. The detailed objectives are listed below:

(a) To give a comprehensive review of the mixture theory, and the limitations of the mixture theory in the phase change problems should also be pointed out.

(a) To develop a general mixture theory based framework to model the phase change problems of PCMs and PCM composites, and give our definitions to each terms.

(d) To develop a more rational mixture model for the phase change problems of PCM and PCM composites melting in a cavity.

(c) To experimentally test the melting of pure PCMs and PCM/metal foam composites and compare the experimental data with the numerical results by the mixture model in order to validate the rightness of our proposed mathematical models.

The research methods are described in Figure 2.1.

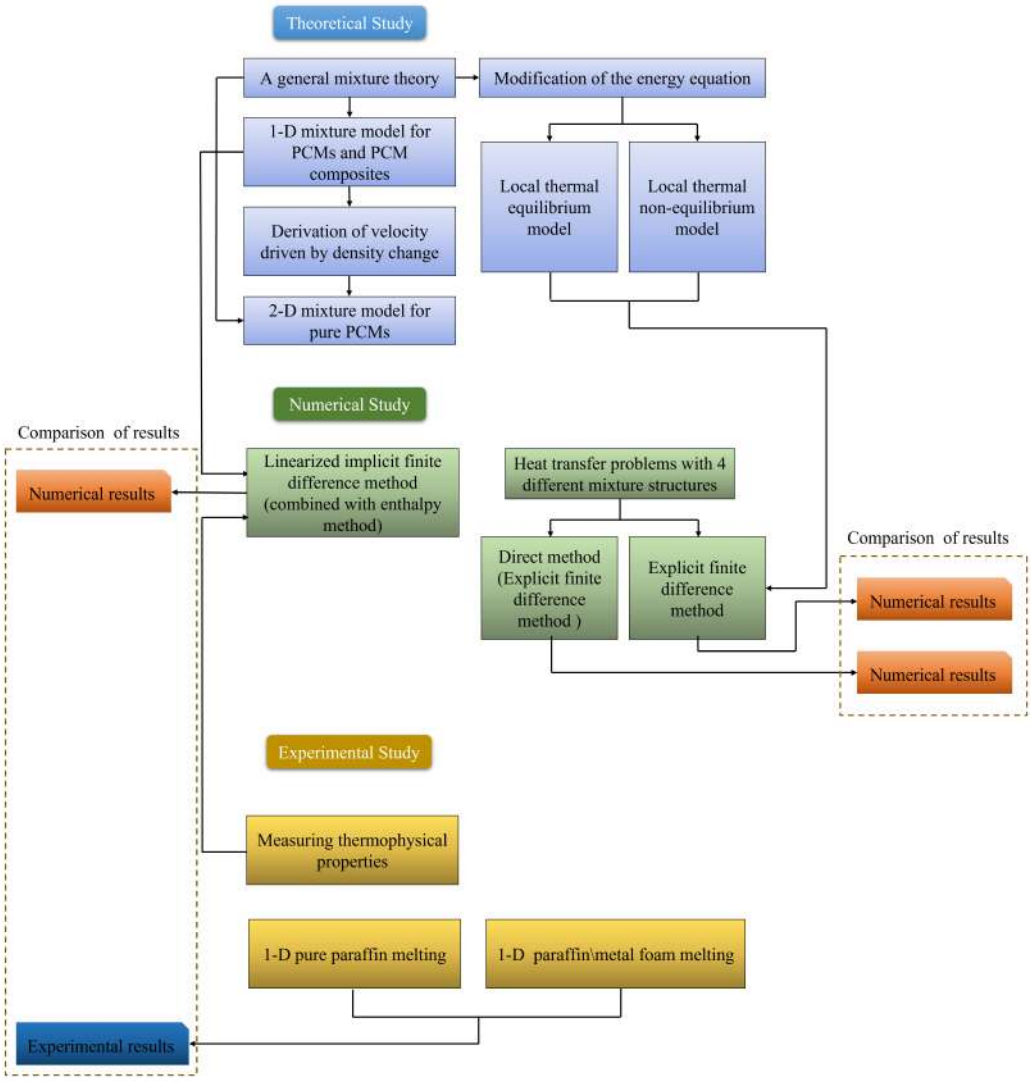

Figure 2.1: Research methodology of the thesis

Chapter 3

A Mixture Theory for PCMs

Since it was proposed by Truesdell and Toupin (1960) in 1960, the mixture theory has been widely utilized to decouple the interactions between constituents in both homogeneous and heterogeneous mixtures in a macroscopic scale. Generally, the mixture theory framework consists of three parts: balance laws of mass, momentum, and energy; entropy inequality, which exerts restrictions to the balance laws; jump conditions that handle singular surfaces where continuity disappears. However, the mixture theory is just a general regime for a mixture such that one need to interpret the equations based on the specific problems. One of the important assumptions for the mixture theory is that several constituents occupy a same spatial potsition at the sametime. However, in real life 2 entities can never overlap. This reflects that the mixture theory framework is a macroscopic method and can not deal with the microscopic structure of a mixture. Also, some terms in the mixture

theory,like the thermal interaction coefficient, are based on a series of assumptions and highly dependent on empirical relations. Moreover, because the some definitions of terms in the mixture theory can be ambiguous, the terms can be defined differently in different studies. For example, the stress tensor of the mixture is given by

$$\mathbf{T} = \mathbf{T}_{\mathrm{I}} - \sum_{\alpha} \rho^{\alpha} \mathbf{u}^{\alpha} \otimes \mathbf{u}^{\alpha} \tag{3.1}$$

in the studies of Truesdell and Toupin (1960), Bowen (1980), and Liu (2014). While Green and Naghdi (1969), and Rajagopal (Rajagopal 2007) use a different expression for the same quatity that

$$\mathbf{T} = \mathbf{T}_{\mathrm{I}} \tag{3.2}$$

As a result, it is important to show the mixture theory with consistent definitions for each terms. In this research, we follow the basic definitions given by Truesdell and Toupin (1960). For the balance laws and entropy inequality, we apply the expressions given by Bowen (1980). Further, jump conditions given by Eringen and Ingram (1965) is adopted in order to describe the boundary conditions.

3.1 Kinematics

We here consider an arbitrary deformable continuous body $\mathcal{B}$ in a Euclidean space shown in Figure 3.1. According to continuum physics, an arbitrary material point in the reference configuration Ω_0 is defined by a position vector $\mathbf{X}$. The position of $\mathbf{X}$ in the current configuration Ω is denoted by $\mathbf{x}$. The motion of $\mathbf{X}$ to $\mathbf{x}$ is defined by using a point-to-point mapping $\boldsymbol{\chi}$, where $\mathbf{x} = \boldsymbol{\chi}(\mathbf{X}, t)$. For conventional continuum theory, it is required that the mapping $\boldsymbol{\chi}$ is a one-to-one relationship. Namely the spatial position $\mathbf{x}$ is occupied by a specific material point that is subjected to $\boldsymbol{\chi}$. However, for mixture theory, an arbitrary point $\mathbf{x}$ may consist all constituents, and the motion of constituent α is given by $\boldsymbol{\chi}^\alpha(\mathbf{X}^\alpha, t)$, where $\mathbf{X}^\alpha$ is the position of constituent α in the reference configuration. The velocity of the mixture and the velocity of a single constituent is defined by

$$\mathbf{v} = \frac{\partial \boldsymbol{\chi}}{\partial t}, \qquad \mathbf{v}^\alpha = \frac{\partial \boldsymbol{\chi}^\alpha}{\partial t} \tag{3.3}$$

Since each constituent α has there own motion, every constituent should have their own deformation tensor $\mathbf{F}^\alpha$ that

$$\mathbf{F}^\alpha = \frac{\partial \chi^\alpha}{\partial \mathbf{X}^\alpha} \tag{3.4}$$

which results in a constituential effective stress tensor $\mathbf{T}^{\alpha}$. Moreover, the material derivative of a physical property f can either follow the motion of the mixture or the motion of constituent α, which indicates

$$\frac{Df}{Dt} = \frac{\partial f}{\partial t} + \nabla f \cdot \mathbf{v} \tag{3.5}$$

$$\frac{D^{\alpha} f}{Dt} = \frac{\partial f}{\partial t} + \nabla f \cdot \mathbf{v}^{\alpha} \tag{3.6}$$

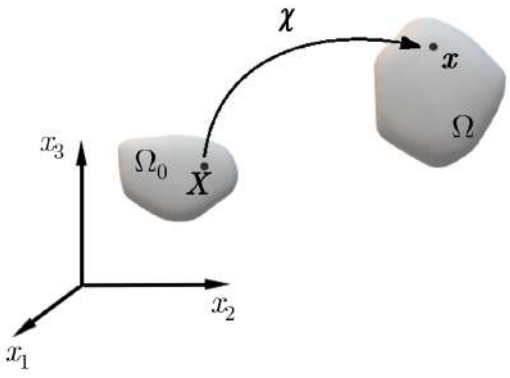

Figure 3.1: Motion of a continuous body $\mathcal{B}$.

3.2 Balance Laws

3.2.1 Balance of Mass

According to aforementioned considerations, the local form of the balance of mass for the mixture using a Euclidean description is given by (Ray M Bowen 1976)

$$\frac{D\rho}{Dt} + \rho\nabla \cdot \mathbf{v} = 0 \tag{3.7}$$

and the local form of the balance of mass for constituent α is

$$\frac{D^\alpha\rho^\alpha}{Dt} + \rho^\alpha\nabla \cdot \mathbf{v}^\alpha = \hat{\rho}^\alpha \tag{3.8}$$

where ρ^α is the bulk density of α and $\hat{\rho}^\alpha$ stands for the mass supply rate to α from other constituents. The relation between mixture density ρ and constituential density ρ^α yields

$$\rho = \sum_\alpha \rho^\alpha \tag{3.9}$$

The mixture velocity $\mathbf{v}$ is defined by

$$\mathbf{v} = \frac{1}{\rho}\sum_\alpha \rho^\alpha\mathbf{v}^\alpha \tag{3.10}$$

According to the definitions for mixture theory by Truesdell and ToupinTruesdell and Toupin 1960, Eq. (3.7) should be equal to the summation of Eq. (3.8), which indicates

$$\sum_{\alpha} \hat{\rho}^{\alpha} = 0 \tag{3.11}$$

For phase change problems of PCMs, many numerical studies use a continuity equation $\nabla \cdot \mathbf{v} = 0$ for the mixture. However, this results in an invariant density while phase changing or no phase transition between constituents. For example, in the mush region of melting paraffin that is a mixture composed by solid paraffin s and liquid paraffin l, $\hat{\rho}^s$ is the mass transition rate from liquid paraffin to solid paraffin while $\hat{\rho}^l$ represents the mass transition rate from solid paraffin to liquid paraffin where $\hat{\rho}^l = -\hat{\rho}^s \neq 0$. If the aforementioned continuity equation is applied, according to Eq. (3.7)-Eq. (3.11) it can be derived that the true density of solid paraffin $\acute{\rho}^s$ equals that of liquid paraffin $\acute{\rho}^l$, which would cause errors for most PCMs suffer a noteworthy density variation during their phase change process. It is important to mention that, which is different from classical continuum physics, the assumption $\nabla \cdot \mathbf{v} = 0$ does not imply an incompressibility for mixtures. Bowen (1980) stated that the mixture is incompressible as long as the true density of each constituent is a constant, though the mixture density ρ might vary.

3.2.2 Balance of Momentum

The angular momentum is always balanced by using some definitions and the demonstration of this conclusion is shown by Jiao (2017).The local form of balance of linear momentum for the mixture and constituent α are defined by (Ray M Bowen 1976)

$$\rho\frac{D\mathbf{v}}{Dt} - \nabla\cdot\mathbf{T} - \rho\mathbf{b} = 0 \tag{3.12}$$

$$\rho^{\alpha}\frac{D^{\alpha}\mathbf{v}^{\alpha}}{Dt} - \nabla\cdot\mathbf{T}^{\alpha} - \rho^{\alpha}\mathbf{b}^{\alpha} - \hat{\mathbf{p}}^{\alpha} = 0 \tag{3.13}$$

where $\mathbf{T}$ is the stress tensor; $\mathbf{b}$ is the external body force vector; $\mathbf{T}^{\alpha}$ is the Cauchy stress tensor of α; $\mathbf{b}^{\alpha}$ is the body force vector for α; $\hat{\mathbf{p}}^{\alpha}$ is the momentum supply to α from all the other constituents. Again, the compatibility between Eq. (3.12) and Eq. (3.13) requires that

$$\mathbf{T} = \mathbf{T}_{\mathrm{I}} + \sum_{\alpha}\rho^{\alpha}\mathbf{u}^{\alpha}\otimes\mathbf{u}^{\alpha} \tag{3.14}$$

and

$$\sum_{\alpha}(\hat{\mathbf{p}}^{\alpha} + \hat{\rho}^{\alpha}\mathbf{v}^{\alpha}) = 0 \tag{3.15}$$

where $\mathbf{u}^\alpha$ is called the diffusion velocity of α which is defined by

$$\mathbf{u}^\alpha = \mathbf{v}^\alpha - \mathbf{v} \tag{3.16}$$

and $\mathbf{T}_\mathrm{I}$ is the inner part of the stress tensor given by

$$\mathbf{T}_\mathrm{I} = \sum_\alpha \mathbf{T}^\alpha \tag{3.17}$$

$\mathbf{T}_\mathrm{I}$ is also symmetric in accordance with Eq. (3.14). Whereas the constituential stress tensor $\mathbf{T}^\alpha$ is unnecessarily symmetric due to local interactions. The expression of body force vector $\mathbf{b}$ in terms of $\mathbf{b}^\alpha$ is given by

$$\mathbf{b} = \frac{1}{\rho} \sum_\alpha \rho^\alpha \mathbf{b}^\alpha \tag{3.18}$$

For phase change problems, the most common body force source is gravity, which is evenly exerted on each constituent. As a result, for many problems it is reasonable to assume a uniform body force vector that $\mathbf{b}^\alpha = \mathbf{b}$.

3.2.3 Balance of Energy

The balance of energy for the mixture and constituent α are given by (Ray M Bowen 1976)

$$\rho\frac{D\varepsilon}{Dt} - \mathbf{T} : \nabla\mathbf{v} + \nabla\cdot\mathbf{q} - \rho\gamma = 0 \tag{3.19}$$

$$\rho^\alpha\frac{D^\alpha\varepsilon^\alpha}{Dt} - \mathbf{T}^\alpha : \nabla\mathbf{v}^\alpha + \nabla\cdot\mathbf{q}^\alpha - \rho^\alpha\gamma^\alpha - \hat{\varepsilon}^\alpha = 0 \tag{3.20}$$

where ε is the mixture internal energy density; $\mathbf{q}$ is the heat flux vector; γ is the heat supply term; ε^α is the internal energy density of constituent α; $\mathbf{q}^\alpha$ is the constituential heat flux vector; γ^α is the heat supply to constituent α from external sources; and $\hat{\varepsilon}^\alpha$ is the energy supply to constituent α from other constituents. The internal energy of the mixture is given by

$$\varepsilon = \varepsilon_{\mathrm{I}} + \frac{1}{\rho}\sum_\alpha \frac{1}{2}\rho^\alpha\mathbf{u}^\alpha\cdot\mathbf{u}^\alpha \tag{3.21}$$

and the heat flux and external heat supply are defined by (Ray M Bowen 1976)

$$\mathbf{q} = \mathbf{q}_{\mathrm{I}} + \frac{1}{2}\sum_\alpha \rho^\alpha(\mathbf{u}^\alpha\cdot\mathbf{u}^\alpha)\mathbf{u}^\alpha \tag{3.22}$$

$$\gamma = \frac{1}{\rho}\sum_{\alpha}\rho^{\alpha}\gamma^{\alpha} \tag{3.23}$$

where ε_{I} and $\mathbf{q}_{\mathrm{I}}$ are the inner part of internal energy density and heat flux respectively that are defined by (Ray M Bowen 1976)

$$\varepsilon_{\mathrm{I}} = \frac{1}{\rho}\sum_{\alpha}\rho^{\alpha}\varepsilon^{\alpha} \tag{3.24}$$

$$\mathbf{q}_{\mathrm{I}} = \sum_{\alpha}[\mathbf{q}^{\alpha} - (\mathbf{T}^{\alpha})^{\mathrm{T}}\cdot\mathbf{u}^{\alpha} + \rho^{\alpha}\varepsilon^{\alpha}\mathbf{u}^{\alpha}] \tag{3.25}$$

Mixture theory requires that Eq. (3.19) can be obtained by taking summation of Eq. (3.20) over all constituents. By using definitions in Eq. (3.21)-(3.25), it is suggested that

$$\sum_{\alpha}(\hat{\varepsilon}^{\alpha} + \bar{\mathbf{p}}^{\alpha}\cdot\mathbf{u}^{\alpha} + \hat{\rho}^{\alpha}(\varepsilon^{\alpha} + \frac{1}{2}\rho^{\alpha}\mathbf{u}^{\alpha}\cdot\mathbf{u}^{\alpha})) = 0 \tag{3.26}$$

The above-mentioned definitions have to be consistent with the balance of energy. Namely, if we substitute (3.21)-(3.25) into the local form of the balance of energy of the mixture described by Eq. (3.19), it can be expanded to the form for individual constituents given in Eq. (3.20). Therefore that the diffusion velocity must yield

$$\sum_{\alpha}\rho^{\alpha}\mathbf{u}^{\alpha} = \mathbf{0} \tag{3.27}$$

Here, in particular, for the cases that the body force is uniform, namely

$$\mathbf{b}^{\alpha} = \mathbf{b} \tag{3.28}$$

we may develop another way of describing the balance of energy. With the aid of (3.27), Eq. (3.19) may be written as

$$\rho\frac{D\varepsilon}{Dt} = \mathbf{T} : \nabla\mathbf{v} - \nabla\cdot\mathbf{q} + \rho\gamma + \mathbf{b}\cdot\sum_{\alpha}\rho^{\alpha}\mathbf{u}^{\alpha} \tag{3.29}$$

It is noticed from (3.27) that the last term on the right of Eq. (3.29) is zero. Next, if the body force is uniform, which is reasonable since the body force acting on most mixtures that we consider is gravity only, we may move **b** in the right hand side of Eq. (3.29) inside the summation. Therefore Eq. (3.29) can be further written as

$$\rho\frac{D\varepsilon}{Dt} = \mathbf{T} : \nabla\mathbf{v} - \nabla\cdot\mathbf{q} + \rho\gamma + \sum_{\alpha}\rho^{\alpha}\mathbf{u}^{\alpha}\cdot\mathbf{b}^{\alpha} \tag{3.30}$$

The left side of Eq. (3.30) can be expanded using (3.21),

$$\rho\frac{D\varepsilon}{Dt} = \rho\frac{D\varepsilon_{\mathrm{I}}}{Dt} + \sum_{\alpha}\left[\rho^{\alpha}\mathbf{u}^{\alpha}\cdot\frac{D^{\alpha}\mathbf{u}^{\alpha}}{Dt} - \nabla\cdot[(\frac{1}{2}\rho^{\alpha}\mathbf{u}^{\alpha}\cdot\mathbf{u}^{\alpha})\mathbf{u}^{\alpha}] + \frac{1}{2}\hat{\rho}^{\alpha}\mathbf{u}^{\alpha}\cdot\mathbf{u}^{\alpha}\right] \tag{3.31}$$

and the first term inside the parenthesis of (3.31) can be expressed as

$$\sum_{\alpha} \rho^{\alpha} \mathbf{u}^{\alpha} \cdot \frac{D^{\alpha} \mathbf{u}^{\alpha}}{Dt} = \sum_{\alpha} \rho^{\alpha} [\mathbf{u}^{\alpha} \cdot \mathbf{a}^{\alpha} - \nabla \mathbf{v} : (\mathbf{u}^{\alpha} \otimes \mathbf{u}^{\alpha})] \tag{3.32}$$

Then Eq. (3.30) is expanded to

$$\begin{aligned} &\rho \frac{D\varepsilon_{\mathrm{I}}}{Dt} + \sum_{\alpha} \left[\rho^{\alpha} \mathbf{u}^{\alpha} \mathbf{a}^{\alpha} - \nabla \mathbf{v} : (\mathbf{u}^{\alpha} \otimes \mathbf{u}^{\alpha}) - \nabla \cdot [(\frac{1}{2} \rho^{\alpha} \mathbf{u}^{\alpha} \cdot \mathbf{u}^{\alpha}) \mathbf{u}^{\alpha}] + \frac{1}{2} \hat{\rho}^{\alpha} \mathbf{u}^{\alpha} \cdot \mathbf{u}^{\alpha} \right] \\ &= (\mathbf{T}_{\mathrm{I}} - \sum_{\alpha} \rho^{\alpha} \mathbf{u}^{\alpha} \otimes \mathbf{u}^{\alpha}) : \nabla \mathbf{v} - \nabla \cdot [\mathbf{q}_{\mathrm{I}} + \frac{1}{2} \rho^{\alpha} \mathbf{u}^{\alpha} \cdot \mathbf{u}^{\alpha}) \mathbf{u}^{\alpha}] \\ &\quad + \sum_{\alpha} \rho^{\alpha} \mathbf{u}^{\alpha} \cdot \mathbf{b}^{\alpha} + \rho \gamma \end{aligned} \tag{3.33}$$

For convenience, let us define a vector $\mathbf{k}$, where

$$\mathbf{k} = \sum_{\alpha} (\mathbf{q}^{\alpha} + \rho^{\alpha} \varepsilon^{\alpha} \mathbf{u}^{\alpha}) \tag{3.34}$$

and accordingly we have

$$\mathbf{T}_{\mathrm{I}} : \nabla \mathbf{v} = \sum_{\alpha} \mathbf{T}^{\alpha} : \nabla \mathbf{v}^{\alpha} + \sum_{\alpha} \mathbf{u}^{\alpha} \cdot \nabla \cdot \mathbf{T}^{\alpha} - \nabla \cdot \mathbf{k} + \nabla \cdot \mathbf{q}_{\mathrm{I}} \tag{3.35}$$

Now by substituting Eq. (3.35) into (3.33), with the aid of the balance of linear momentum, we have

$$\rho\frac{D\varepsilon_{\mathrm{I}}}{Dt} = \sum_{\alpha}\mathbf{T}^{\alpha} : \nabla\mathbf{v}^{\alpha} - \nabla\cdot\mathbf{k} + \rho\gamma - \sum_{\alpha}\mathbf{u}^{\alpha}\cdot\hat{\mathbf{p}}^{\alpha} - \frac{1}{2}\sum_{\alpha}\hat{\rho}^{\alpha}\mathbf{u}^{\alpha}\cdot\mathbf{u}^{\alpha} \quad (3.36)$$

It is noticed that for a solid-liquid phase change problem without energy supply, if the mixture velocity is assumed to be incompressible, Eq. (3.19) is reduced to

$$\rho\frac{D\varepsilon}{Dt} + \nabla\cdot\mathbf{q} = 0 \quad (3.37)$$

Furthermore, if the mechanical part is not taken into account, for pure PCM with a constant specific heat capacity C_P, the internal energy density is written as

$$\varepsilon = C_P T + \varphi L \quad (3.38)$$

where T is the averaging temperature of the mixture; φ is the volume fraction of liquid phase; L is the latent heat of the PCM. Eq. (3.37) together with Eq. (3.38) is usually used to avoid modeling the moving interface for phase change problems which is known as the enthalpy method.

3.2.4 Entropy Inequality

Instead of formulating equations for individual constituents, the entropy inequality is postulated for the whole mixture to avoid unexpected constrains (Bedford and Drumheller 1983). Obtained by Bowen and Wiese (1969), the local form of entropy inequality is expressed as

$$\rho\frac{D\eta}{Dt} + \sum_{\alpha} \nabla \cdot \frac{\mathbf{h}^{\alpha}}{T^{\alpha}} - \sum_{\alpha} \frac{\rho^{\alpha}\gamma^{\alpha}}{T^{\alpha}} \geqslant 0 \tag{3.39}$$

where T^{α} is the temperature of constituent α, η is the entropy density of the mixture which is defined by

$$\eta = \frac{1}{\rho}\sum_{\alpha} \rho^{\alpha}\eta^{\alpha} \tag{3.40}$$

where η^{α} is the entropy density of constituent α, and $\mathbf{h}^{\alpha}$ is a flux vector given by

$$\mathbf{h}^{\alpha} = \mathbf{q}^{\alpha} + T^{\alpha}\rho^{\alpha}\eta^{\alpha}\mathbf{u}^{\alpha} \tag{3.41}$$

where η is the entropy density of the mixture defined by

$$\eta = \frac{1}{\rho}\sum_{\alpha} \rho^{\alpha}\eta^{\alpha} \tag{3.42}$$

and η^α is the entropy density for constituent α. Using (3.42), Eq. (3.39) may be expanded to

$$\sum_\alpha [\rho^\alpha \frac{D^\alpha \eta^\alpha}{Dt} + \nabla \cdot (\frac{\mathbf{h}^\alpha}{\theta^\alpha} - \rho^\alpha \eta^\alpha \mathbf{u}^\alpha) - \frac{\rho^\alpha \gamma^\alpha}{\theta^\alpha} + \hat{\rho}^\alpha \eta^\alpha] \geqslant 0 \tag{3.43}$$

Next, with the aid of the local form of the balance of energy given in Eq. (3.20), the term $\rho^\alpha \gamma^\alpha$ is replaced in (3.43). Therefore Eq. (3.43) becomes

$$\begin{aligned}\sum_\alpha \Bigg[& \rho^\alpha \frac{D^\alpha \eta^\alpha}{Dt} + \frac{1}{\theta^\alpha} \nabla \cdot \mathbf{h}^\alpha - \frac{\mathbf{h}^\alpha \cdot \nabla \theta^\alpha}{(\theta^\alpha)^2} - \nabla \cdot (\rho^\alpha \eta^\alpha \mathbf{u}^\alpha) \\ & - \frac{1}{\theta^\alpha} [\rho^\alpha \frac{D^\alpha \varepsilon^\alpha}{Dt} - \mathbf{T}^\alpha : \nabla \mathbf{v}^\alpha + \nabla \cdot \mathbf{q}^\alpha - \hat{\varepsilon}^\alpha] + \hat{\rho}^\alpha \eta^\alpha \Bigg] \geqslant 0\end{aligned} \tag{3.44}$$

By introducing a new scalar $\hat{e}^\alpha$ which is defined by

$$\hat{e}^\alpha = \hat{\varepsilon}^\alpha + \mathbf{u}^\alpha \cdot \hat{\mathbf{p}}^\alpha + \hat{\rho}^\alpha (\varepsilon^\alpha + \frac{1}{2} \mathbf{u}^\alpha \cdot \mathbf{u}^\alpha) \tag{3.45}$$

Eq. (3.44) is written as

$$\begin{aligned}\sum_\alpha \frac{1}{\theta^\alpha} [\rho^\alpha (\theta^\alpha \frac{D^\alpha \eta^\alpha}{Dt} - \frac{D^\alpha \varepsilon^\alpha}{Dt}) + \mathbf{T}^\alpha : \nabla \mathbf{v}^\alpha - \frac{\mathbf{h}^\alpha \cdot \nabla \theta^\alpha}{\theta^\alpha} + \nabla \cdot (\mathbf{h}^\alpha - \mathbf{q}^\alpha) \\ - \theta^\alpha \nabla \cdot (\rho^\alpha \eta^\alpha \mathbf{u}^\alpha) - \hat{\rho}^\alpha (\varepsilon^\alpha - \theta^\alpha \eta^\alpha + \frac{1}{2} \mathbf{u}^\alpha \cdot \mathbf{u}^\alpha) + \hat{e}^\alpha - \mathbf{u}^\alpha \cdot \hat{\mathbf{p}}^\alpha] \geqslant 0\end{aligned} \tag{3.46}$$

At this point, the definition of the flux vector $\mathbf{h}^\alpha$ is given by

$$\mathbf{h}^\alpha = \mathbf{q}^\alpha + \theta^\alpha \rho^\alpha \eta^\alpha \mathbf{u}^\alpha \tag{3.47}$$

By substituting (3.47) into the general form of the entropy inequality for individual constituents is obtained, which is rewritten as

$$\begin{aligned}\int_{\mathcal{V}^\alpha} \frac{\partial}{\partial t}(\rho\eta)\, dv \geqslant & -\int_{\partial\mathcal{V}^\alpha} \sum_\alpha \rho^\alpha \eta^\alpha \mathbf{v}^\alpha \cdot \mathbf{n}\, da \\ & -\int_{\partial\mathcal{V}^\alpha} \sum_\alpha \frac{\mathbf{q}^\alpha}{\theta^\alpha} \cdot \mathbf{n}\, da + \int_{\mathcal{V}^\alpha} \sum_\alpha \frac{\rho^\alpha \gamma^\alpha}{\theta^\alpha}\, dv\end{aligned} \tag{3.48}$$

Moreover, inequality (3.46) may be written as

$$\begin{aligned}&\sum_\alpha \frac{1}{\theta^\alpha}[\rho^\alpha(\theta^\alpha \frac{D^\alpha \eta^\alpha}{Dt} - \frac{D^\alpha \eta^\alpha}{Dt}) + \mathbf{T}^\alpha : \nabla \mathbf{v}^\alpha - \\ &\frac{1}{\theta^\alpha}(\mathbf{q}^\alpha \cdot \nabla\theta^\alpha) + \hat{e}^\alpha - \mathbf{u}^\alpha \cdot \hat{\mathbf{p}}^\alpha - \hat{\rho}^\alpha(\varepsilon^\alpha - \theta^\alpha \eta^\alpha + \frac{1}{2}\mathbf{u}^\alpha \cdot \mathbf{u}^\alpha)] \geqslant 0\end{aligned} \tag{3.49}$$

For mixtures subjected to a uniform temperature, we may obtain an alternative form of the inequality. To this end, we introduce the Helmholtz free energy which is defined by

$$\psi^\alpha = \varepsilon^\alpha - \eta^\alpha \theta^\alpha \tag{3.50}$$

and the material derivative of ψ following the motion of constituent α is

$$\frac{D^\alpha \psi^\alpha}{Dt} = \frac{D^\alpha \varepsilon^\alpha}{Dt} - \eta^\alpha \frac{D^\alpha \theta^\alpha}{Dt} - \theta^\alpha \frac{D^\alpha \eta^\alpha}{Dt} \tag{3.51}$$

By substituting (3.51) back into Eq. (3.49), with the understanding that $\theta^\alpha = \theta$, we obtain

$$\begin{aligned} \sum_\alpha [& -\rho^\alpha (\frac{D^\alpha \psi^\alpha}{Dt} + \eta^\alpha \frac{D^\alpha \theta}{Dt}) \\ & + \mathbf{T}^\alpha : \nabla \mathbf{v}^\alpha - \frac{1}{\theta}(\mathbf{q}^\alpha \cdot \nabla \theta) + \hat{e}^\alpha - \mathbf{u}^\alpha \cdot \hat{\mathbf{p}}^\alpha - \hat{\rho}^\alpha (\psi^\alpha + \frac{1}{2}\mathbf{u}^\alpha \cdot \mathbf{u}^\alpha)] \geqslant 0 \end{aligned} \tag{3.52}$$

Moreover, if the mixture is subjected to a uniform body force, it can be shown that

$$\sum_\alpha \hat{e}^\alpha = 0 \tag{3.53}$$

Therefore the entropy inequality is further reduced to

$$\begin{aligned} \sum_\alpha [& -\rho^\alpha (\frac{D^\alpha \psi^\alpha}{Dt} + \eta^\alpha \frac{D^\alpha \theta}{Dt}) + \mathbf{T}^\alpha : \nabla \mathbf{v}^\alpha - \frac{1}{\theta}(\mathbf{q}^\alpha \cdot \nabla \theta) \\ & - \mathbf{u}^\alpha \cdot \hat{\mathbf{p}}^\alpha - \hat{\rho}^\alpha (\psi^\alpha + \frac{1}{2}\mathbf{u}^\alpha \cdot \mathbf{u}^\alpha)] \geqslant 0 \end{aligned} \tag{3.54}$$

3.3 Jump Conditions

In real situations, the mixture can not always continuous, and as a result, physical properties can suffer a jump where discontinuity appears. We should state that the discontinuities are not referring to the property differences between the local constituents, but the macroscopic jumps like the interface between two mixtures. Most PCMs and PCM composites can be regarded as continuous mixture because they are homogeneous or heterogeneous. However, if there is a suddenly change in the structures of PCMs and PCM composites, we should expect some properties could suffer jumps including temperature, velocity, pressure, density, etc. Moreover, we do not consider the gap and overlap of constituents in this mixture theory framework, which indicates that the motion of the mixture is always continuous. In this thesis, the jump conditions are not used for calculation because the PCMs and PCM composites we study are assumed to be continuous, yet we would like to show the expressions of the jumps conditions because it is a significant part of the mixture theory and would be essential for our studying the discontinuities in PCMs in the future. We follow the definitions given by Casey (2011) , who claimed that a jump can be considered as an infinitesimally narrow material region that is called a singular surface. For an arbitrary field property Φ, its jump across a singular

surface Γ is given by (Casey 2011)

$$[[\Phi]] \cdot \mathbf{n} = (\Phi_+ - \Phi_-) \cdot \mathbf{n} \tag{3.55}$$

where Φ_+ and Φ_- are the two one-sided limits of property Φ at Γ, and $\mathbf{n}$ is a unit normal on Γ that point into $+$ side.

The local form of jump of mass for the mixture is given by

$$[[\rho \mathbf{u}_\Gamma]] \cdot \mathbf{n} = 0 \tag{3.56}$$

where $\mathbf{u}_\Gamma$ is the diffusion velocity relative to the singular surface for the mixture defined by the difference between mixture velocity $\mathbf{v}$ and velocity of the singular surface $\mathbf{v}_\Gamma$

$$\mathbf{u}_\Gamma = \mathbf{v} - \mathbf{v}_\Gamma \tag{3.57}$$

The jump of mass for constituent α is given by

$$[[\rho^\alpha \mathbf{u}_\Gamma^\alpha]] \cdot \mathbf{n} = \bar{\rho}^\alpha \tag{3.58}$$

where $\mathbf{u}_\Gamma^\alpha$ is the diffusion velocity relative to the singular surface for α, and $\bar{\rho}^\alpha$ is

the mass supply rate to α from other constituents on Γ that follows

$$\sum_{\alpha} \bar{\rho}^{\alpha} = 0 \tag{3.59}$$

The jump of linear momentum for the mixture is given by

$$[[\rho \mathbf{v} \otimes \mathbf{u}_{\Gamma} - \mathbf{T}]] \cdot \mathbf{n} = 0 \tag{3.60}$$

and the jump of linear momentum for constituent α is expresses as

$$[[\rho^{\alpha} \mathbf{v}^{\alpha} \otimes \mathbf{u}_{\Gamma}^{\alpha} - \mathbf{T}^{\alpha}]] \cdot \mathbf{n} = \bar{\mathbf{s}}^{\alpha} \tag{3.61}$$

with the momentum supply rate term $\bar{\mathbf{s}}^{\alpha}$ defined by

$$\bar{\mathbf{s}}^{\alpha} = \bar{\rho}^{\alpha} \mathbf{v}^{\alpha} + \bar{\mathbf{p}}^{\alpha} \tag{3.62}$$

where the first term on the right hand side stands for the momentum supply on Γ by mass supply, and the second term indicates the momentum supply from chemical reaction or phase change.

The jump conditions of energy are given by

$$[[\rho(\varepsilon + \frac{1}{2}\mathbf{v} \cdot \mathbf{v})\mathbf{u}_{\Gamma} - \mathbf{T}^{\mathrm{T}} \cdot \mathbf{v} + \mathbf{q}]] \cdot \mathbf{n} = 0 \tag{3.63}$$

$$[[\rho^\alpha(\varepsilon^\alpha + \frac{1}{2}\mathbf{v}^\alpha \cdot \mathbf{v}^\alpha)\mathbf{u}_\Gamma^\alpha - (\mathbf{T}^\alpha)^{\mathrm{T}} \cdot \mathbf{v}^\alpha + \mathbf{q}^\alpha]] \cdot \mathbf{n} = \bar{w}^\alpha \tag{3.64}$$

where $\bar{w}^\alpha$ is the rate of energy supply on the singular surface Γ defined by

$$\bar{w}^\alpha = \bar{\rho}^\alpha(\varepsilon^\alpha + \frac{1}{2}\mathbf{v}^\alpha \cdot \mathbf{v}^\alpha) + \bar{\mathbf{p}}^\alpha \cdot \mathbf{v}^\alpha + \bar{\varepsilon}^\alpha \tag{3.65}$$

Eq. (3.65) suggests that the energy supply rate to α on Γ consists of three components. The first part is the energy carried by the mass supply involving internal energy and kinetic energy, the second part is from the momentum supply on the singular surface, and the third part is the energy transfer rate from contact.

As stated previously, the entropy inequality can not be postulated for individual constituents. Likewise, the jump of entropy should be presented the the mixture. With the relation $\sum_\alpha(\mathbf{h}^\alpha/T^\alpha) = \mathbf{h}/T$, the local for of the jump of entropy is given by

$$[[\rho\eta\mathbf{u}_\Gamma + \frac{\mathbf{h}}{T}]] \cdot \mathbf{n} \geqslant 0 \tag{3.66}$$

3.4 Approxiamation of Momentum Equation

Although we have the balance laws for the mixture, they can not be directly solved for the number of unknowns is greater than the number of equations, and as a result

we need some constitutive relations or approximations to constrain the balance laws. It is noticed that in the mushy zone generated in the phase change processes of PCMs is of a porous structure, and most heat transfer enhancement materials like metal foams and carbon materials can be regarded as porous materials. Intuitively we can use Darcy's equation to approximate the momentum equation[1]. Now let us consider a binary mixture consists of a solid constituent s and a liquid constituent l. For porous media, the inertia force is usually neglected (Ray M Bowen 1980, Qiao et al. 2018), and if we ignore the viscous stress for liquid components that

$$\mathbf{T}^l = -p\mathbf{I} \tag{3.67}$$

and say the body force is uniform, Eq. 3.13 for the liquid fraction becomes

$$-\nabla p + \acute{\rho}^l \varphi^l \mathbf{b} + \mathbf{p}^l = 0 \tag{3.68}$$

Though we have ignored the viscosity effect of the liquid, the drag from the solid can not be ignored and should be included in the term $\mathbf{p}^l$. According to the exper-

[1] Darcy's equation is also referred to as the Darcy's law, which initially was an empirical relation founded by Darcy (1856). Yet Rajagopal (2007) suggested that this relation should not be conferred as a "law" because it is just an approximation of the momentum equation. In this research, we apply this proposition and use "Darcy's equation" refer to this approximation.

iment studies it was found that

$$\mathbf{p}^l = -\alpha(\mathbf{v}^l - \mathbf{v}^s) \tag{3.69}$$

where the negative symbol indicated that the direction of the drag is opposite to that of velocity. Here we say the body force solely comes from gravity that

$$\mathbf{b} = \begin{pmatrix} 0 \\ 0 \\ -g \end{pmatrix} \tag{3.70}$$

Such that we have

$$\mathbf{v}^l = \frac{1}{\alpha}(-\nabla p + \acute{\rho}^l \varphi^l \mathbf{b}) \tag{3.71}$$

which is the Darcy's equation. Rewire the drag coefficient α in terms of intrinsic permeability $\mathcal{K}$ and viscosity μ that

$$\alpha = \frac{\mu}{\mathcal{K}} \tag{3.72}$$

The above derivation process is consistent with Freeze (1979) and Rajagopal (1995). However the above derivation is not pure theoretical because an empirical relation

Eq. 3.69 is used from which the resulted restrictions are not clear. In view of this, we may apply the entropy inequality to the momentum equation and obtain the same equation as Eq. 3.71 to find out the assumptions we need to make. Consider a mixture consists of multiple incompressible liquids and multiple incompressible elastic solids. If the mixture is of local thermal equilibrium that $T^{\alpha} = T$ and acceleration of liquid constituents is ignored, Bowen (1980) showed that Eq. (3.39) requires the balance of momentum for any liquid constituent l to be

$$\varphi^{l}\mathbf{v}^{l} = -\frac{\mathbf{K}^{l}}{\mu^{l}} \cdot (\nabla P^{l} - \acute{\rho}^{l}\mathbf{b}^{l}) \tag{3.73}$$

which is the general form of the Darcy's equation, where $\mathbf{K}^{l}$ is the permeability tensor of l, μ^{l} is the viscosity of l, and P^{l} is called the pore pressure for constituent l. The same equation wasw obtained by Liu (2014) by using Lagrange multipliers. In obtaining Eq. (3.73), the following assumption's are made: (1) inertia of the fluid constituents is ignored; (2) The solid constituents are rigid; (3) deformations are isothermal and there is no local temperature difference between different constituents; (4) constituents are incompressible and there is no mass exchange between constituents; (5) the drags only exist between solid and liquid constituents. Although the Darcy's equation has been applied by some studies (Voller et al. 1985) to describe the fluid flow in the porous structures of PCMs and PCM composites, some aforementioned assumptions do not follow the real

situations from the aspect of the mixture theory. First, inside the mushy zone there is mass exchange between solid PCMs and liquid PCMs; second, if the thermal conductivities between extra additives and PCMs vary significantly, which is quite common, there would be local thermal non-equilibrium; third, deformation could exist for some solid constituents like solid PCMs and carbon materials; last, sometimes the acceleration of the fluid constituents can not be ignored. In order to overcome these restrictions, on one hand, we can revise the Darcy's equation to a more general form. If we now consider the liquid constituents are Newtonian, Eq. (3.73) can be revised to the

$$\varphi^l \mathbf{v}^l = -\frac{\mathbf{K}^l}{\mu^l} \cdot (\nabla P^l - \rho^l \mathbf{b}^l) + \frac{\mathbf{K}^l}{\varphi^l} \cdot \nabla(\nabla \cdot \mathbf{v}^l) \tag{3.74}$$

which is equivalent to the Brinkman's equation. Regarding this topic, Rajagopal (2007) gave the expression of the revised Darcy's equation for the unsteady viscous flow through a rigid solid, and Preziosi and Farina (2002) derived the Darcy's equation for the mixtures with mass interactions between constituents. On the other hand, we can avoid using the Darcy's equation by using different mathematical models. The most complicated region for the phase change problems of PCMs and PCM composites is the mushy zone where the solid PCM, liquid PCM, and additives coexist. Recall that the purpose of using Darcy's equation is to find the approximate form of the momentum equation to obtain the velocity field. In

this case, if we can use the mass equation together with some other constitutive relations to find the velocity field, the momentum equation is not needed. This idea is applied in this research to find the velocity field inside the mushy zone and the details are shown in the following chapter.

Chapter 4

A Mixture Model for PCMs and PCM Composites

In this chapter, we build the mathematical model for one-dimensional melting of pure PCM and PCM composites based on the general mixture theory shown in the previous chapter. Each source term for an individual constituent is fully considered. A new expression for heat flux terms is defined including heat conduction terms between different constituents that have not been presented before. A new expression for the internal energy supply terms is also given. By analyzing the governing equations, it is suggested that the nonlinearity of one-dimensional melting problems only comes from the phase change itself, and the addition of metal foam does not introduce extra complexity. Three different problems: pure PCM melting, PCM melting in a copper foam, and PCM melting in a nickel foam, are

numerically solved using a finite difference method based on the modified mixture theory model. The PCM used in this study is paraffin wax with three phase change processes. Considering the densities of liquid paraffin and solid paraffin are different, the velocity profile is obtained by the balance of mass. It is shown that this velocity, which is rarely considered by researchers, has a noticeable influence on the precise prediction of temperature profile. The absence of local thermal equilibrium is considered in this model. The result shows that the temperature difference between metal foam and paraffin is trivial except near the heating side at the beginning of the melting process. Experiments are designed to validate the numerical results. It is shown that the numerical calculation based on the modified mixture theory model well predicts the phase change process by comparing the temperature profile.

4.1 One-dimensional Melting

4.1.1 Problem Description

The one-dimensional melting of PCM and PCM/metal foam composite is shown in Figure 4.1. A constant temperature T_b, which is higher than the melting point of the PCM, is exerted on the top boundary. Thus, the effect of buoyancy difference on the direction of fluid velocity can be ignored so that the melting is assured to be

one-dimensional all time. This type of one dimensional problem is usually seen in PVT systems, which is filled with PCMs and heated from top. By building the model, we can model the one-dimensional heat transferring and predict the leakage problem. The rest of three boundaries are insulated. Accordingly, the melting direction should be from the top boundary to the bottom, and the melting direction is chosen to be the positive direction of the coordinate. Conventionally, the melting region can be divided into three regions: the liquid region, the mushy zone, and the solid region. Since the density of solid PCM is usually higher than its liquid state (Ukrainczyk et al. 2010), a negative velocity u should exist in both the mushy zone and the liquid region. In view of the consistency, here the liquid PCM is allowed to pass through the top boundary freely as a heat loss. If the densities of liquid PCM and solid PCM are assumed to be constant, the velocity in the liquid region is fully developed and should also be constant. The mushy zone is the place where the melting taking place, inside which the liquid phase and the solid phase coexist. Yang et al. (X. Yang et al. 2019) experimentally investigated the microscopic morphology of the mushy zone, indicating the liquid fraction along the melting direction is changing nonlinearly. Hence the velocity inside the mushy zone should be correlated to x. It should be noticed that PCMs like paraffin wax are usually chemically mixtures instead of pure substances, which would result in more than one phase change process. This phenomenon has been observed for different types of PCMs (Sun et al. 2016; W. Wu et al. 2015; S. Yang et al. 2014).

As a result, the possible solid-solid phase change inside the solid region should be considered.

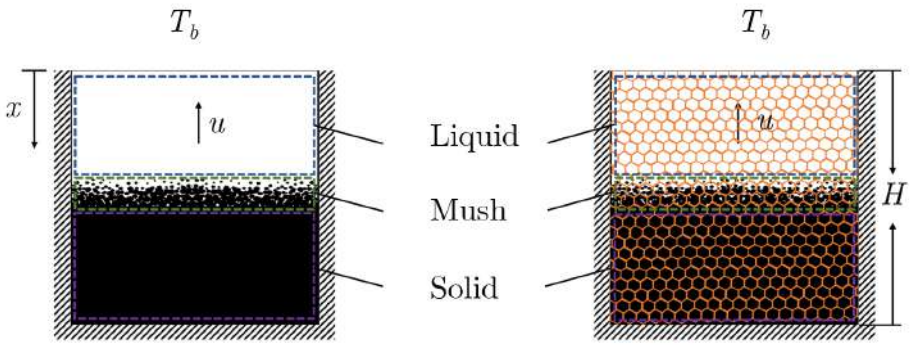

Figure 4.1: One-dimensional PCM and PCM/metal foam melting.

4.1.2 Governing Equations

For one dimensional melting problems shown in Figure 4.1, it is assumed that the motion of liquid PCM is driven by the phase change only, and there is no pressure change, viscous dissipation, or momentum supply. Moreover, because the heating side is at the top boundary, the body force can be ignored. Thus, the momentum is automatically balanced, and we only need mass equation and energy equation to model the problem. The local form of the balance of mass for constituent α using a Euclidean description is given by Eq. (3.8). By using Eq.(3.6), Eq.(3.8) is

expanded to

$$\frac{\partial \rho^\alpha}{\partial t} + \mathbf{v}^\alpha \nabla \rho^\alpha + \rho^\alpha \nabla \cdot \mathbf{v}^\alpha = \hat{\rho}^\alpha \tag{4.1}$$

where the apparent density ρ^α is

$$\rho^\alpha = \varphi^\alpha \acute{\rho}^\alpha \tag{4.2}$$

φ^α is the volumetric fraction of constituent α, and $\acute{\rho}^\alpha$ is the true density of α. In the melting problems, for convenience, properties of the liquid PCM, solid PCM, and metal foam are super-scripted with l, s, and m, respectively. Next, we assume that the true density of solid PCM $\acute{\rho}^s$ does not change along with the solid-solid phase change. Moreover, it is assumed that the solids are rigid, which implies that $u^s = 0$ and $u^m = 0$. Based on the above assumptions and notations, the balance of mass Eq. (4.1) for the melting problem shown in Figure 4.1 can be rewritten into

$$\acute{\rho}^l \frac{\partial \varphi^l}{\partial t} + \acute{\rho}^l \frac{\partial}{\partial x}(\varphi^l u^l) = \hat{\rho}^l \tag{4.3}$$

$$\acute{\rho}^s \frac{\partial (1 - \varphi^l - \varphi^m)}{\partial t} = \hat{\rho}^s \tag{4.4}$$

The mass equation for the metal foam vanishes because the metal is not involved in any physical or chemical changing so that its mass is always balanced. For pure PCM melting, φ^m is just 0. By using Eq. (3.11) and Eq. (4.4) in Eq. (4.3), the velocity of the liquid is obtained as

$$u^l = -\frac{\acute{\rho}^s}{\varphi^l + \sigma}\left(\frac{1}{\acute{\rho}^l} - \frac{1}{\acute{\rho}^s}\right)\int_x^{x=H} \frac{\partial \varphi^l}{\partial t} dx \tag{4.5}$$

where σ is a small number to avoid 0 divisor.

Recall the balance of energy for constituent α that

$$\rho^\alpha \frac{D^\alpha \varepsilon^\alpha}{Dt} - \mathbf{T}^\alpha : \nabla \mathbf{v}^\alpha + \nabla \cdot \mathbf{q}^\alpha - \rho^\alpha \gamma^\alpha - \hat{\varepsilon}^\alpha = 0 \tag{4.6}$$

where ε^α is the internal energy density of constituent α; $\mathbf{q}^\alpha$ is the constituential heat flux vector; γ^α is the heat supply to constituent α from external sources; and $\hat{\varepsilon}^\alpha$ is the energy supply to constituent α from other constituents. In this one dimensional phase change problem, the fluid flow is solely driven by the density difference between liquid PCM and solid PCM, and the scale of the velocity is quiet small. Moreover, usually the viscosity of liquid PCM is not significant (for paraffin OP42E, μ=5.52$\times 10^{-3}$ Pa·s). As a result, we assume the viscous dissipation is negligible and ignore the viscosity term $\mathbf{T}^\alpha : \nabla \mathbf{v}^\alpha$. Since there is no chemical reaction or other heat sources, the heat source term $\rho^\alpha \gamma^\alpha$ is also ignored.

The equations of energy Eq. (4.6) for each constituent are reduced to

$$\varphi^l \acute{\rho}^l (\frac{\partial \varepsilon^l}{\partial t} + u^l \frac{\partial \varepsilon^l}{\partial x}) = -\frac{\partial q^l}{\partial x} + \hat{\varepsilon}^l \tag{4.7}$$

$$\varphi^s \acute{\rho}^s \frac{\partial \varepsilon^s}{\partial t} = -\frac{\partial q^s}{\partial x} + \hat{\varepsilon}^s \tag{4.8}$$

$$\varphi^m \acute{\rho}^m \frac{\partial \varepsilon^m}{\partial t} = -\frac{\partial q^m}{\partial x} + \hat{\varepsilon}^m \tag{4.9}$$

Because of the phase transition, φ^l and φ^s should be dependent on both position and time. Thus Eqs. (4.7) and (4.8) should be nonlinear, whereas Eq. (4.9) is linear since φ^m is constant. Furthermore, if another solid additive is added into the system, we just need to include a linear energy equation with the form of Eq. (4.9), hence the nonlinearity of one-dimensional melting of PCM totally comes from the phase change process itself and the addition of additives does not increase the order of the system. Eqs. (4.3), (4.4), and (4.7) - (4.9) are the governing equations for the melting problems of PCM and PCM/metal foam composite. Nevertheless, problems can not be solved merely by those equations because some terms like the heat flux are in a general form and therefore we need to interpret them in terms of known quantities and field properties. Here we give our interpretation for the undefined terms and the relationship between some filed properties.

Constituential Heat Flux

In the mixture theory, it is assumed that a spatial point contains every constituentRay M Bowen 1976. Assuming **x** is an arbitrary spatial point in a continuous body that consists of a binary mixture (constituent α and constituent β), then α and β can coexist at **x** ($\mathbf{X}^{\alpha}$ and $\mathbf{X}^{\beta}$). In this study, we assumed that the temperatures of solid PCM and liquid PCM are the same, which means that there is no local heat transfer between $\mathbf{X}^{\alpha}$ and $\mathbf{X}^{\beta}$. However, $\mathbf{X}^{\alpha}$ and $\mathbf{X}^{\beta}$ are subjected to heat transfers from its surrounding αs and βs. For example, $\mathbf{X}^{\alpha}(\mathbf{x})$ would lose or gain heat from surrounding mixtures - both $\mathbf{X}^{\alpha}(\mathbf{x}+\Delta r)$ and $\mathbf{X}^{\beta}(\mathbf{x}+\Delta r)$, where $\Delta r \to 0$. As a result, the liquid PCM should revive heat flux from nearby liquid PCM, solid PCM, and metal foam. In this study, the temperature difference between solid PCM and liquid PCM is ignored. The reason is that if we assume a different temperature between liquid paraffin and solid paraffin, by solving the model proposed by this study, the temperature difference $|T^s - T^l|$ would have an order of 10^{-2}K at most, which is considered to be negligible. Accordingly, the constituential heat flux vector for liquid PCM is given by

$$q^l = -\varphi^l \left[\varphi^l k^l \frac{\partial T}{\partial x} + \varphi^s k^{ls} \frac{\partial T}{\partial x} + \varphi^m k^{lm} \lim_{h \to 0} \frac{T^m(x+h,t) - T(x,t)}{h} \right] \quad (4.10)$$

where T is the temperature of the PCM and $k^{\alpha\beta}$ (k^{ls} and k^{lm} in Eq. (4.10)) is the effective thermal conductivity between constituent α and β defined by

$$\frac{2}{k^{\alpha\beta}} = \frac{1}{k^{\alpha}} + \frac{1}{k^{\beta}} \tag{4.11}$$

For pure PCM melting, the term related to metal foam vanishes by making $\varphi^m = 0$ in Eq. (4.10). Inside the liquid region, we would have $\varphi^s = 0$. Similarity, q^s and q^m in Eq. (4.8) and Eq. (4.9) are defined by

$$q^s = -\varphi^s \left[\varphi^s k^s \frac{\partial T}{\partial x} + \varphi^l k^{ls} \frac{\partial T}{\partial x} + \varphi^m k^{sm} \lim_{h \to 0} \frac{T^m(x+h,t) - T(x,t)}{h} \right] \tag{4.12}$$

$$\begin{aligned} q^m = -\varphi^m \Bigg[& \varphi^m k^m \frac{\partial T^m}{\partial x} + \varphi^l k^{lm} \lim_{r \to 0} \frac{T(x+r,t) - T^m(x,t)}{r} \\ & + \varphi^s k^{sm} \lim_{r \to 0} \frac{T(x+r,t) - T^m(x,t)}{r} \Bigg] \end{aligned} \tag{4.13}$$

Local Energy Supply

For the energy source terms $\hat{\varepsilon}^m$, here we use the expression given by Costa (1992) that

$$\hat{\varepsilon}^m = h(T - T^m) \tag{4.14}$$

where h is a heat transfer coefficient related to local solid structure and local liquid velocity. Here we use the expression given by Dixon and Cresswell (1979):

$$h = a_{Pm} h^* \tag{4.15}$$

where a_{Pm} is the specific surface area. According to Calmidi and Mahajan (2000), the specific surface area for metal foam is

$$a_{Pm} = \frac{3\pi d_f}{{d_p}^2} \tag{4.16}$$

where d_f is the diameter of the fibre and d_p is pore size of the metal foam. Parameter h^* in Eq. (4.15) is given by

$$h^* = \frac{\mathrm{Nu}_{Pm} k^{ls}}{d_P} \tag{4.17}$$

Since local thermal non-equilibrium assumption is made, the local heat transfer coefficient h should not be reduced to 0 even for points where liquid velocity is zero. Following Wakao and Kaguei (1982), the Nusselt number from PCM to metal foam is given by

$$\mathrm{Nu}_{Pm} = 2 + 1.1 \mathrm{Pr}^{\frac{1}{3}} \mathrm{Re}_p^{0.6} \tag{4.18}$$

where Pr is the local Prandtl number and Re is the Reynolds number based on d_p. Such that the heat transfer coefficient would not vanish for pure solid region

However, the expression Eq. (4.14) is not suitable for $\hat{\varepsilon}^s$ and $\hat{\varepsilon}^l$ because a phase change process is involved between liquid PCM and solid PCM. Based on the expression given by Bowen (1980), if we ignore the momentum supply and kinetic energy from diffusion velocity, the local energy supply terms should follow the correlation:

$$\hat{\varepsilon}^l + \hat{\varepsilon}^s + \hat{\varepsilon}^m + \hat{\rho}^s \varepsilon^s + \hat{\rho}^l \varepsilon^l = 0 \tag{4.19}$$

Since we have assumed the temperatures of liquid PCM and solid PCM are the same, there should be no heat supply from temperature difference, i.e., $|T^s - T^l|$. Moreover, it is assumed that the heat supply from metal foam to liquid PCM and solid PCM is allocated linearly in associate with φ^s and φ^l. By substituting Eqs. (4.3)-(4.4) and Eq. (4.14) into Eq. (4.19), we have

$$\hat{\varepsilon}^l = \acute{\rho}^s \frac{\partial \varphi^l}{\partial t} \varepsilon^s - \frac{\varphi^l}{\varphi^s + \varphi^l} \hat{\varepsilon}^m \tag{4.20}$$

$$\hat{\varepsilon}^s = -\acute{\rho}^s \frac{\partial \varphi^l}{\partial t} \varepsilon^l - \frac{\varphi^s}{\varphi^s + \varphi^l} \hat{\varepsilon}^m \tag{4.21}$$

It should be highlighted that for pure PCM melting, $\hat{\varepsilon}^m = 0$ in Eqs. (4.20) and (4.21).

Relations of Field Properties

Considering the PCM could experience both solid-solid and solid-liquid phase transitions, by denoting the latent heat of the two processes with L^{ss} and L^{sl}, ignoring the work done by the PCM, the relationship between internal energy ε^{α} and the local temperature for liquid PCM, solid PCM and metal foam should be

$$\varepsilon^{l} = Cp^{l}T + L^{ss} + L^{sl} \tag{4.22}$$

$$\varepsilon^{s} = Cp^{s}T + \varphi^{s1-s2}L^{ss} \tag{4.23}$$

$$\varepsilon^{m} = Cp^{m}T^{m} \tag{4.24}$$

where Cp^{α} is the specific heat of constituent α, and φ^{s1-s2} is the proportion of $s2$ to the whole PCM during the solid-solid phase change from $s1$ to $s2$. With Eqs. (4.22)-(4.24), the temperature profile can be obtained by knowing the current internal energy densities. However, in the mushy zone, the temperature T should be evaluated by ε^{s} and ε^{l} together. We define the internal energy density of the PCM as

$$\varepsilon^{pa} = (\varphi^{l}\acute{\rho}^{l}\varepsilon^{l} + \varphi^{s}\acute{\rho}^{s}\varepsilon^{s})/(\varphi^{l}\acute{\rho}^{l} + \varphi^{s}\acute{\rho}^{s}) \tag{4.25}$$

and if Cp^l and Cp^s are assumed to be equal to an average value Cp^{pa}, we have

$$\varepsilon^{pa} = Cp^{pa}T + \frac{\varphi^s\varphi^{s1-s2} + \varphi^l}{\varphi^l + \varphi^s}L_{ss} + \frac{\varphi^l}{\varphi^l + \varphi^s}L_{sl} \tag{4.26}$$

4.1.3 Experiment Method

4.1.3.1 PCM and Metal Foam Materials

The PCM used in this study is a paraffin wax OP42E provided by Ruhr Tech Company, Hangzhou, China. The melting point of the paraffin is around 40°C by a preliminary test. Hence the latent heat and melting range of the paraffin were measured from 0 °C to 90 °C by using a differential scanning calorimeter (DSC, Mettler Toledo DSC3). Figure 4.2 shows the DSC curve of the paraffin with an empty line subtracted. The sample size for the DSC test is 8.00 mg and the heating rate is 1.5 °C/min. It is noticed that there exist three peaks. The first two peaks are ascribed to solid-solid phase transitions, and the third peak represents the solid-liquid phase change. Since the experiments was conducted under the room temperature T_∞ (24 °C - 26 °C), the first peak is ignored in the following calculations. By assuming the specific heat capacity of the paraffin is linearly dependent on the temperature, the baseline is interpolated by lining the beginning of DSC curve to its end. Here, the extrapolated onset peak temperatures T_{e1} and T_{e2} are supposed to be the starting point for phase transitions, which are intersections of the baseline

and the tangents of the left side of the peaks. T_{in}s are initial temperatures of each peak, which are determined by intersecting the DSC curve with a tangent parallel to the baseline. We assume that the finial temperature of the second peak coincide with T_{i3}, and assume the final temperatures of each peaks are the end point of phase transitions. The range of the solid-solid phase change (the second peak) is T_{e1} to T_{i3}, and the melting range is T_{e2} to T_f. The latent heat of the two peaks, L^{ss} and L^{sl} are evaluated by integrating the grey area in Figure.4.2 from T_∞ to T_{i3}, and from T_{i3} to T_f, respectively. Accordingly, φ^{s1-s2} in Eq. (4.25) is defined by

$$\varphi^{s1-s2} = \begin{cases} 0 & \varepsilon^{pa} < \varepsilon^{pa}_{T_{e1}} \\ \frac{\varepsilon^{pa}_{T_{e1}} - \varepsilon^{pa}}{\varepsilon^{pa}_{T_{e1}} - \varepsilon^{pa}_{T_{i3}}} & \varepsilon^{pa}_{T_{e1}} \leq \varepsilon^{pa} < \varepsilon^{pa}_{T_{i3}} \\ 1 & \varepsilon^{pa}_{T_{i3}} \leq \varepsilon^{pa} \end{cases} \tag{4.27}$$

and the liquid fraction φ^l is

$$\varphi^l = \begin{cases} 0 & \varepsilon^{pa} < \varepsilon^{pa}_{T_{e2}} \\ \frac{\acute{\rho}^s(\varepsilon^{pa}_{T_{e2}} - \varepsilon^{pa})(1-\varphi^m)}{\varepsilon^{pa}(\acute{\rho}^l - \acute{\rho}^s) - \acute{\rho}^l \varepsilon^{pa}_{T_f} + \acute{\rho}^s \varepsilon^{pa}_{T_{e2}}} & \varepsilon^{pa}_{T_{e2}} \leq \varepsilon^{pa} < \varepsilon^{pa}_{T_f} \\ 1 - \varphi^m & \varepsilon^{pa}_{T_f} \leq \varepsilon^{pa} \end{cases} \tag{4.28}$$

The thermophysical properties of the paraffin are given in Table 4.1. The heat capacity of the paraffin is measured by using sapphire method (Mettler Toledo

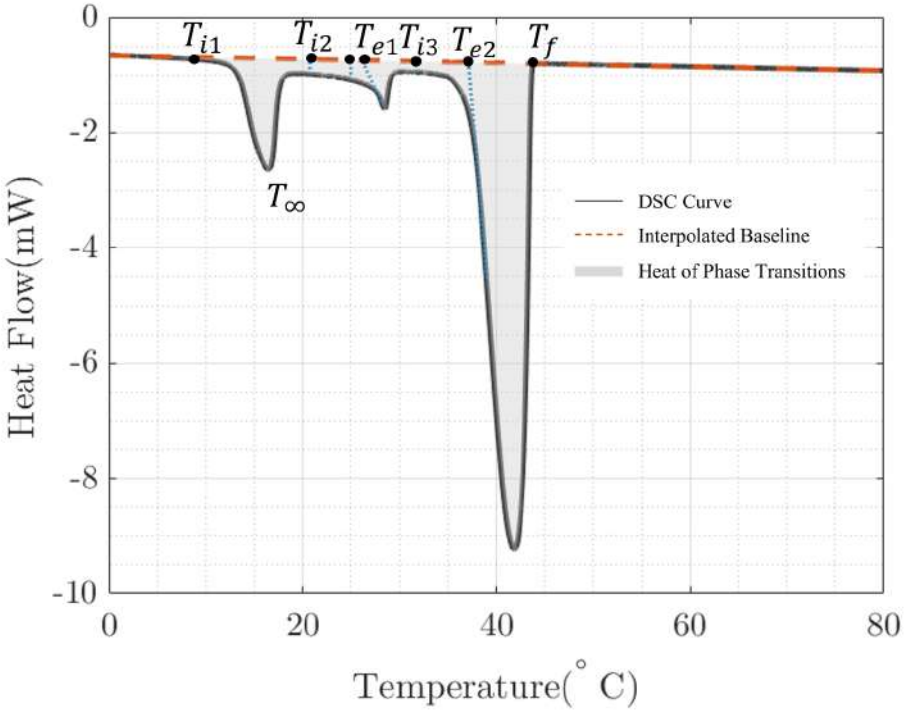

Figure 4.2: DSC curve of OP42E paraffin. (Sample size: 8.00 mg; heating rate: 1.5 °C/min.)

DSC3); solid and liquid densities of the paraffin are measured at 25°C and 80°C using a electronic densimeter (DH-300, DAHO); the thermal conductivity of solid paraffin and that of liquid paraffin are tested at 25°C and 80°C by hot wire method using a thermal conductivity meter (TC3000E, XIATECH).

In the PCM/metal foam composite experiment, two metal foams are used in this experiment: a 100 mm × 100mm × 10 mm nickel foam with 96% porosity and a a 100 mm × 100mm × 10 mm copper foam with 97% porosity. The properties related to the metal foams are shown in Table 5.1.

Table 4.1: Thermophysical properties of OP42E paraffin.

Properties	Value	Unit
Average heat capacity	2701	J/(kg·K)
Thermal conductivity of solid paraffin	0.26	W/(m·K)
Thermal conductivity of liquid paraffin	0.18	W/(m·K)
Specific latent heat of solid-solid phase change	12538	J/kg
Specific latent heat of solid-liquid phase change	176333	J/kg
True density of solid paraffin	913	kg/m^3
True density of liquid paraffin	784	kg/m^3
Onset temperature of the solid-solid phase change	26.1	°C
Final temperature of the solid-solid phase change	31.6	°C
Onset temperature of the solid-liquid phase change	37.1	°C
Final temperature of the solid-liquid phase change	43.8	°C

Table 4.2: Properties related to the metal foams.

Properties	Copper foam	Nickel foam	Unit
Specific heat capacity	385	440	J/(kg·K)
Thermal conductivity	401.0	90.7	W/(m·K)
True density	8960	8902	kg/m^3
Porosity	97%	96%	N/A
Pore size	6.38	4.00	mm
Fibre diameter	0.72	0.52	mm

4.1.3.2 Experiment Apparatus and Procedures

Figure 4.3 shows the experimental setup for the 1-dimensional melting problem. A 100 mm $\times$ 100 mm $\times$ 10 mm acrylic cavity was made to contain the PCM and PCM/ metal foam composites. Expanded polystyrene foam with a thickness of 30 mm was used for insulation materials, of which the thermal conductivity was tested to be 0.037 W/(m·K). The top of the cavity is covered with a copper plate. Two rows of 0.9 mm holes were drilled on the plate as shown in Figure 4.3 with an interval of 5 mm. The purpose of the holes was to let the fluid driven by the melting pass through the top boundary while keeping the velocity direction undisturbed. A water block connected to a hot water tank was attached on top of the copper plate to provide a constant temperature boundary of 70 °C. Five T-type thermocouples were placed with an interval of 20 mm as shown in Figure 4.3 to measure the temperature profile at the boundary (T_b), x=20 mm (T_1), x=40 mm (T_2), x=60 mm (T_3), and x=80 mm (T_4), respectively, based on the coordinate in Figure 4.1. Before experiment test, the thermocouples were connected to the data logger, and temperatures of each measuring points were confirmed to match the current room temperature. The temperature of the water in the water block was also confirmed to reach the setting temperature before attaching it to the copper plate, and silicone grease was used to eliminate the thermal resistance of air between the water block and the copper plate. Three groups of experiment were conducted: melting of pure

paraffin, melting of paraffin/nickel foam, and melting of paraffin/copper foam, and the temperature profiles were recorded in a duration of 2 hours.

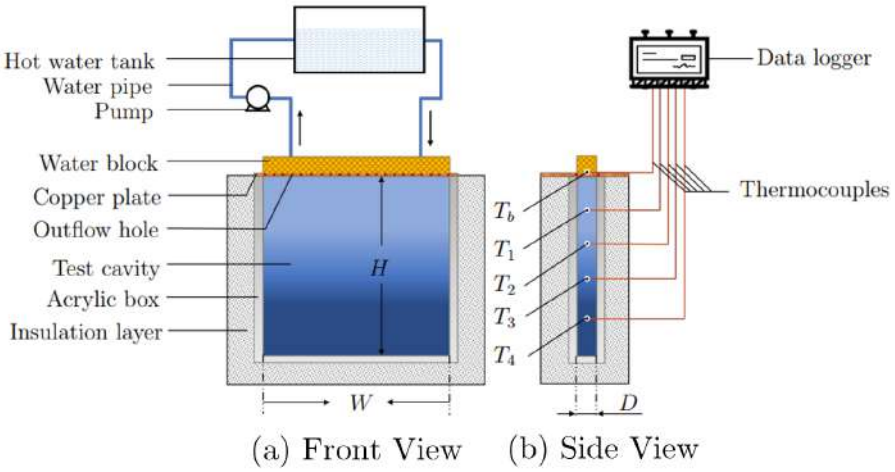

Figure 4.3: Schematic of the experimental setup.

4.1.4 Numerical Method

In this study, governing equations Eqs. (4.3), (4.4), and (4.7) - (4.9) were numerically solved using GNU Octave by finite difference method. An enthalpy method is used to avoid modeling of the moving boundary. Since Eqs. (4.7) and (4.8) are nonlinear, we froze the values of φ^αs at every time step to linearize the problem following the method given by Zikanov (Zikanov 2019). The idea is: making internal energy implicit in time and making volumetric fraction explicit in time. By doing this, at every time step, φ^αs and the quantities related to φ^αs including

u^l and $\partial\varphi^l/\partial t$ are constants. The values of ε^αs are iterated using Gauss-Seidel method until they meet the convergence criteria:

$$R = \frac{1}{N}\left[\sum_i^N (\varepsilon_i^{pa,n+1,I+1} - \varepsilon_i^{pa,n+1,I})^2\right]^{\frac{1}{2}} < 10^{-5} \tag{4.29}$$

where N is the number of grids; n is the current time step; I is the iteration times. The temperature filed should also be updated using Eqs. (4.22) - (4.25) in every iteration. After the values of ε^αs at time $n+1$ converged, φ^{s1-s2}, u^l, φ^l and φ^s are updated using Eqs. (4.5), (4.27) and (4.28), and the updated values were frozen and used for iterations at the next time step.

The optimized grid size Δx and time step Δt were determined by doing a grid sensitivity analysis based on the pure paraffin melting problem. First, the optimum grid size was found with a fixed time step. Then the optimum time step was determined with the optimum grid size found previously. Here the residual is defined by the L^2 norm of the temperature field between each refinement:

$$\text{Residual} = \left[\sum_i^N (T_i^{Ref} - T_i^{Ref+1})^2\right]^{\frac{1}{2}} \tag{4.30}$$

Figure 4.4 shows that the residual does not change significantly where the number of grids is over 160. As a result, Δx is determined as 5×10^{-4} m, and the value is used for the sensitivity analysis of Δt. Figure 4.5 indicates that the residual is

almost a constant when Δt is shorter than 6 s. In the numerical calculations, Δt is selected to be 1 s. A small time step is chosen here because the energy supply terms $\hat{\varepsilon}^{\alpha}$s are source terms for the energy equations, and the utilization of a small Δt could ease their stiffness, which could lead the iterations to divergence.

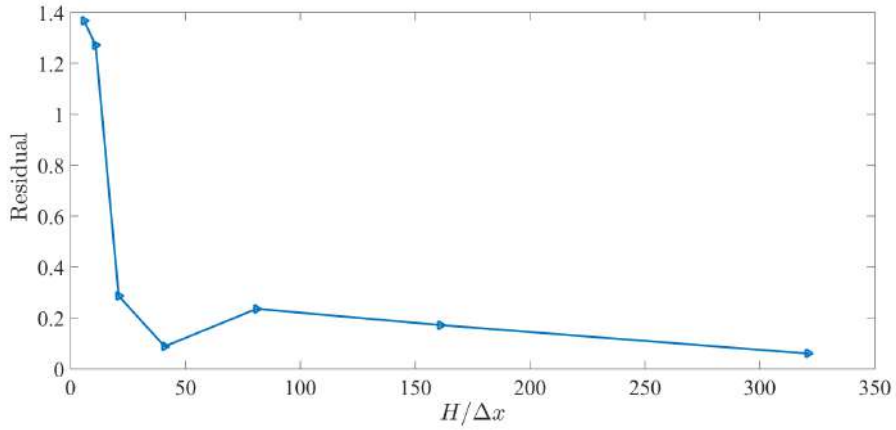

Figure 4.4: Relationship between residual and number of grids. (Time: 600 s; Δt: 4 s)

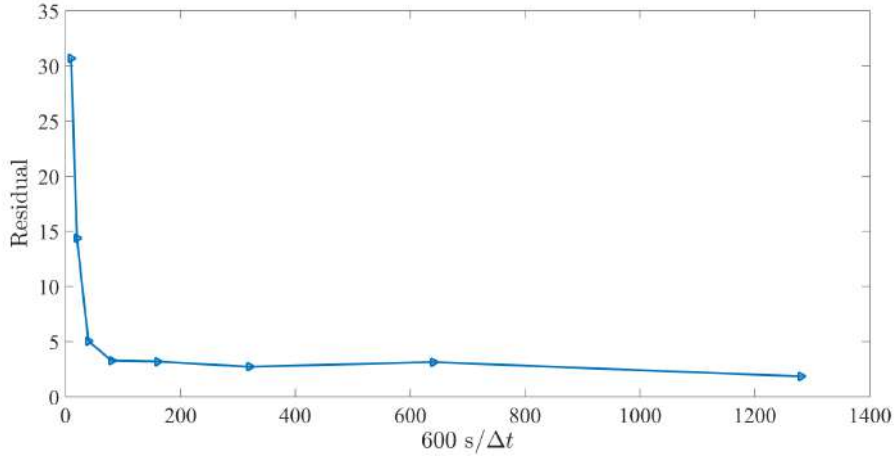

Figure 4.5: Relationship between residual and number of time steps in 600 s. (Δx: 5×10^{-4} m)

4.1.5 Model Validation

Comparison of Numerical Results and Experimental Data

The temperature profiles of paraffin temperature T that recorded in the experiments are compared to the numerical results to validate the modified mixture theory model.For pure paraffin melting, analytical solution given by Weber and Riemann (1919) is also introduced to validate the mixture theory model using individual density, individual thermal conductivity, and an averaging melting temperature 40.25°C. Figure 4.6 shows the temperatures of pure paraffin at each measuring points shown in Figure 4.3. At $x = 20$ mm, the numerical results shows a better match to the experiment data than the analytical solution, whereas at the other three positions, the temperature profiles obtained by analytical method and numerical method are very close. The maximum difference between experimental data and numerical results is 1.73 °C that occurs at $x = 20$ mm at $t = 1202$ s. The average difference between experimental data and numerical results is 0.58 °C, and the average relative deviation is 1.84% ($(T - T_{experiment})/T_{experiment}$, based on Celsius degree). Whereas for analytical results, the average relative deviation from the experimental data is 2.33%. For the paraffin/nickel foam composite melting, Figure 4.7 shows that the maximum difference between experimental data and numerical results is 2.36 °C that occurs at $x = 20$ mm at $t = 414$ s. The average difference from T_1 - T_4 is 0.75 °C and the average relative deviation is 2.32%. Fig-

ure 4.8 shows the temperature profile of paraffin/copper foam composite melting, and the maximum difference is 2.83 °C that occurs at $x = 20$ mm at $t = 6814$ s. The average difference from T_1 - T_4 is 1.01 °C and the average relative deviation is 2.83%. The comparison shows that the numerical results have a satisfying agreement with the experimental data, indicating the mixture theory model is suitable for solving one-dimensional pure PCM and PCM/metal foam composite phase change problems. Consequently, the validated model is used for further analysis in the following studies.

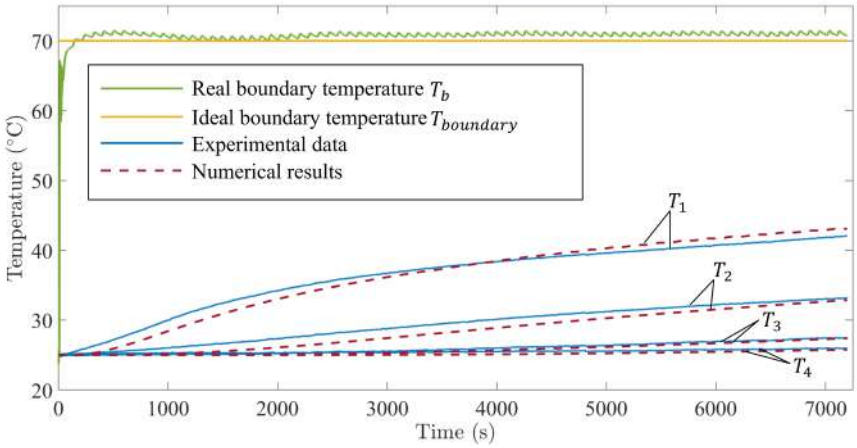

Figure 4.6: Temperature profile of pure paraffin melting.

4.1.5.1 The Influence of Liquid Velocity

Figure 4.9 shows the liquid velocity at $x = 0$ obtained by numerical calculation. The oscillations come from the mixed explicit-implicit numerical method, which is to linearize the problem. The velocity at every time step is frozen until the iteration

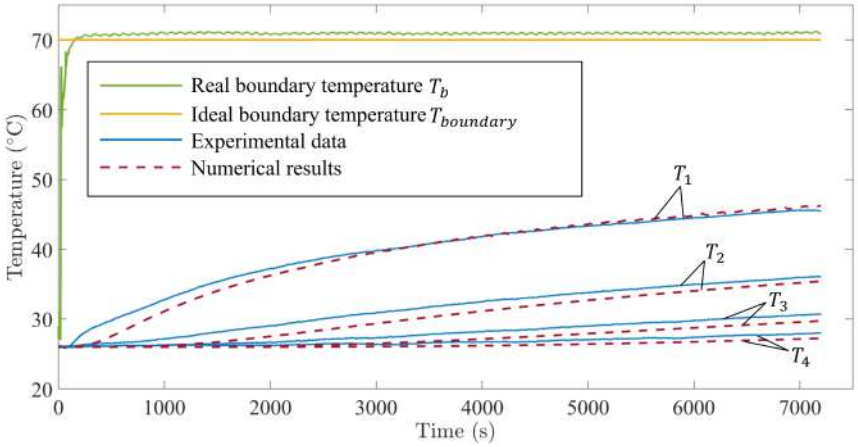

Figure 4.7: Temperature profile of paraffin/nickel foam composite melting.

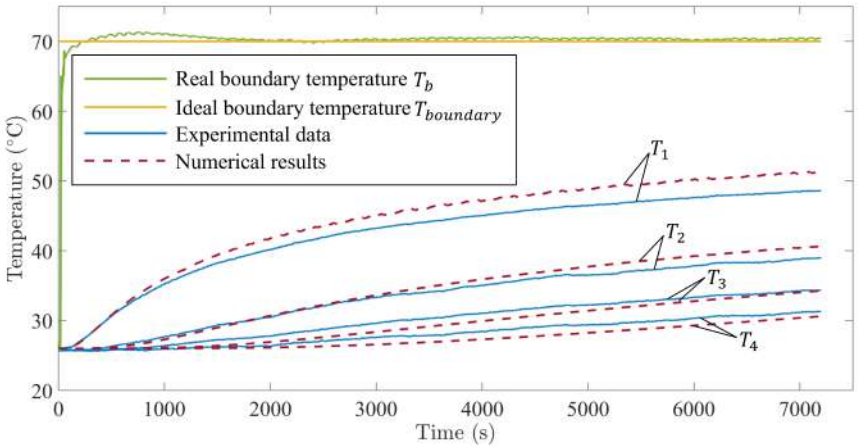

Figure 4.8: Temperature profile of paraffin/copper foam composite melting.

converges, and then the velocity is updated according to the converged internal energy densities. As a result, as moved to the next time step, the numerical liquid velocity sharply changes. A decreasing trend is observed for all the three melting problems. This tendency is because, initially a 70 °C temperature is exerted on the top boundary, where the heat flux injected into the paraffin is expected to the

highest. As the mushy zone moves to a deeper position of the cavity, the heat flux that the solid paraffin receives decreases because the temperature distribution inside the mushy zone is stable, and as a result the melting rate represented by the liquid velocity is becoming steady.

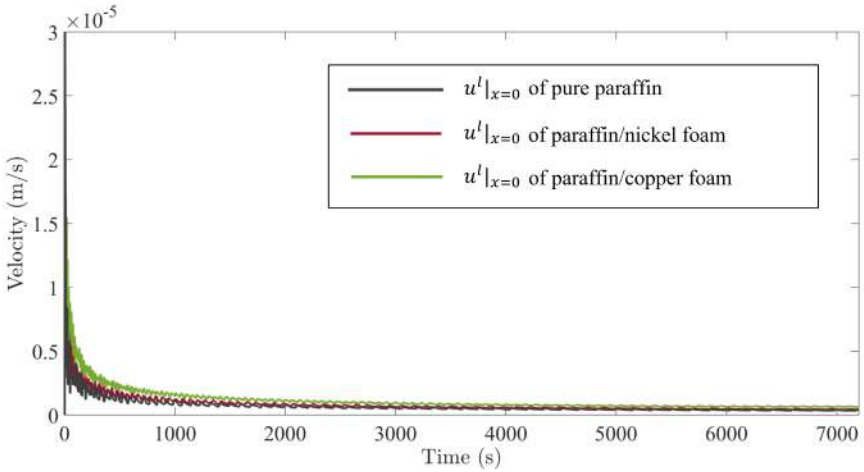

Figure 4.9: Velocity of liquid paraffin at the top boundary by numerical calculation.

Overall, $u^l|_{x=0}$ for the paraffin/copper foam composite is the highest, and that is the lowest for the pure paraffin. This result is as expected as the thermal conductivity of copper is higher than nickel while the conductivity of nickel is still much higher than pure paraffin. The average $u^l|_{x=0}$ after 2000 s for paraffin/copper foam, paraffin/nickel foam, and pure paraffin are 7.89×10^{-7} m/s, 5.67×10^{-7} m/s, and 4.67×10^{-7} m/s, respectively. Although the scale of the velocity is very small, those velocities are important in predicting the phase change processes. Figure 4.10, Figure 4.11, and Figure 4.12 show the temperatures of T_1 by the experiment,

by the original numerical results, and by the numerical results ignoring u^l throughout the computation, respectively. It is suggested that the numerical results without considering u^l gradually lose their credibility as the paraffin transfers from solid state to liquid state. The reasons can be ascribed to the following two aspects: (1) u^l describes the fluid flow out of top boundary that restrain the heat transfer from boundary; (2) u^l brings the liquid paraffin from low temperature area to high temperature area.

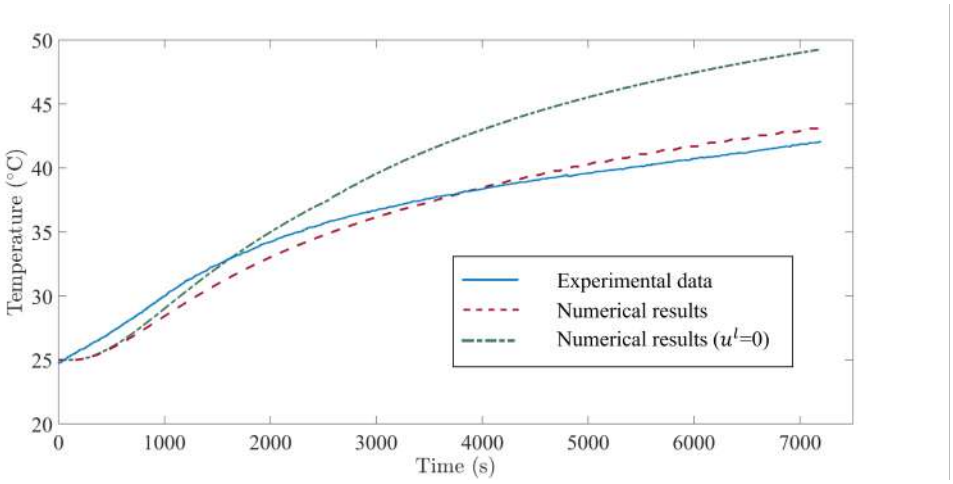

Figure 4.10: Experimental data and numerical results of T_1 of pure paraffin melting.

4.1.5.2 Local Thermal Non-equilibrium

Figure 4.13 shows the difference between T^m and T of paraffin/metal foam composite melting at $x = 0$ to 10 mm during the first 200 s. It is indicated that the local thermal non-equilibrium only exists around the heating side in the first few

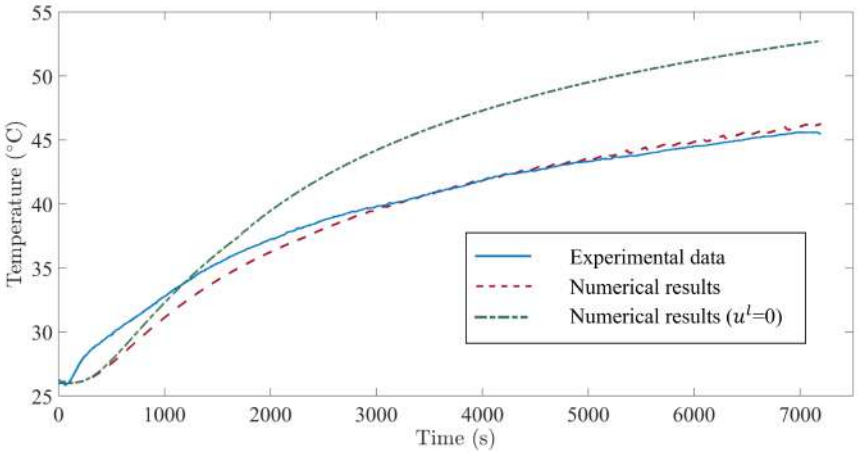

Figure 4.11: Experimental data and numerical results of T_1 of paraffin/nickel foam composite melting.

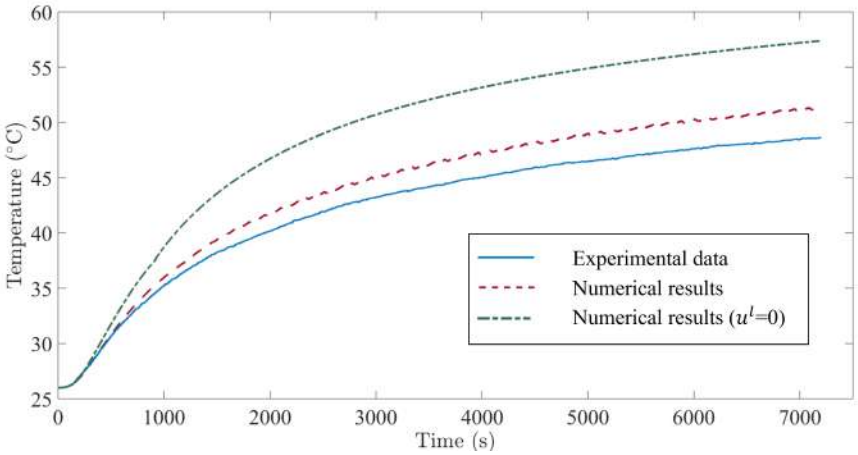

Figure 4.12: Experimental data and numerical results of T_1 of paraffin/copper foam composite melting.

minutes. The maximum temperature difference $|T - T^m|$ is observed at $x = 0$ at $t = 1$ s for both paraffin/nickel foam and paraffin/copper foam. The maximum temperature difference between paraffin and nickel is 12.41 °C, and the maximum temperature difference between paraffin and copper is 20.12 °C. However, as time

marches, the maximum temperature difference at a particular time step deviates from the top boundary. For example, for paraffin/copper foam the maximum differences between T^m and T at $t = 10$ s, $t = 20$ s, $t = 40$ s, and $t = 100$ s are located at $x = 1.5$ mm, $x = 2$ mm, $x = 2.5$ mm, and $x = 3$ mm, respectively. The reason for this phenomenon is that: T and T^m both approaches the boundary temperature $T_{boundary}$ around $x = 0$ so that the difference between T and T^m gradually decreases, but the thermal energy previously stored in the metal has not completely dispersed into the surrounding paraffin since the thermal conductivity of paraffin is much lower than that of metal materials. With the heat flux at the boundary becoming stable, the temperature difference between metal and paraffin gradually vanishes. The maximum $|T - T^m|$ decreases to an order of 10^{-1} as $t > 194$ s for paraffin/nickel foam, and the maximum $|T - T^m|$ decreases to an order of 10^{-1} as $t > 505$ s for paraffin/copper foam.

4.1.5.3 Evolution of the Mushy Zone

Figures 4.14, 4.15, and 4.16 show the evolution of φ^l along x in 7200 s. It is suggested that the thickness of mushy zone is increasing with time. If the mushy zone is defined by the area where $0 < \varphi^l < 1-\varphi^m$, the thickness of the mushy zone at 7200s for pure paraffin melting is 9.5 mm; for paraffin/nickel foam composite, the thickness is 12.0 mm; for paraffin/copper foam composite, the thickness is 16.5 mm. It is also observed directly from Figures 4.14 - 4.16 that the metal foams

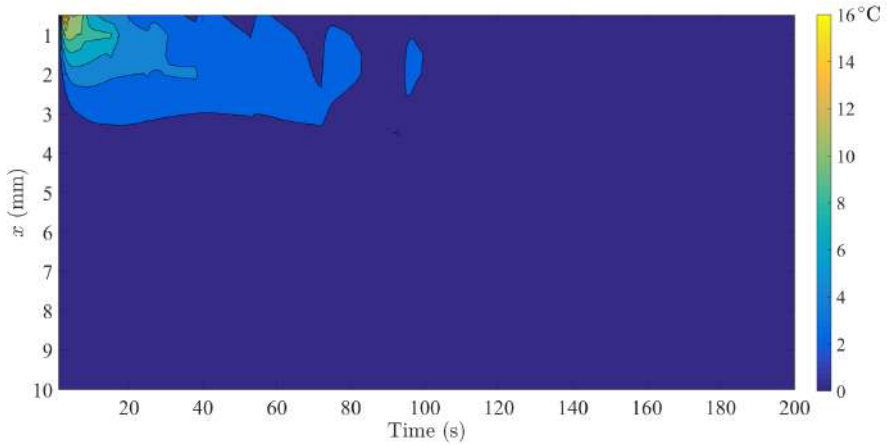

(a) Praffin/nickel foam

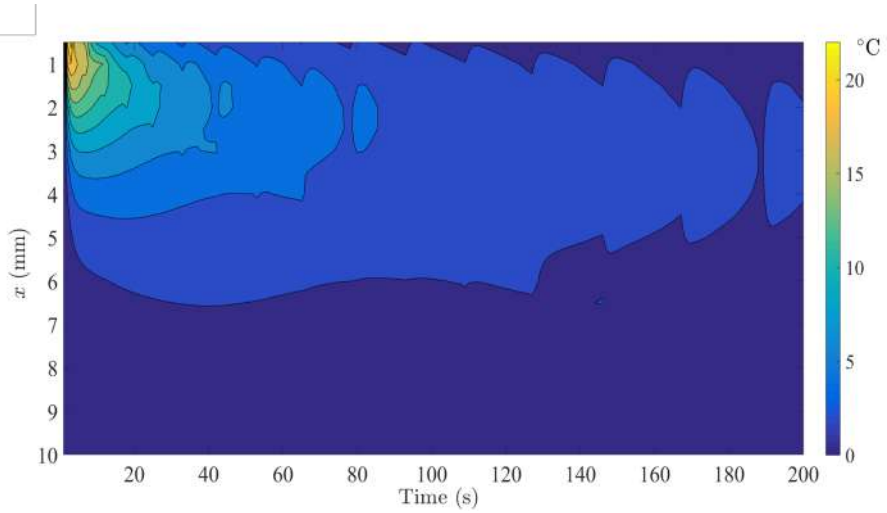

(b) Praffin/copper foam

Figure 4.13: Difference between T^m and T.

increase the melting speed of paraffin. The thicknesses of the liquid region at 7200s of pure paraffin melting, paraffin/nickel foam melting, paraffin/copper foam melting are 19 mm, 23 mm, and 32.5 mm, respectively. The melting rates for pure paraffin, paraffin/nickel foam, paraffin/copper foam are 10.84 kg/(m^2·h), 13.24 kg/(m^2·h), and 18.60 kg/(m^2·h), respectively.

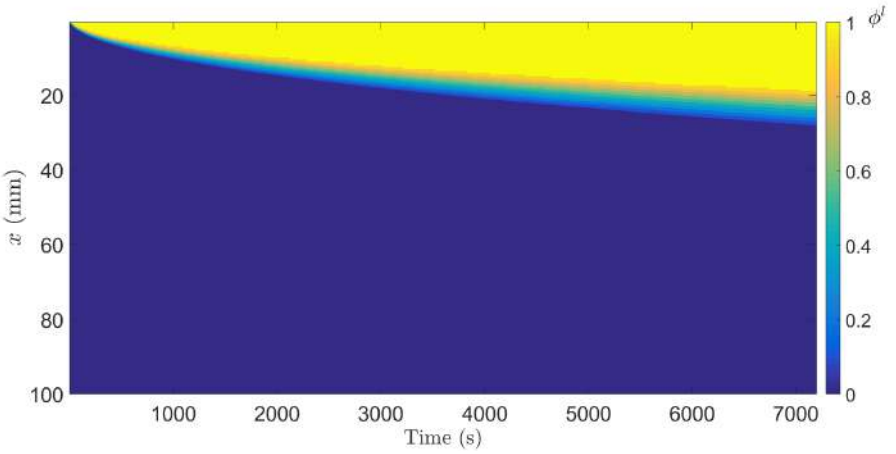

Figure 4.14: Evolution of φ^l along x for pure paraffin melting.

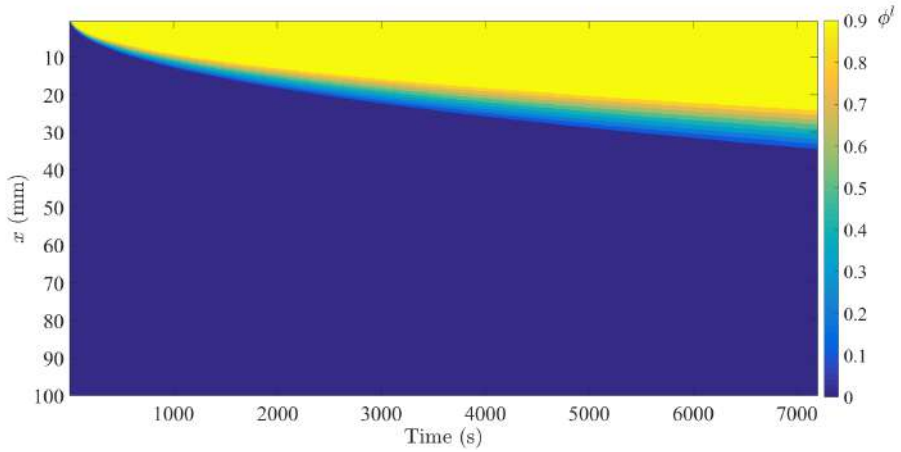

Figure 4.15: Evolution of φ^l along x for paraffin/nickel foam composite melting.

4.1.5.4 Error Analysis

The errors in this study consist of three parts: (1) the error from the mixture theory model; (2) the error from experiment equipment and measurement; (3) the error from numerical calculation.

The first type of error mainly comes from the assumptions made for the math-

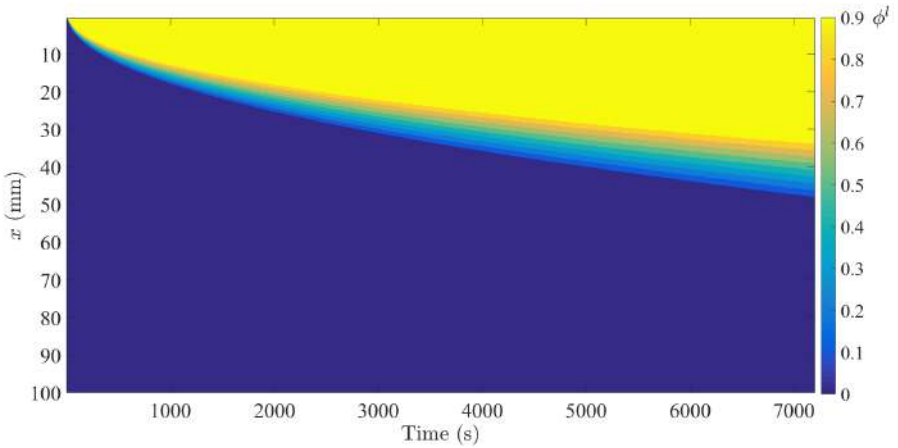

Figure 4.16: Evolution of φ^l along x for paraffin/copper foam composite melting.

ematical model. For example, the kinetic energy of velocity, of which the energy comes from the phase change, is ignored. Also, the specific heat capacity of paraffin is assumed to be a constant, whereas it is increasing with temperature as suggested by the baseline in Figure 4.2. As a result, the numerical prediction of temperatures should be lower than the real value at low temperature, and greater than the real value at high temperature, which is indicated in Figures 4.6 - 4.8. Also, the mixture theory has its intrinsic inaccuracy. On one hand, the mixture theory is still based on the classical continuum mechanics that assumes the materials are continuous while real materials are composed of discrete particles. One the other hand, the constituents can not be so well mixed that two constituents occupy the same spatial position as we proposed in the mixture theory.

The second type of error is partially from the inaccuracy of experiment equipment itself. For example, the error of T-type thermocouples is ± 0.1 °C. The error

from the DSC analysis also a big contribution in this study. As shown in Table 4.1, the thermal conductivity of paraffin is very small, which could cause a thermal lag in doing the DSC test. Although we used a small sample size, the smearing of the DSC curve is inevitable (McNaughton et al. 2003). Furthermore, in the study the temperature range of phase changes is determined by intersecting the baseline with the tangent of peaks, which is consistent with the method used by many other studies (W. Li et al. 2012; Rao and G. Zhang 2011; W. Wu et al. 2015). However, in fact the the melting point of paraffin can not be found accurately (Jin et al. 2014). Finally, as shown in Figure 4.2, the DSC curve does not go back to the baseline near the finial temperature T_{i3} of the second peak, implying that the second peak and the third peak is possible merged into each other. However, in this study we assumed the the two peaks are separate.

The third types of error include the intrinsic error of the finite difference method with an order of $O(\Delta t, \Delta x)$, and the errors from the linearization method used in the numerical calculation. In this study, we have done a grid sensitivity test to reduce the numerical errors. However, the numerical method we used in this study still cause a discontinuity of properties related to φ^l as shown in Figure 4.9.

4.2 A Mixture Model for Two-Dimensional PCM Melting

For the two-dimensional melting of PCMs, the effect of nature convection need to be considered. Thus we need to model the flow inside the porous structures. As discussed in Section 2.4, Darcy's equation as well as its extended forms is not theoretically rigorous to model the liquid flow in a porous structure with mass interactions. In this section, we propose a novel fluid model for the melting of pure PCMs that circumvents the usage of Darcy's equation. In Section 3.1.2, it is shown that the velocity field of the liquid fraction of PCM can be determined solely by using the balance of mass because the density variation is the exclusive source to drive the flow. Following the same idea, we may assume the fluid field inside the mushy zone can be determined by using the mass equation for two reasons: first, the velocity of the natural convection driven flow in the liquid region is small; second, the mushy zone is of a porous structure for which the inertia is usually neglected. As a result, the flow in the liquid region would not penetrate the mushy zone such that the flow in the mushy zone is irrelevant to the liquid in the liquid region. Following this idea, we can model the melting PCM for 3 different regions separately and couple the three equation sets using the enthalpy method. The basic assumptions for our two-dimensional model are: (1) the properties of the PCM are constants and assumed to be the same for liquid PCM and solid PCM except for

density; (2) there is no local thermal non-equilibrium throughout the phase change process; (3) the liquid is Newtonian; (4) the solid PCM is rigid and not moving; (5) the volume expansion is only considered in the mushy zone. The equation set for the solid region is

$$\rho^s \frac{\partial \varepsilon}{\partial t} = k\nabla^2 T \tag{4.31}$$

The equation set for the liquid region is

$$\frac{\partial u^l}{\partial x} + \frac{\partial v^l}{\partial y} = 0 \tag{4.32}$$

$$\rho^l(\frac{\partial u^l}{\partial t} + u^l\frac{\partial u^l}{\partial x} + v^l\frac{\partial u^l}{\partial y}) = -\frac{\partial P}{\partial x} + \mu(\frac{\partial^2 u^l}{\partial x^2} + \frac{\partial^2 u^l}{\partial y^2}) \tag{4.33}$$

$$\rho^l(\frac{\partial v^l}{\partial t} + u^l\frac{\partial v^l}{\partial x} + v^l\frac{\partial v^l}{\partial y}) = -\frac{\partial P}{\partial y} + \mu(\frac{\partial^2 v^l}{\partial x^2} + \frac{\partial^2 v^l}{\partial y^2}) + \acute{\beta}\rho^l g(T - T_f) \tag{4.34}$$

$$\rho^l(\frac{\partial \varepsilon}{\partial t} + u^l\frac{\partial \varepsilon}{\partial x} + v^l\frac{\partial \varepsilon}{\partial v}) = k\nabla^2 T \tag{4.35}$$

where $\acute{\beta}$ is the volumetric thermal expansion coefficient, and T_f is the offset temperature of the solid-liquid phase change indicating the right boundary temperature

of the liquid region. The equation set for the mushy zone is

$$(\acute{\rho^s} - \acute{\rho^l})\frac{\partial \varphi^l}{\partial t} = u^l \frac{\partial \varphi^l}{\partial x} + v^l \frac{\partial \varphi^l}{\partial y} \tag{4.36}$$

$$\frac{\mathbf{v}^l}{|\mathbf{v}^l|} = \frac{\nabla T}{|\nabla T|} \tag{4.37}$$

$$\rho(\frac{\partial \varepsilon}{\partial t} + u\frac{\partial \varepsilon}{\partial x} + v\frac{\partial \varepsilon}{\partial v}) = k\nabla^2 T \tag{4.38}$$

where u and v are the velocities of the mixture. The relation between volumetric fraction and internal energy density is consistent with Eq. (4.27) and Eq. (4.28). Figure 4.17 shows the pattern of melting of paraffin with a boundary temperature 70 °C at $t =_3 0$ min. Figure 4.18 shows the volumetric fraction of liquid paraffin at t=30min with boundary temperature 70 °C at $t = 30$ min. By comparing the two figures, it is shown that the two-dimensional mixture model provides a satisfying result to predict the real situation. Figure 4.19 shows the stream function of the paraffin $t = 30$ min. It is shown that the liquid paraffin is circulating inside the liquid region and does not penetrate into the mushy zone.

Still this model is for pure PCM melting, and one can add another rigid solid constituent in the model for PCM composites for local thermal equilibrium situa-

Figure 4.17: Pattern of the melting of paraffin at t=30min

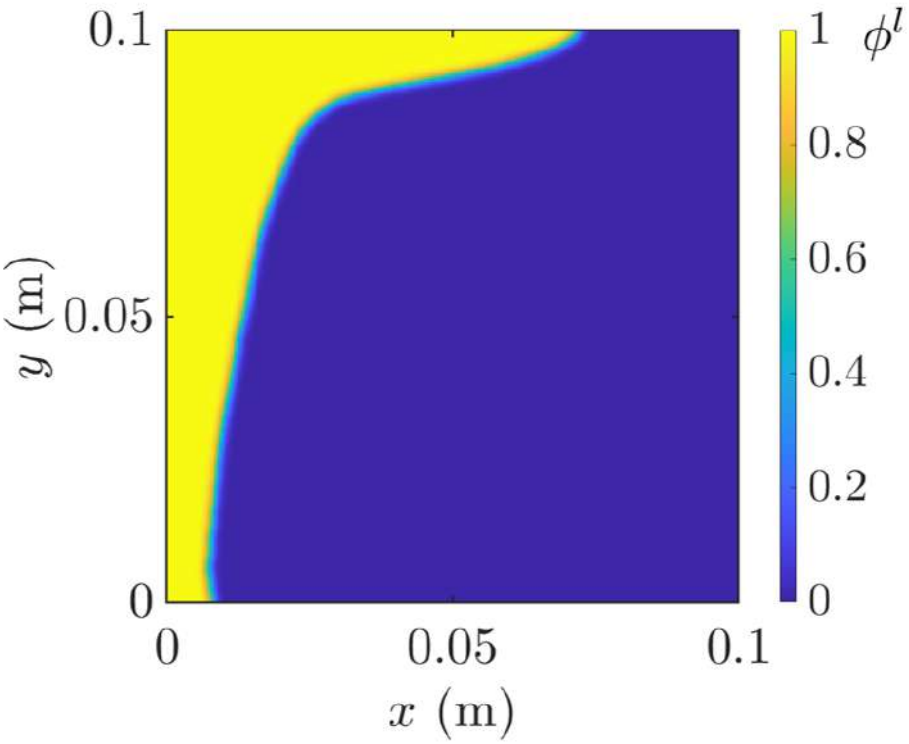

Figure 4.18: Volumetric fraction of liquid paraffin at t=30min

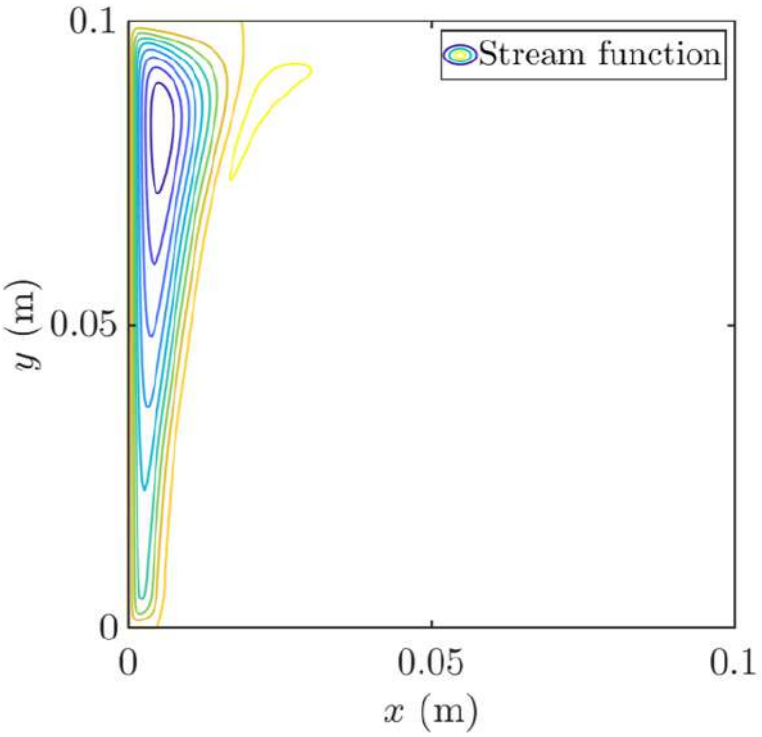

Figure 4.19: Stream function of paraffin at t=30min

tions and the addition of a stable solid does not increase the order of the problem. However, for local thermal non-equilibrium situations, one should be careful because one still need to model the flow in the liquid region using Darcy's equation and its extended forms while that for local thermal non-equilibrium situations is yet to be developed.

Chapter 5

Modification of the Energy Equation

In Chapter 2, we show the model for pure PCMs and PCM composites. However, there are some unignorable problems regarding the energy equations in the mixture theory based model: first, the numerical data seemingly overestimate the heat transfer performance of paraffin/metal foam composites; second, only local thermal non-equilibrium situation is considered in the model.However sometimes a local thermal equilibrium is preferred for saving the numerical resources; 3. the model does not consider the influence of specif structures of the mixture.

In this chapter, we propose a new heat conduction model based on the energy equations of the mixture theory, which is valid for both local thermal equilibrium and local thermal non-equilibrium situations. Mixture structures are considered in the model by introducing the effective volumetric fraction which is defined as the volumetric fraction that is continuous along the heat flow direction. For the

local thermal equilibrium situations, we give a new expression for the effective thermal conductivity of the mixture. For the local thermal non-equilibrium situations, revised definitions of heat flux terms and local thermal interactions terms are proposed to illustrate the heat transfers between each constituent. Four mixture structures are evaluated in this research, which can serve as analogies to different materials such as porous materials and nanoparticle-embedded materials, and the related heat transfer problems are solved by two methods: 1. using the classical heat equation and analyzing every constituent individually, which represents the real situations; 2. treating the mixture as a whole and applying our revised mixture model. By comparing the numerical results by the two methods, it is shown that the mixture theory can provide satisfying predictions to the real situations for both local thermal equilibrium and local thermal non-equilibrium 2 situations, even if the mixture structures do not strictly follow the assumptions of the mixture theory.

5.1 Method

5.1.1 Balance of Energy in the Mixture Theory

For a static mixture, the constituential velocity of constituents are 0, and as a result the stress term can be ignored. Further, if there is no other heat source like radiation

or chemical reaction, the constituential energy equation Eq. (5.14) is reduced to

$$\rho^{\alpha}\frac{\partial \varepsilon^{\alpha}}{\partial t} = -\nabla \cdot \mathbf{q}^{\alpha} + \hat{\varepsilon}^{\alpha} \tag{5.1}$$

Specifically, for a 2-constituent mixture (α and β), since a spatial point consists of α and β at the same time, constituent α should receive thermal energy by heat conduction from both surrounding α and β, and the amount of energy from the two sources should be related to the volumetric fraction of each constituent. If we use the same expression in Eq. (4.14) for the thermal interaction term, and rewrite the apparent density to the product of true density and volumetric fraction, Eq. (5.1) becomes

$$\begin{aligned}\varphi^{\alpha}\acute{\rho}^{\alpha}\frac{\partial \varepsilon^{\alpha}}{\partial t} &= \varphi^{\alpha}\nabla \cdot (\varphi^{\alpha}k^{\alpha}\nabla T^{\alpha} + \varphi^{\beta}k_m \lim_{r\to 0}\frac{T^{\beta}(x_i + r, t) - T^{\alpha}(x_i, t)}{r}\mathbf{e}_i \\ &\quad + h(T^{\beta} - T^{\alpha}) \qquad (5.2)\\ \varphi^{\beta}\acute{\rho}^{\beta}\frac{\partial \varepsilon^{\beta}}{\partial t} &= \varphi^{\beta}\nabla \cdot (\varphi^{\alpha}k_m \lim_{r\to 0}\frac{T^{\alpha}(x_i + r, t) - T^{\beta}(x_i, t)}{r}\mathbf{e}_i + \varphi^{\beta}k^{\beta}\nabla T^{\beta} \\ &\quad + h(T^{\alpha} - T^{\beta}) \qquad (5.3)\end{aligned}$$

where x_i is the index notation of the Cartesian coordinate and $\mathbf{e}_i$ is the according unit vector, which follows the summation rule; k_m is the average thermal conduc-

tivity defined by

$$k_m = \frac{k^\alpha + k^\beta}{2} \tag{5.4}$$

Eq. (5.2) and Eq. (5.3) suggest that for the heat conduction of constituent α with a volumetric fraction φ^α, it is receiving thermal energy from the heat conduction between α and α with a proportion $\varphi^\alpha\varphi^\alpha$ (if there is no mass exchange between α and β), the heat conduction between α and β with a proportion $\varphi^\alpha\varphi^\beta$, and the local thermal interaction between α and β. If a mixture is well-mixed which means that the heat transfer coefficient h becomes sufficiently large, the local temperature difference $|T^\beta - T^\alpha|$ is trivial and it is reasonable to assume $T^\alpha = T^\beta = T$. By adding up Eq. (5.2) and Eq. (5.3), for a saturated mixture without mass exchange that $\varphi^\alpha + \varphi^\beta = 1$, by assuming the true densities of the 2 constituents are constants, we get

$$\rho\frac{\partial \varepsilon_I}{\partial t} = \nabla \cdot [(\varphi^\alpha k^\alpha + \varphi^\beta k^\beta)\nabla T] \tag{5.5}$$

where ρ is the density of the mixture given by and ε_I is the inner part of the internal energy density given by

$$\varepsilon_I = \frac{1}{\rho}(\rho^\alpha \varepsilon^\alpha + \rho^\beta \varepsilon^\beta) \tag{5.6}$$

For a static mixture, the kinetic energy from the diffusion velocity can be ignored, such that ε_I is identical to the internal energy density of the whole mixture ε. Eq. (5.5) indicates that the effective heat transfer coefficient for a mixture with local thermal equilibrium is exactly the weighted mean of the thermal conductivities of the 2 constituents, and this conclusion can be extended to a mixture containing more than 2 constituents. However, one can find this conclusion does not match the results reported by many studies especially for nano-materials (Ren et al. 2005; Naghdbishi et al. 2020; Choi and Eastman 1995; Sheikholeslami et al. 2019). This is because though Eqs. (5.2), (5.3) and (5.5) are derived by assuming both two constituents are always continuous, however, although nanoparticle-embedded mixtures can be homogeneous with local thermal equilibrium, the nanoparticles are discrete instead of continuous. Therefore Eq. (5.2) and Eq. (5.3) are not applicable and as a result Eq. (5.5) is not suitable for describing heat conduction of a mixture involving discontinuous constituents. Hence, Eqs. (5.2) and (5.3) need to be modified based on the structure of the mixture so that they can be more practicable.

5.1.2 Structures of a Mixture

Carson et al. (2005) suggested that the structures of porous materials can be divided into internal porosity materials and external porosity materials based on

which constituent the major heat flow is passing through. Following this idea, 4 types of heat transfer unit are defined to represent the different structures of mixtures as shown in Figure 5.1. Each unit is a square shape consists of 2 constituents and the volume ratio is 2:8. Suppose the side length of the square is a non-dimensional value 1, for Type 1 and Type 2 units, the breadth of the minor constituents is expected to be 0.2; for Type 3 unit, the width of the beam of the cross is chosen to be 0.1, and a lump is made in the center to assure the volumetric fraction of the minor constituent is exactly 0.2; for Type 4 unit, the minor constituent is of a square form and the side length is $\sqrt{5}/5$. These mixture structures may represent some actual mixtures. For example, Type 3 unit may represent the unit structure of metal-foam-embedded materials, and Type 4 unit may represent the unit structure of nanoparticle-embedded materials. Now consider a 2-dimensional heat conduction problem shown in Figure 5.2, a constant temperature is exerted on the left boundary of a 0.1 m$\times$0.1 m cavity, while the other 3 boundaries are insulated. The cavity is filled with one type of the heat transfer units shown in Figure 5.1. The number of heat transfer units along x_1 direction is m, and therefore the total number of the units in the cavity is m^2. By prescribing the unit type and m, the overall structure in the cavity can be determined and therefore the evolution of the temperature filed can be easily obtained by a finite difference method.

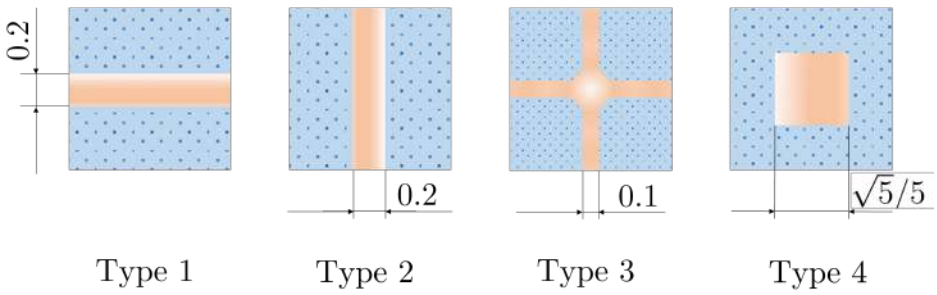

Figure 5.1: 4 different structures of a 2-constituent mixture. The volumetric fraction of the minor constituent (bronze in color) is 0.2.

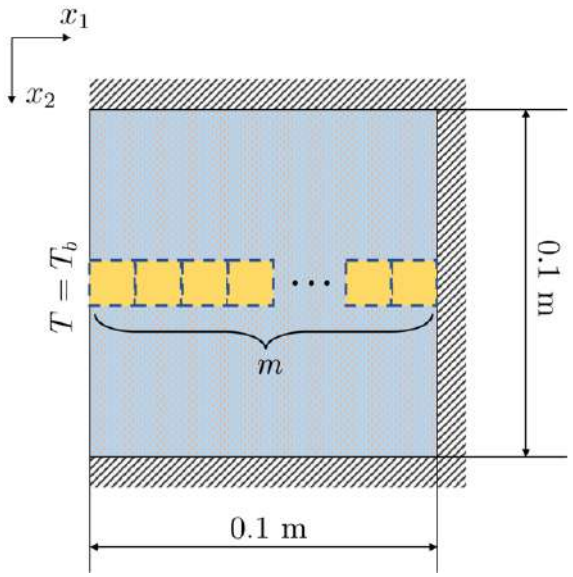

Figure 5.2: Schematic of a 2 dimensional heat conduction problem in a square cavity. The yellow squares represents the heat transfer units in Figure 5.1

.

5.1.3 Numerical Result of Temperature Profiles

Before solving the heat conduction problem, the 2 constituents should first be specified. Here, we assume the major constituent is OP42E paraffin and the minor

constituent is nickel. The boundary temperature is chosen to be $50°$C. It should be noticed that paraffin could also suffer phase change processes, however this physical phenomenon is irrelevant to the purpose of this section, and as a result, the latent heat of the phase changes is ignored such that the internal energy densities of each constituent is the product of its specific heat and temperature. The thermophysical properties of the 2 materials are given in Table 4.1 and 5.1. By assuming the properties of the 2 constituents are constants, the 2-dimensional heat conduction equation and its according finite difference equation in explicit form is given by

$$\acute{\rho}Cp\frac{\partial T}{\partial t} = k(\frac{\partial^2 T}{\partial {x_1}^2} + \frac{\partial^2 T}{\partial {x_2}^2}) \tag{5.7}$$

$$\acute{\rho}Cp\frac{T_{l,j}^{n+1} - T_{l,j}^{n}}{\Delta t} = k(\frac{T_{l+1,j}^{n} - 2T_{l,j}^{n} + T_{l-1,j}^{n}}{\Delta {x_1}^2} + \frac{T_{l,j+1}^{n} - 2T_{l,j}^{n} + T_{l,j-1}^{n}}{\Delta {x_2}^2}) \tag{5.8}$$

where n is the time layer, Δt is the time step, Δx_1 and Δx_2 are grid sizes, and i and j are grid number along x_1 and x_2 direction. In this stage, heat conduction problems of the 4 structures shown in Figure 5.1 with m=4, 8, 16, 32 are numerically solved with a uniform initial temperature $T_{initial} = 0°$C. For convenience, the gird sizes in x_1 direction and x_2 direction are set to be the same that $\Delta x = \Delta x_1 = \Delta x_2$. Additionally, since the thermal conductivity difference between paraffin and nickel is considerable ($k^{ni}/k^{pa} = 349$), it would lead to an abundant waste of computation resources if a uniform time step Δt is used.

Therefore, we utilize different time step for nickel and paraffin in Eq. (5.8) that

$$\Delta t^{pa} = 200\Delta t^{ni} \tag{5.9}$$

Grid sensitivity tests are conducted for each problem separately to ensure the credibility of the numerical results. The optimized grid sizes and time steps are shown in the appendix. Figures 5.16-5.19 show the temperature distributions of the cavity filled by Type 1-4 heat transfer units at 1000s, respectively. It is suggested that although all the cavities possess 20% nickel, their temperature profiles are dissimilar. The effective thermal conductivities of the four units from high to low are Type 1, Type 3, Type 4, and Type 2. As expected, it is shown that the cavities filled with continuous units Type 1 and Type 3 exhibit a much higher heat transfer efficiency than those filled with discontinuous units Type 2 and Type 4. Nevertheless, it is noticed that the difference between the heat transfer performances between Type 1 and Type 3 is still significant especially with a big m by comparing the temperature profiles Figure 5.6 and Figure 5.14. This is because, as m increases, the temperature distribution along x_2 direction is homogenizing and the two-dimensional problems are reducing to one-dimensional problems, and as a result the heat transfer enhancement effect of the nickel in x_2 direction becomes negligible. Therefore, the volumetric fraction in the right hand side of Eq. (5.2) and Eq. (5.3) should first be equivalized before applying to a certain mixture struc-

ture.

5.1.4 Modified Heat Transfer Equation

Local thermal equilibrium

As suggested by Figures 5.16-5.19, the heated-from-side heat conduction problems are losing their two-dimensionality as the number of heat transfer units increases, which implies that the local temperature difference between the major and minor constituents would become inconsequential. It can be imagined that if the number of units is sufficiently large, the temperatures of the two constituents would coincide at the same position. Therefore, the key point for the local thermal equilibrium problems is to determine the effective thermal conductivities for different structured mixtures. For convenience, from now on we use "Type-1 mixture" to represent the mixture formed by Type 1 units, etc. For Type-1 mixtures involving 2 constituents, each constituent is always continuous along the direction along the heat flux which fulfils the assumption for deriving Eq. (5.5), and thus the effective thermal conductivity should equal the weighted mean given by

$$k_{wm} = \varphi^{\alpha} k^{\alpha} + \varphi^{\beta} k^{\beta} \tag{5.10}$$

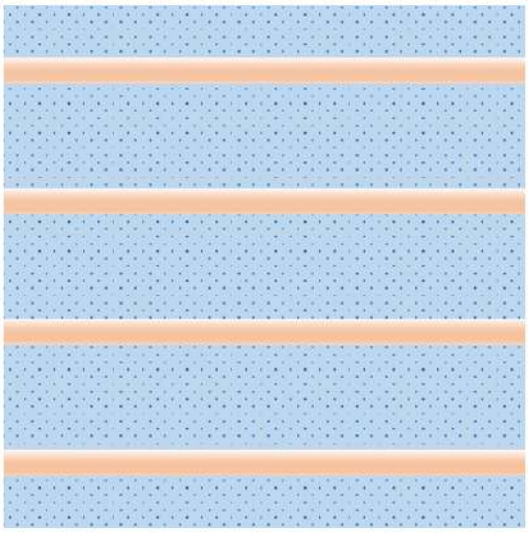

(a)

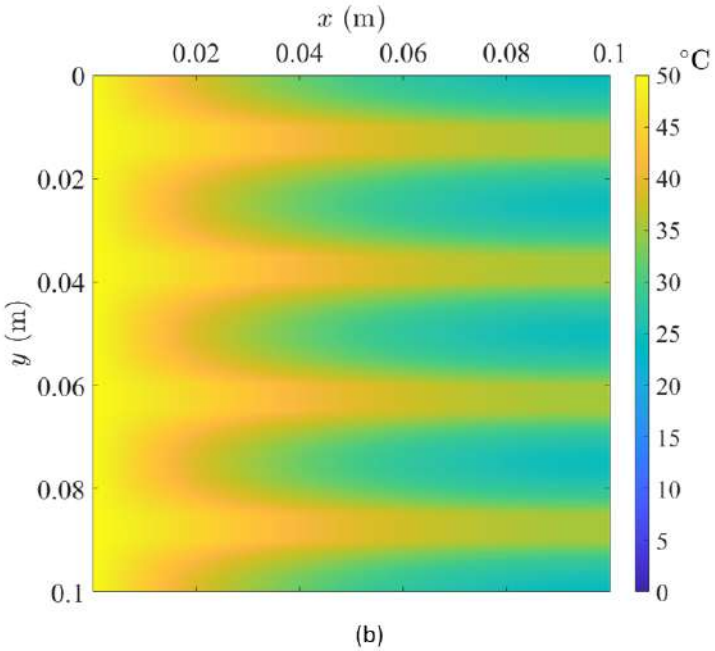

(b)

Figure 5.3: The cavity with Type 1 units when $m = 4$. (a) Mixture structure. (b) The temperature distribution at $t = 1000$s.

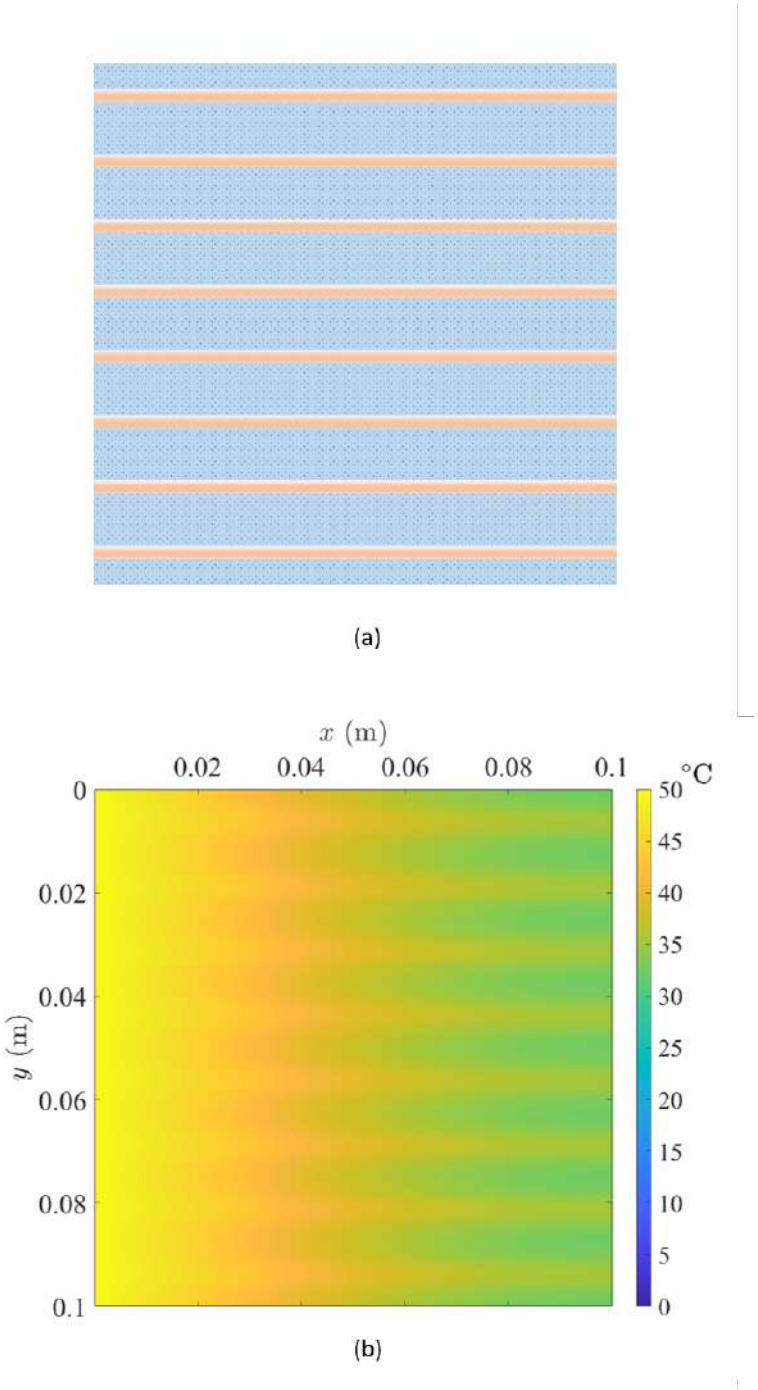

Figure 5.4: The cavity with Type 1 units when $m = 8$. (a) Mixture structure. (b) The temperature distribution at $t = 1000$s.

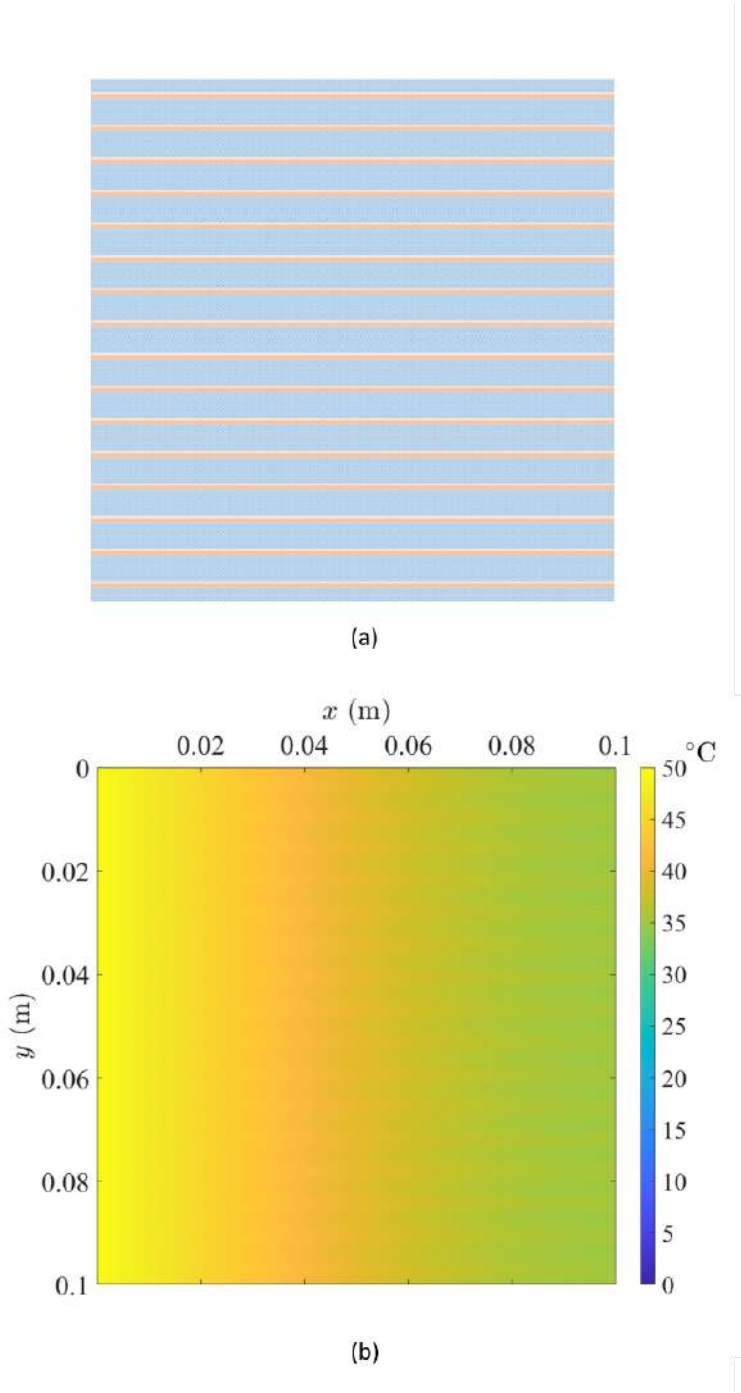

Figure 5.5: The cavity with Type 1 units when $m = 16$. (a) Mixture structure. (b) The temperature distribution at $t = 1000$s.

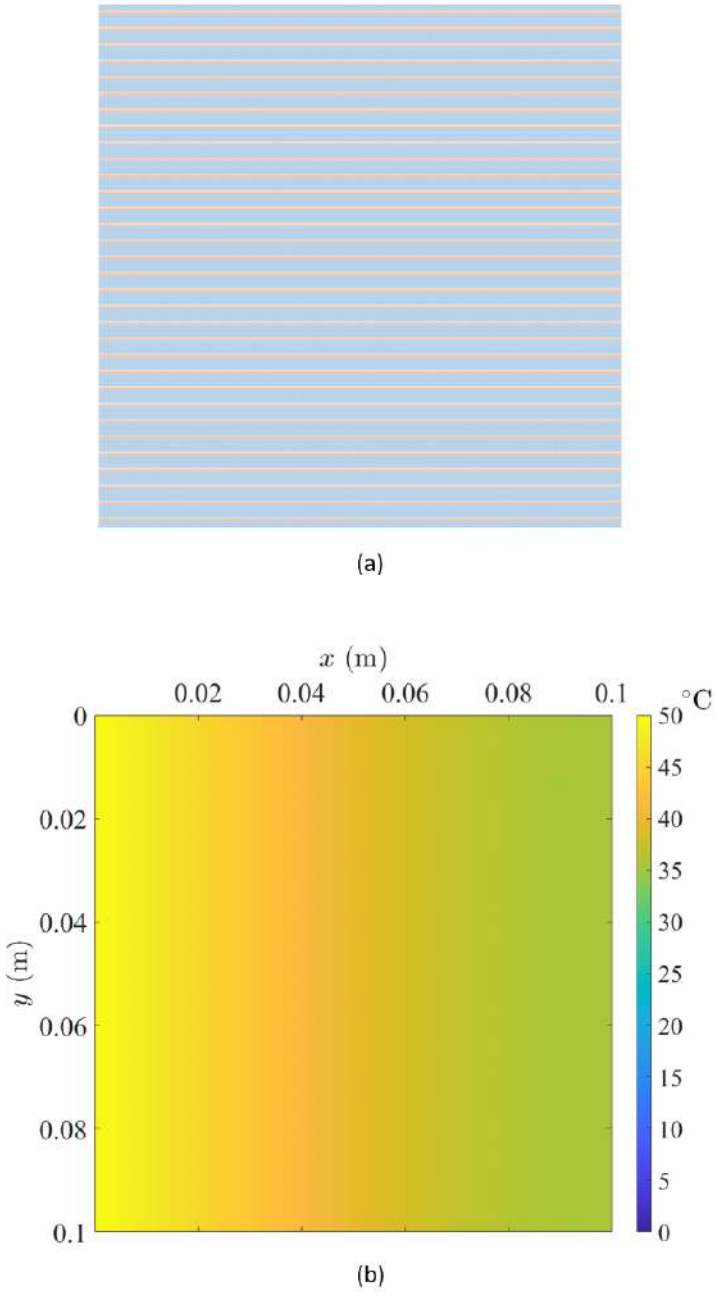

Figure 5.6: The cavity with Type 1 units when $m = 32$. (a) Mixture structure. (b) The temperature distribution at $t = 1000$s.

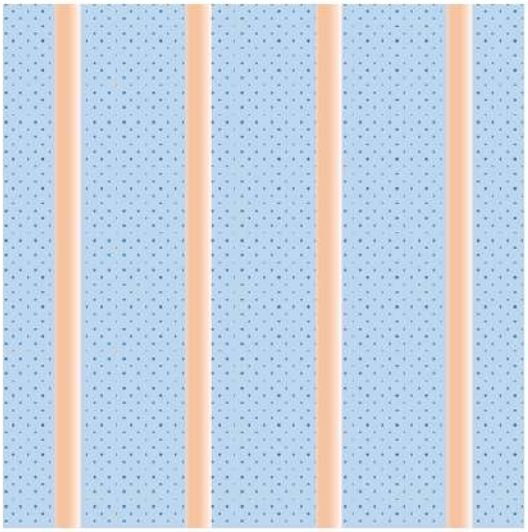

(a)

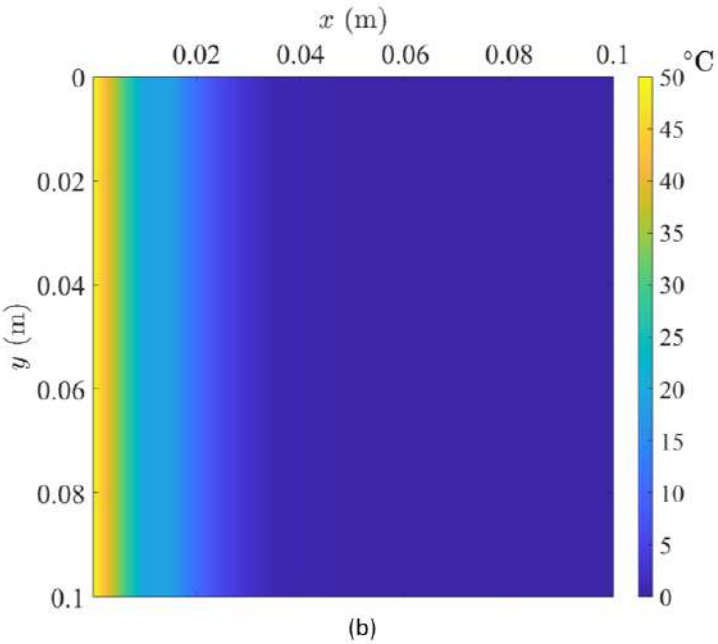

(b)

Figure 5.7: The cavity with Type 2 units when $m = 4$. (a) Mixture structure. (b) The temperature distribution at $t = 1000$s.

For Type-2 mixtures, the heat transfer problems can be simplified to one-dimensional heat flow traveling through two types of thermal resistances, for which the effective thermal conductivity is the harmonic mean that

$$\frac{1}{k_{hm}} = \frac{\varphi^{\alpha}}{k^{\alpha}} + \frac{\varphi^{\beta}}{k^{\beta}} \tag{5.11}$$

Figures 5.11-5.14 show that the heat transfer performance of Type-3 mixtures is in the middle between Type-1 mixtures and Type-2 mixtures. As indicated in section 5.1.2, the heat transfer rate of Type-3 mixtures is mainly dominated by the 10% minor constituent while the contribution from the rest of the 10% is little. If we decouple the cross of the Type 3 unit according to the orientations of the minor constituent, it is a combination of the part of minor constituent that is parallel to the heat flow direction and the rest is discontinuous along the heat flow direction. If we further extend this conclusion, the effective heat transfer coefficient for any saturated mixture is given by

$$k_{e,i} = \varphi^{\alpha}_{e,i} k^{\alpha} + (1 - \varphi^{\alpha}_{e,i} - \varphi^{\beta}_{e,i})^2 \frac{k^{\alpha} k^{\beta}}{(\varphi^{\alpha} - \varphi^{\alpha}_{e,i}) k^{\beta} + (\varphi^{\beta} - \varphi^{\beta}_{e,i}) k^{\alpha}} + \varphi^{\beta}_{e,i} k^{\beta} \tag{5.12}$$

where $\varphi^{\alpha}_{e,i}$ is the volumetric fraction of the continuous part of constituent α in x_i direction, and from now on we would call this quantity the effective volumetric

fraction for convenience. The is in Eq. (5.12) arises because the mixtures may not be isotropic and the heat flows can travel in different directions, and therefore the effective thermal conductivity should be evaluated in different directions if needed. It is noticed that Eq. (5.12) is a general form to estimate the effective thermal conductivity of a two-constituent mixture. For example, for Type-1 mixtures, both minor constituent and major constituent are continuous along the heat flow direction and their effective volumetric fractions are identical to their actual volumetric fractions. By substituting $\phi_e^\alpha = \phi^\alpha$ and $\phi_e^\beta = \phi^\beta$ into Eq. (5.12), it would reduce to Eq. (5.10) such that $k_e = k_{wm}$. For Type-2 mixtures, none of the two constituents are continuous along the heat flow direction, and thus $\phi_e^\alpha = \phi_e^\beta = 0$. Accordingly, Eq. (5.12) is reduced to Eq.(5.12) that $k_e = k_{hm}$. For Type-3 mixtures, the effective volumetric fraction of the minor constituent is not simply 0.1 because the lump in the center of the cross needd to be considered (Bhattacharya et al. 2002). Figure 5.20(a) shows the heat flux field as well as the temperature field of a lump in Type-3 mixture when m=4. It is suggested that when the heat flow comes into the lump, some heat deviates from the mainstream of the heat flow. If we only consider the heat transfers inside the cross, this part of deviant heat can be further divided into two parts: the part of heat flowing into the discontinuous part of the minor constituent, and the part of heat hitting the right sides of the lump and flowing back to the mainstream. As a result, the latter part of heat should be considered while estimating the effective volumetric fraction of the minor constituent.

Table 5.1: Values of the effective volumetric fractions. α: the minor constituent.

Mixture Type	ϕ_e^α	ϕ_e^β
1	0.2	0.8
2	0	0
3	1.084	0
4	0	0.553

Figure 5.20(b) shows the area to estimate the effective volumetric fraction of the minor constituent where point B is the midpoint of side AC, which is an approximately guess according to the heat flux field shown in Figure 5.20(a). For Type-4 mixtures, the major constituent is continuous while the minor constituent is discrete along the direction of the heat flow. The values of the effective volumetric fractions for each type of mixture are given in Table 5.1.

Local thermal non-equilibrium

Sometimes the internal heat transfer coefficient h of mixtures is not large enough to eliminate the local temperature differences. As shown by Figures 5.16-5.19, the temperature differences between the two constituents are much more evident with a small m number, and therefore the local thermal non-equilibrium effect needs to be considered. On the other hand, Eq. (5.2) and Eq. (5.3) is not suitable to be directly used for two reasons: first, two particles of the two constituents can never occupy the same spatial position in real situations, and even if the mixture is so well mixed that we can ignore the spatial deviation between the two constituents,

such degree of mixing would result in a very large h so much so that it is meaningless to deal with the local thermal non-equilibrium; second, as suggested by the different structures in Figure 5.1, the constituents may not be always continuous along the heat flow direction, such that using k_m to predict the heat transfer between the two constituents would misinterpret the thermal interactions between the two constituents especially when their thermal conductivities are notably different. Hence, we use the same idea in deriving the effective thermal conductivity in Eq. (5.12) and divide the constituents into continuous and discontinuous parts, and Eq. (5.2) and Eq. (5.3) can be revised to

$$\varphi^{\alpha}\rho'^{\alpha}\frac{\partial\varepsilon^{\alpha}}{\partial t} = \nabla\cdot\left[k^{\alpha}\boldsymbol{\varphi}_{e}^{\alpha}\circ\nabla T^{\alpha} + (\varphi^{\alpha}\mathbf{J}_{3,1} - \boldsymbol{\varphi}_{e}^{\alpha})\circ\mathbf{k}_{hm}\circ\nabla T^{\alpha}\right] + h(T^{\beta} - T^{\alpha}) \tag{5.13}$$

$$\varphi^{\beta}\rho'^{\beta}\frac{\partial\varepsilon^{\beta}}{\partial t} = \nabla\cdot\left[k^{\beta}\boldsymbol{\varphi}_{e}^{\beta}\circ\nabla T^{\beta} + (\varphi^{\beta}\mathbf{J}_{3,1} - \boldsymbol{\varphi}_{e}^{\beta})\circ\mathbf{k}_{hm}\circ\nabla T^{\beta}\right] + h(T^{\alpha} - T^{\beta}) \tag{5.14}$$

where $\mathbf{J}_{3,1}$ is a 3×1 all-ones vector; $\circ$ is the operator representing Hadamard product; $\boldsymbol{\varphi}_{e}^{\alpha}$ is the effective volumetric fraction vector of constituent α defined by

$$\boldsymbol{\varphi}_{e}^{\alpha} = \varphi_{e,i}^{\alpha}\mathbf{e}_{i} \tag{5.15}$$

and the meaning of $\varphi_{e,i}^{\alpha}$ here is consistent with that in Eq. (5.12); $\mathbf{k}_{hm}$ is the thermal conductivity vector that interprets the heat conduction between the discontinuous part of a constituent α and its surrounding constituents, and the subscript hm indicates that these thermal conductivities are evaluated by harmonic means given by

$$\mathbf{k}_{hm} = k_{hm,i}\mathbf{e}_i \tag{5.16}$$

$$k_{hm,i} = \frac{(1-\varphi_{e,i}^{\alpha}-\varphi_{e,i}^{\beta})k^{\alpha}k^{\beta}}{(\varphi^{\alpha}-\varphi_{e,i}^{\alpha})k^{\beta}+(\varphi^{\beta}-\varphi_{e,i}^{\beta})k^{\alpha}} \tag{5.17}$$

Unlike Eq. (5.2) and Eq. (5.3), in Eq. (5.13) and Eq. (5.14) we use a term with $\mathbf{k}_{hm}$ to explain the energy transfer rate to the discontinuous part of the constituent from its surrounding environment. Here the temperature gradient ∇T^{α} can not be replaced by the temperature gradient across the two constituents because the effect of constituent β is already included in $\mathbf{k}_{hm}$, and if doing so the temperature would be overestimated. Eq. (5.13) and Eq. (5.14) are written in three-dimensional to emphasize that the effective volumetric fraction of a constituent should be evaluated from different directions. For the specific problem described in Figure 5.2, Eq (5.13) and Eq. (5.14) are reduced to be one-dimensional because the heat is only exerted on one side of the cavity.

The next step is to determine the expression for the local heat transfer coefficient h. For convenience, we define the concept ”local” as an infinitesimal mate-

rial region inside which the local thermal interaction can be interpreted as the heat conduction between 2 lumped systems, and the local heat transfer coefficient is given by

$$h = \frac{2A^2 k^\alpha k^\beta}{\varphi^\beta V^2 (k^\alpha + k^\beta)} \tag{5.18}$$

where V is the volume of the mixture, A is the total contact area between the 2 constituents, and β here is the constituent with the smaller thermal conductivity. It should be noticed that the meaning of the local heat transfer coefficient h in Eqs. (5.13) and (5.14) is different from that in Eq. (3.3). Nevertheless, if we assume the structure of the mixture is homogeneous and both constituents are always continuous along the heat flow direction, i.e., $\varphi^\alpha = \varphi^\alpha_e$ and $\varphi^\beta = \varphi^\beta_e$, Eqs. (5.13) and (5.14) is reduced to Eq. (3.3). Moreover, Eq. (5.12) can be obtained by assuming $T^\alpha = T^\beta$ in Eqs. (5.13) and (5.14). Yet we should state that Eqs. (5.13) and (5.14) are not applicable to mixtures involving mass interactions between constituents such as phase change processes and chemical reactions, in which case one needs to consider the energy transfer through mass transfer between constituents.

5.2 Results and Discussion

In this section, we compare the numerical results for the heat transfer problems described in Figure 5.2 obtained by the two methods: one is the direct method used in Section 5.1.2, and the other is the modified mixture theory based heat energy equations proposed in Section 5.1.4. Therefore, the modified mixture theory based energy equations can be validated. The time steps and grid sizes used in the numerical calculation are obtained by grid sensitivity tests. Also, it can be found out the scope of the mixture theory framework and to what extent a mixture's structure is suitable for using the modified energy equations.

Local thermal equilibrium

For the heat transfer problems with local thermal equilibrium assumption, for each type of mixture the effective thermal conductivity is evaluated using Eq. (5.12), and by substituting it to Eq. (5.8), the heat transfer problems can be solved by an explicit finite difference method. Since there exists temperature deviations between the two constituents as shown by Figures 5.16-5.19 while T^{α} is identical to T^{β} for the local thermal equilibrium assumption, the temperature profiles can not be directly compared. As a result, the rate of heat transfer through the left boundary of the cavity is used to evaluate the results. Figures 5.21-5.24 show the rate of heat transfer on the boundary of the cavity in the first 1000s with respect to

different mixture types.

For Type-1 mixtures, the total thermal energy that injects into the cavity over 1000s for unit number m =4, 8, 16, 32 is 980.55 kJ, 1066.39 kJ, 1087.50 kJ, and 1090.78 kJ, respectively, while the thermal energy calculated by using the effective thermal conductivity k_e is 1096.01 kJ. It is suggested that the thermal energy calculated by k_e has a good match with the real situations when m is large. By comparing the amount of heat transfer at each time step obtained by using k_e with that of the Type-1 mixture with $m = 32$, the average deviation is 19.84 J and the relative deviation is 1.15%. For Type-2 mixtures, the total thermal energy that injects into the cavity over 1000s for unit number m =4, 8, 16, 32 is 146.12 kJ, 158.52, 161.16, and 161.66 kJ, respectively. The thermal energy calculated by using the effective thermal conductivity k_e is 163.27 kJ. By comparing the amount of heat transfer at each time step obtained by using k_e with that of the Type-1 mixture with $m = 32$, the average deviation between the amount of heat transfer at each time step obtained by using k_e and that of the Type-1 mixture with $m = 32$ is 3.36J and the relative deviation is 1.66%. For Type-3 mixtures, the total thermal energy that injects into the cavity over 1000s for unit number m =4, 8, 16, 32 is 848.97 kJ, 879.65 kJ 883.59 kJ, and 886.90 kJ, respectively. The thermal energy calculated by using the effective thermal conductivity k_e is 871.51 kJ. By comparing the amount of heat transfer at each time step obtained by using k_e with that of the Type-1 mixture with $m = 32$, the average deviation between

the amount of heat transfer at each time step obtained by using k_e and that of the Type-1 mixture with $m = 32$ is 24.19 J and the relative deviation is 2.40%. For Type-4 mixtures, the total thermal energy that injects into the cavity over 1000s for unit number m =4, 8, 16, 32 is 137.09 kJ, 152.81 kJ, 184.81 kJ, and 185.80 kJ, respectively. The thermal energy calculated by using the effective thermal conductivity k_e is 188.85 kJ. By comparing the amount of heat transfer at each time step obtained by using k_e with that of the Type-1 mixture with $m = 32$, the average deviation between the amount of heat transfer at each time step obtained by using k_e and that of the Type-1 mixture with $m = 32$ is 3.21 J and the relative deviation is 1.66%.

The comparison shows that as the total unit number increases, i.e., m increases, the differences between the results by using the effective thermal conductivity shown in Eq. (5.12) and the real situations are decreasing. On one hand, Eq. (5.12) is testified as a valid expression for the effective thermal conductivity for different mixture structures. On the other hand, it is suggested that the effect of local thermal non-equilibrium is weakened when m grows, and it is reasonable to predict that the deviation between the temperatures of the two constituents would become negligible when m is sufficiently large.

Local thermal non-equilibrium

Figures 5.25-5.40 show the average temperature profiles of nickel and paraffin along x_1 direction together with the numerical results calculated by Eqs. (5.13) and (5.14), where the subscript $LTNE$ indicates the numerical results obtained by the local thermal non-equilibrium model. For the paraffin part in Type-1 mixtures, the average deviations between the mixture theory based results and the real situations for m =4, 8, 16, 32 are 2.55 °C, 0.76 °C, 0.25 °C, and 0.13 °C, respectively; while the average deviations for the nickel part are 0.09 °C, 0.19 °C, 0.12 °C, and 0.01 °C, respectively. It is shown that for Type-1 mixtures, the results calculated by the local thermal non-equilibrium assumption is satisfactory even if the structures of the mixtures with a small m number do not strictly follow the assumption of mixture theory that all constituents coexist at the same spatial position. Specifically, Figures 5.25-5.28 indicate that for the nickel part the results by the mixture theory is very close to the situation. This is because the thermal conductivity of nickel is much higher than that of paraffin and thus the temperature profiles of nickel is almost one-dimensional, which coincides the mixture theory heat transfer equations. Moreover, for the paraffin part there are notable deviations between the mixture theory results and the real situation when m is small, which is because the mean temperatures are used to compare the results while the temperature gradient along x_2 direction inside paraffin is not negligible in real situ-

ations. For Type-2 mixtures, Figures 5.29-5.32 show that the temperature profiles of nickel and paraffin by using mixture theory almost coincide with each other. The reason is that although both paraffin and nickel are discontinuous along the heat flow direction, the energy equations Eqs. (5.13) and (5.14) are always continuous which can not show the discontinuity of the structures. Still, the mixture theory results are getting close to real situations as m increases. For Type-3 mixtures, the average deviations for the nickel part are 0.65 °C, 0.26 °C, 0.19 °C, and 0.02 °C, respectively. Here we only compare the temperatures of nickel because the paraffin is discontinuous. For Type-4 mixtures, the average deviations for the paraffin part are 0.96 °C, 0.61 °C, 0.44 °C, and 0.42 °C, respectively. The comparisons show that the mixture theory based energy equations can well predict the temperature variations for each constituent even though the mixture is not well mixed. However, it is determined by the nature of the Eqs. (5.13) and (5.14) that the temperature profiles calculated by the equations are continuous and smooth, and thus the discontinuities in the mixtures can not be expressed.

According to the results, the heat transfer performance of a structure is dependent on the contact area and the volumetric fraction of the high-thermal-conductivity material that is parallel to the heat flow direction. However, as the contact area increases, the heat transfer performance is constrained by the effective volumetric fraction. So for designing the heat transfer structures for thermal energy storage systems, the priority of the effective volumetric fraction is the highest to obtain

the optimized heat transfer performance.

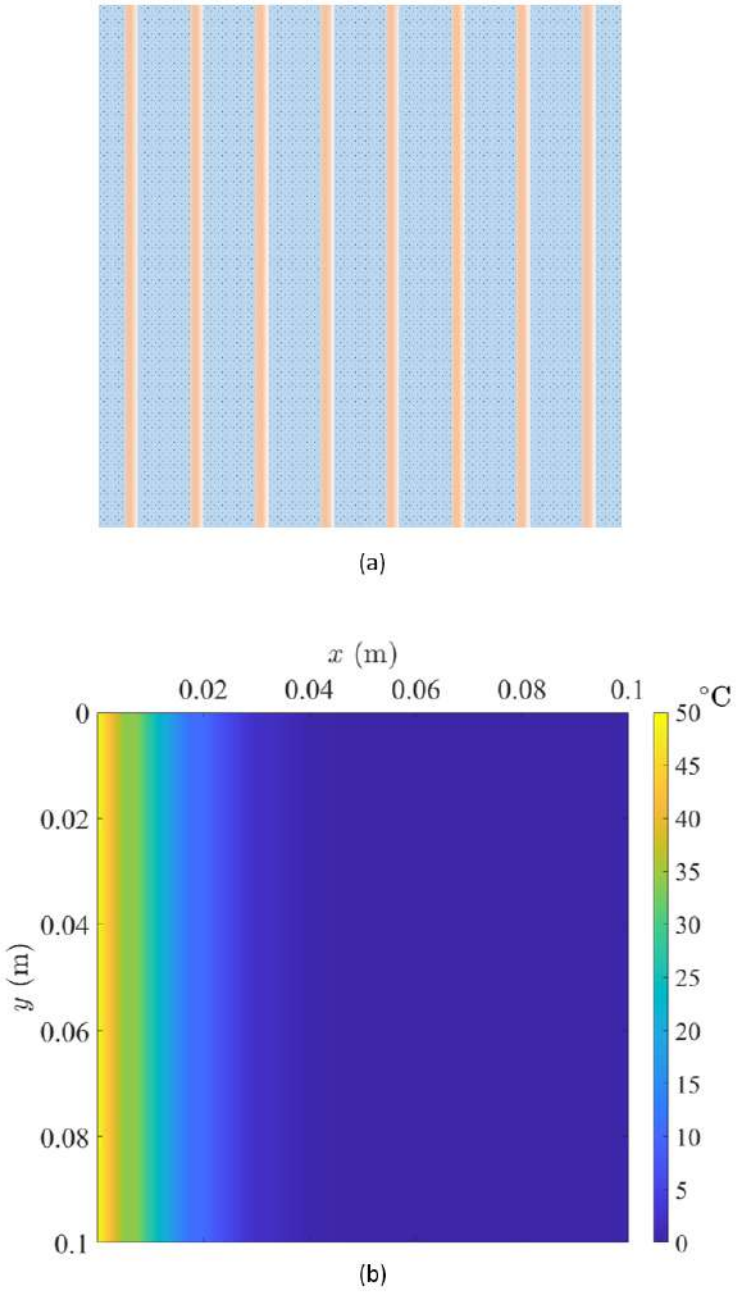

Figure 5.8: The cavity with Type 2 units when $m = 8$. (a) Mixture structure. (b) The temperature distribution at $t = 1000$s.

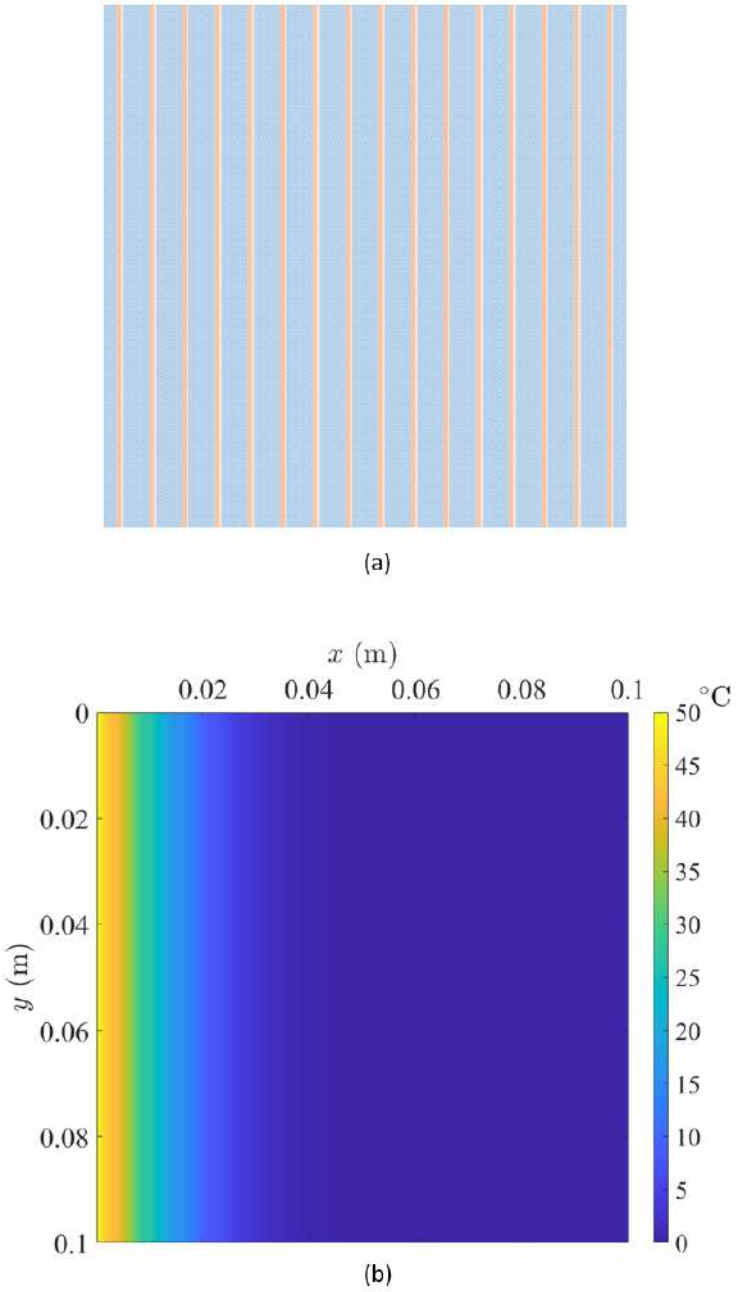

Figure 5.9: The cavity with Type 2 units when $m = 16$. (a) Mixture structure. (b) The temperature distribution at $t = 1000$s.

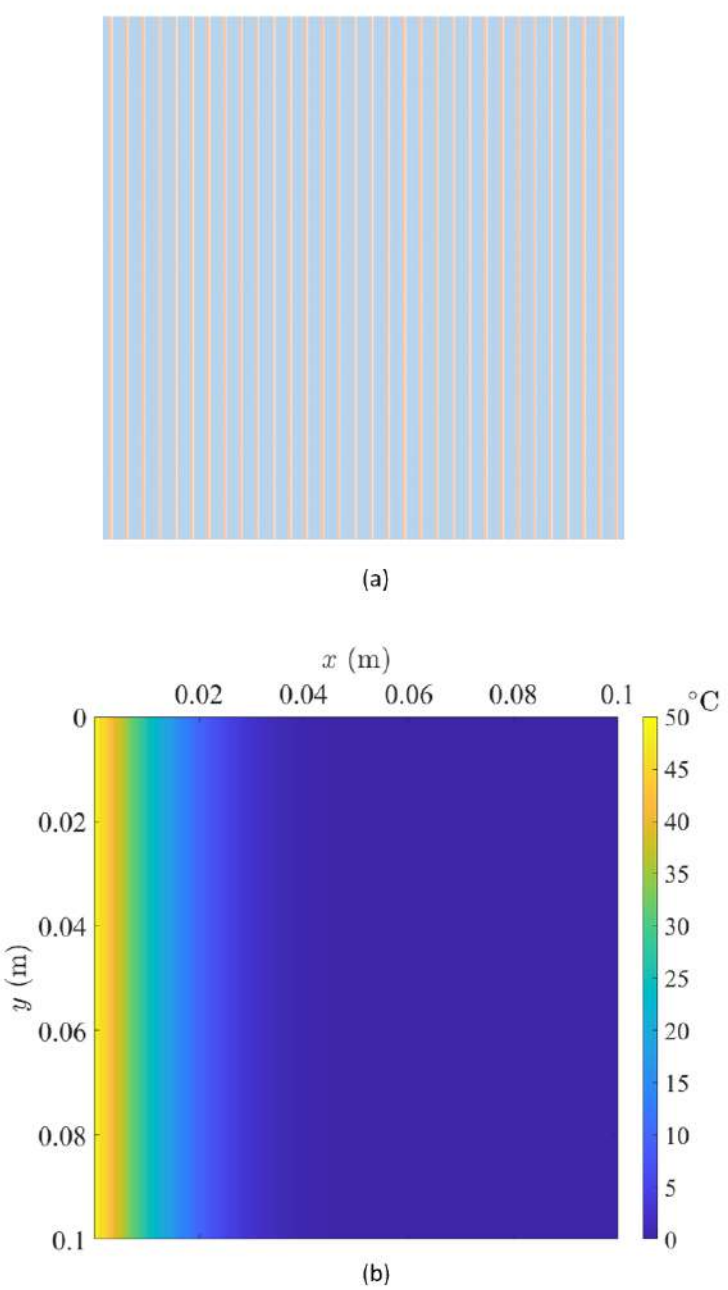

Figure 5.10: The cavity with Type 2 units when $m = 32$. (a) Mixture structure. (b) The temperature distribution at $t = 1000$s.

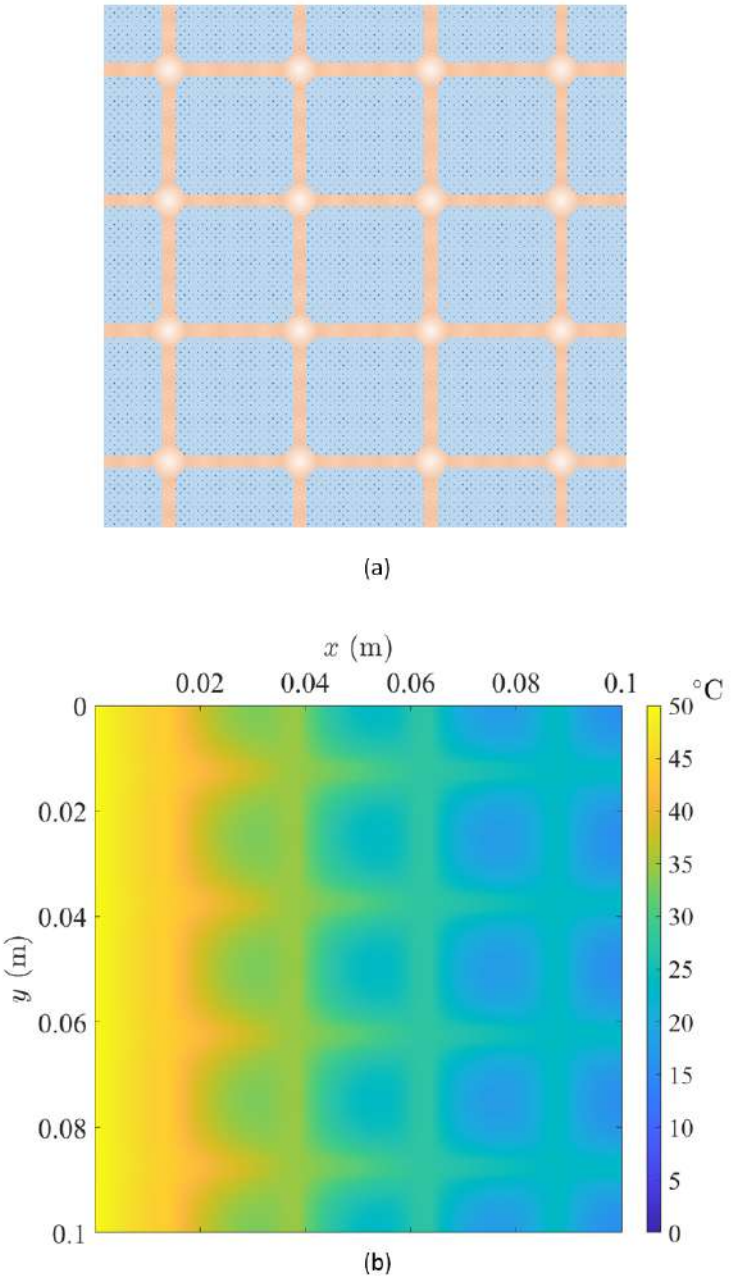

Figure 5.11: The cavity with Type 3 units when $m = 4$. (a) Mixture structure. (b) The temperature distribution at $t = 1000$s.

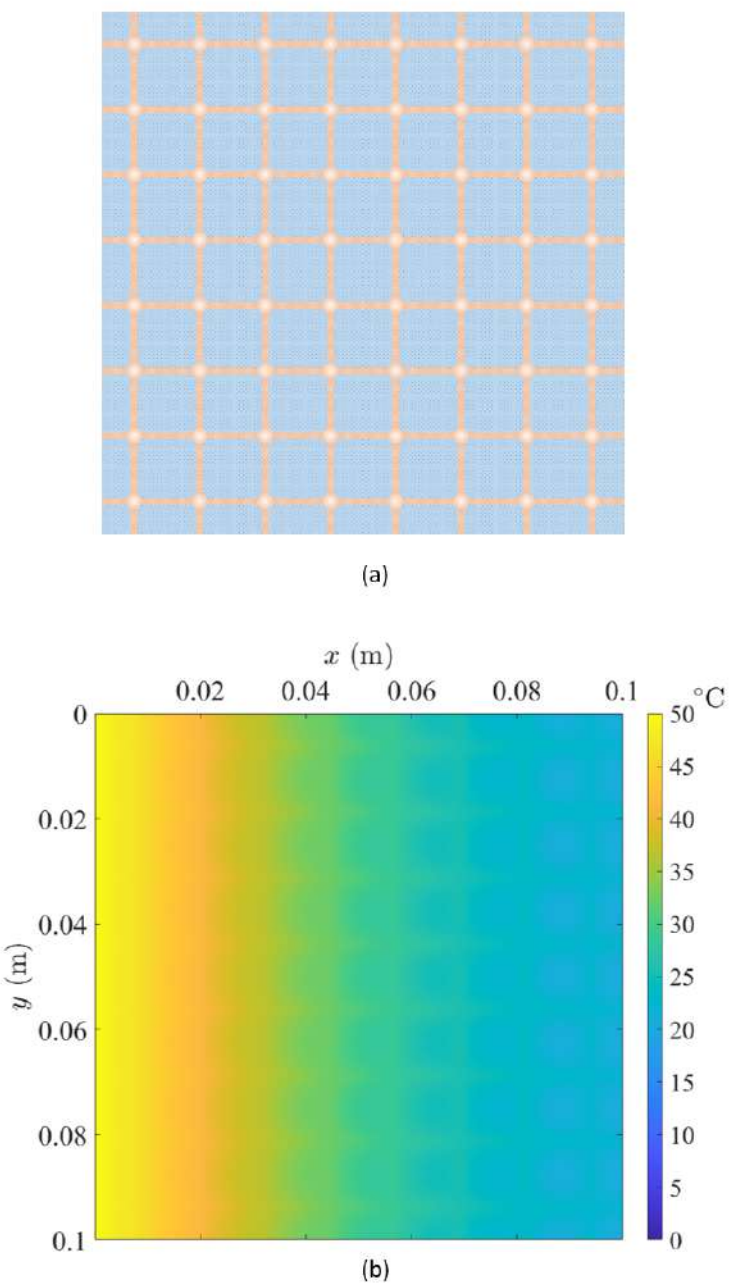

Figure 5.12: The cavity with Type 3 units when $m = 8$. (a) Mixture structure. (b) The temperature distribution at $t = 1000$s.

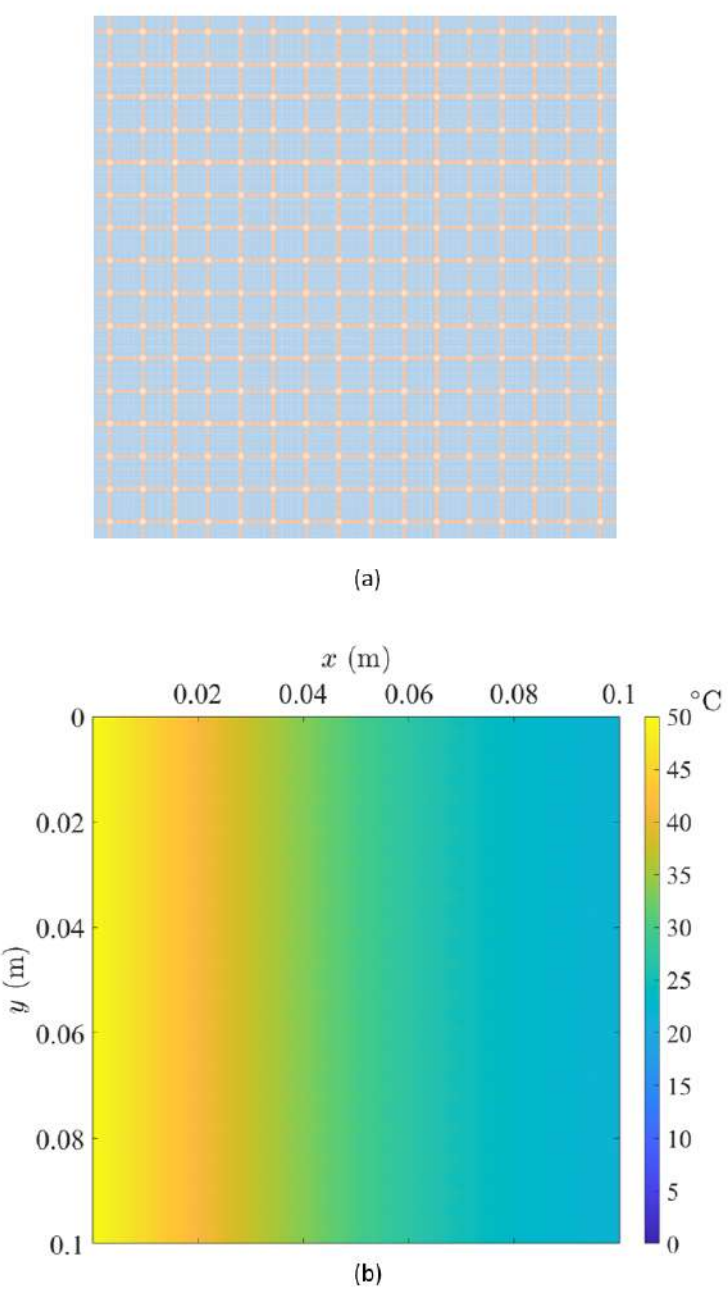

Figure 5.13: The cavity with Type 3 units when $m = 16$. (a) Mixture structure. (b) The temperature distribution at $t = 1000$s.

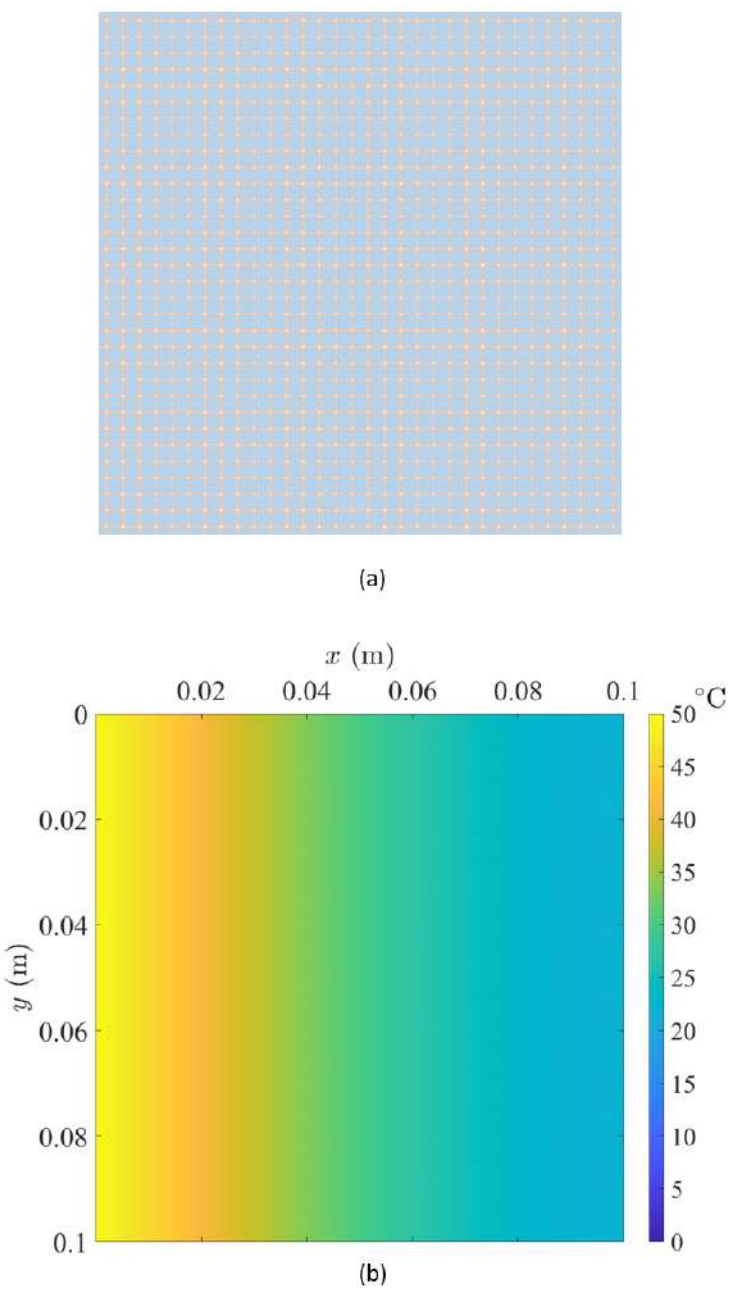

Figure 5.14: The cavity with Type 3 units when $m = 32$. (a) Mixture structure. (b) The temperature distribution at $t = 1000$s.

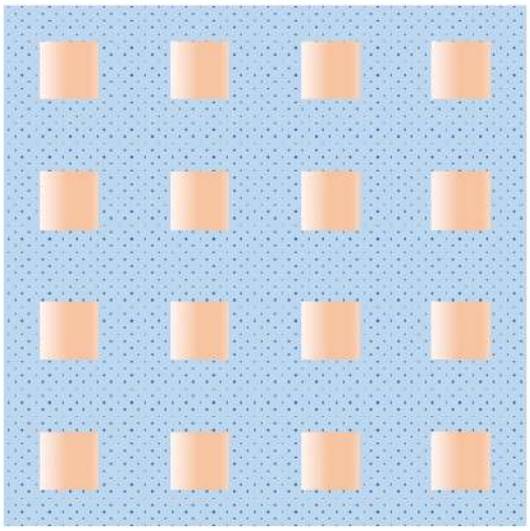

(a)

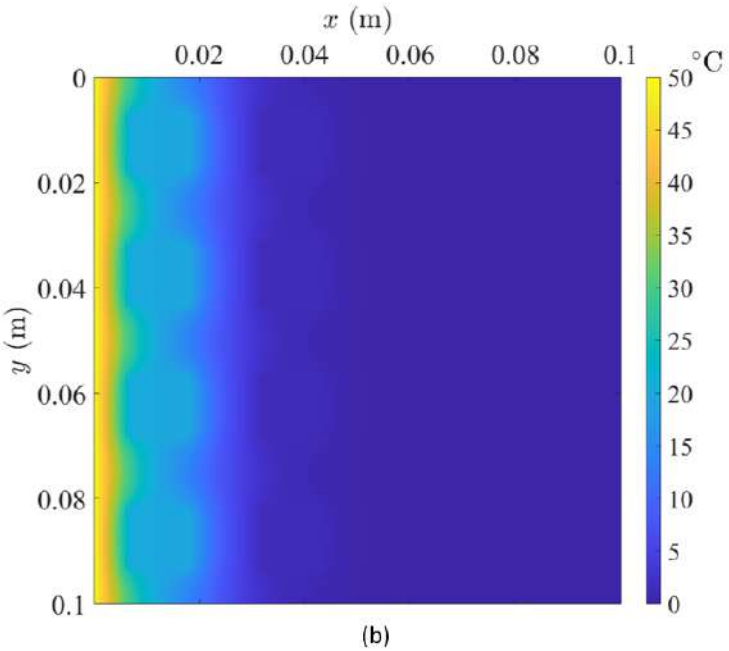

(b)

Figure 5.15: The cavity with Type 4 units when $m = 4$. (a) Mixture structure. (b) The temperature distribution at $t = 1000$s.

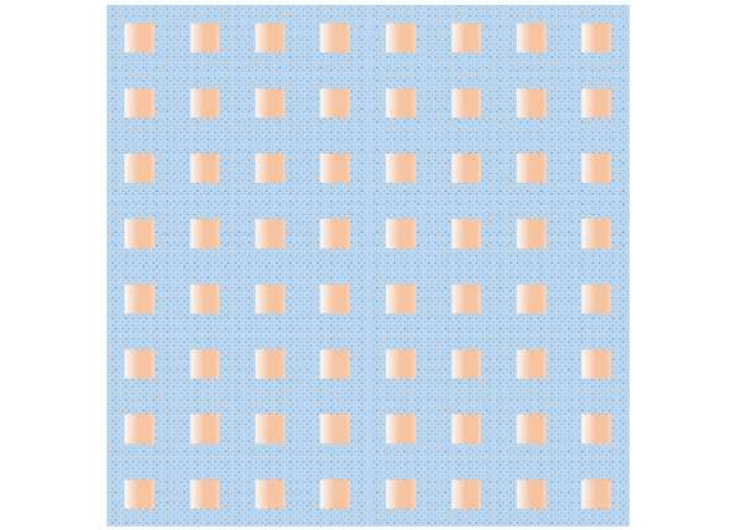

(a)

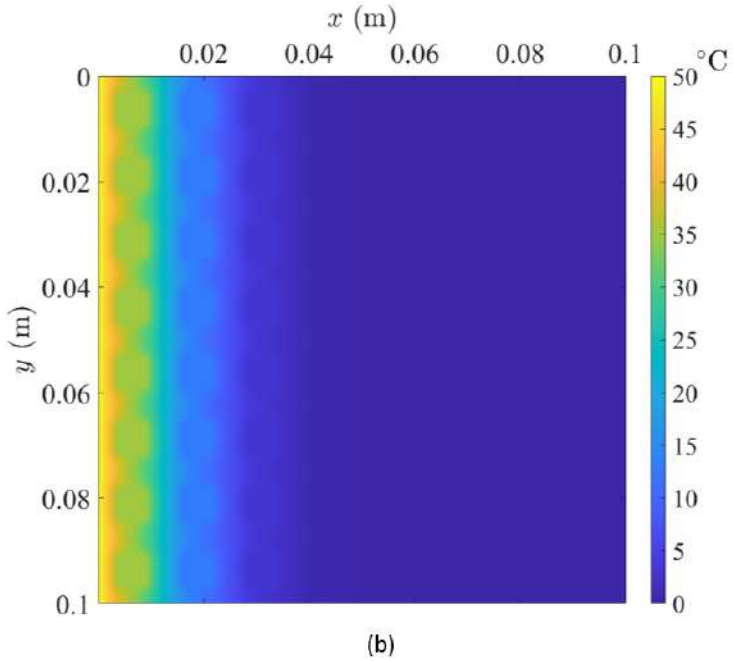

(b)

Figure 5.16: The cavity with Type 4 units when $m = 8$. (a) Mixture structure. (b) The temperature distribution at $t = 1000$s.

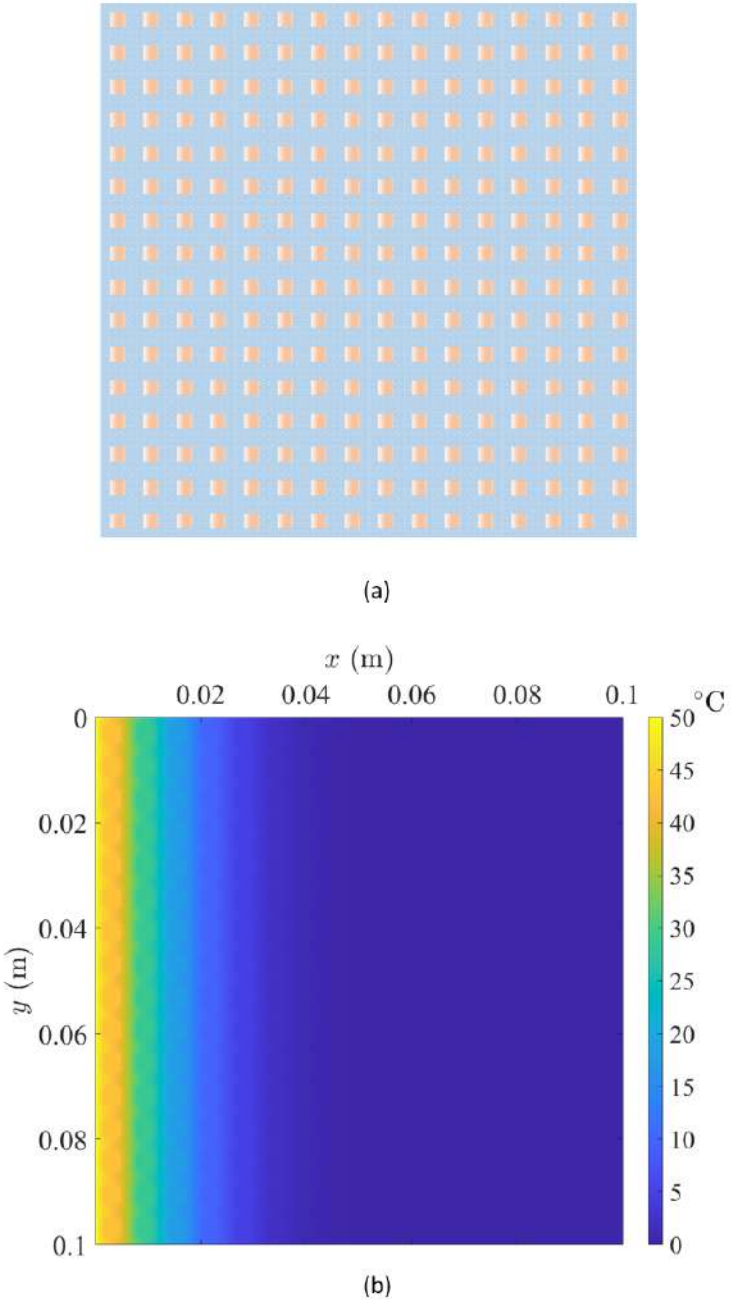

Figure 5.17: The cavity with Type 4 units when $m = 16$. (a) Mixture structure. (b) The temperature distribution at $t = 1000$s.

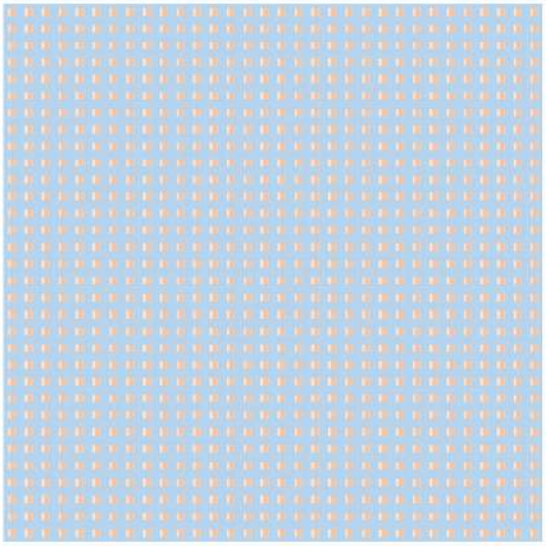

(a)

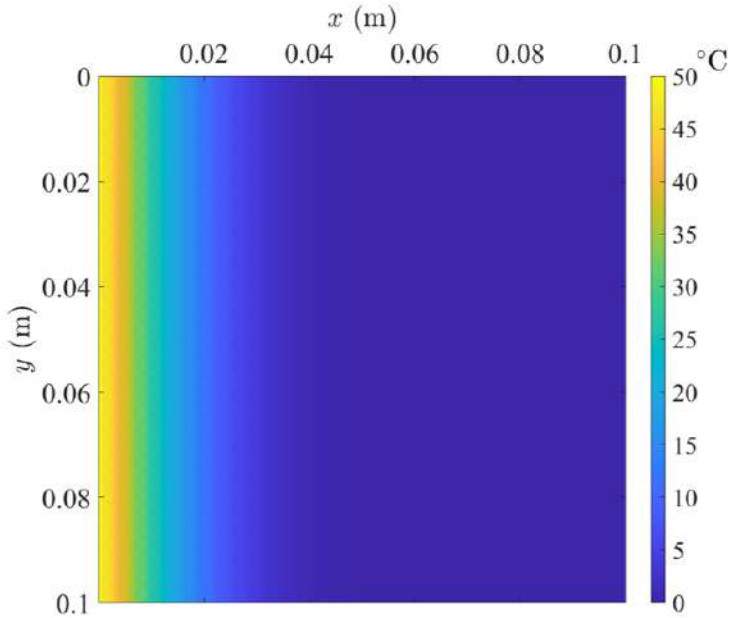

(b)

Figure 5.18: The cavity with Type 4 units when $m = 32$. (a) Mixture structure. (b) The temperature distribution at $t = 1000$s.

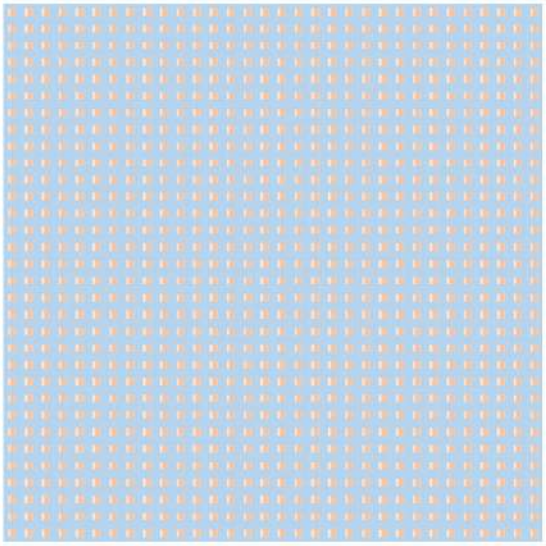

(a)

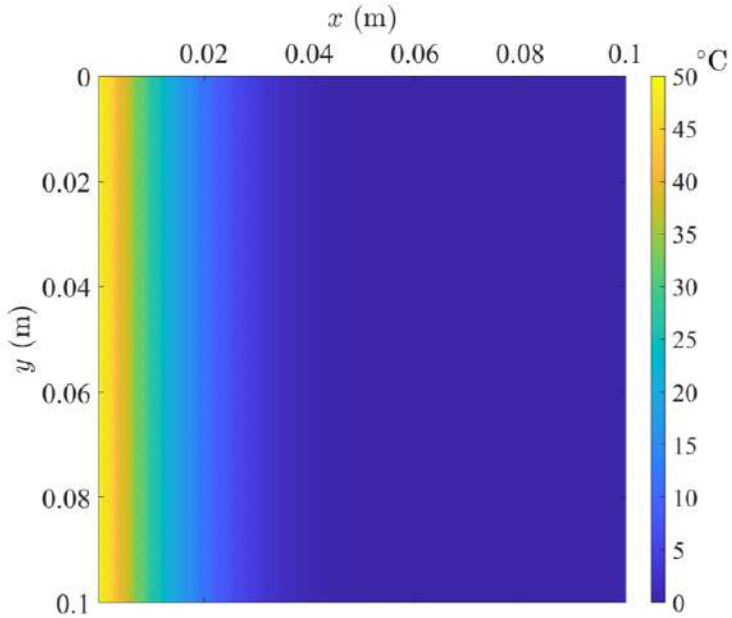

(b)

Figure 5.19: The cavity with Type 1 units when $m = 4$. (a) Mixture structure. (b) The temperature distribution at $t = 1000$s.

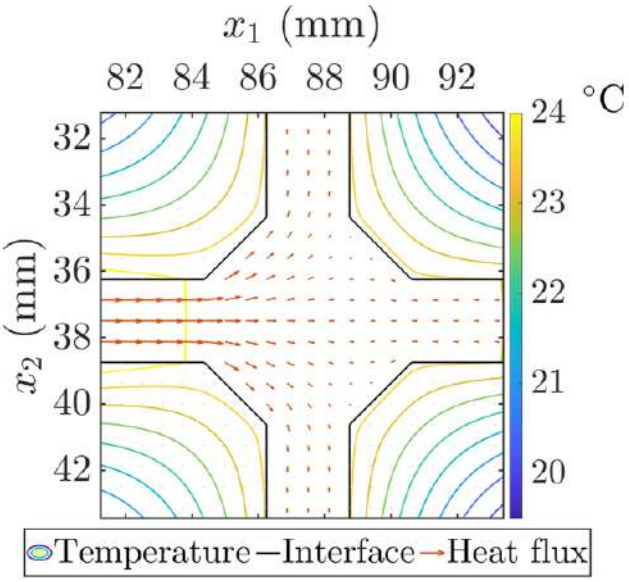

Figure 5.20: A lump in Type-3 mixture ($m = 4$). (a) Heat flux field and temperature field of the lump. (b) The area to estimate the effective volumetric fraction.

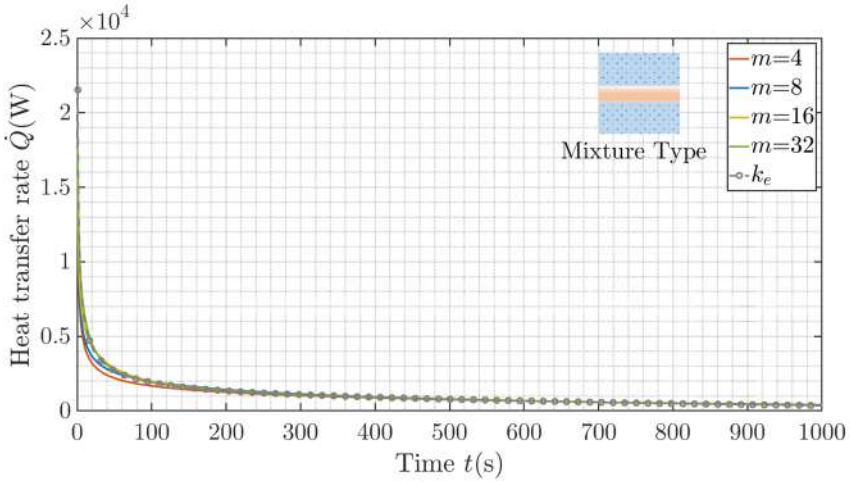

Figure 5.21: Rate of heat transfer through the left boundary of the cavity for Type-1 mixtures in the first 1000 s.

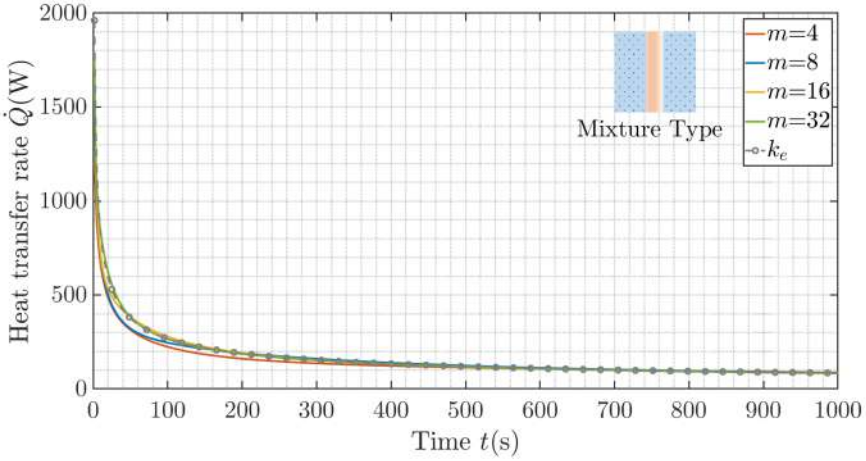

Figure 5.22: Rate of heat transfer through the left boundary of the cavity for Type-2 mixtures in the first 1000 s.

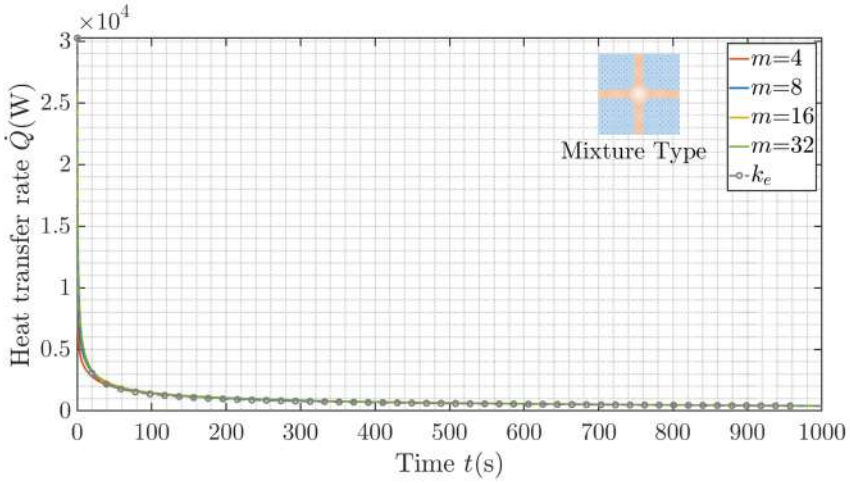

Figure 5.23: Rate of heat transfer through the left boundary of the cavity for Type-3 mixtures in the first 1000 s.

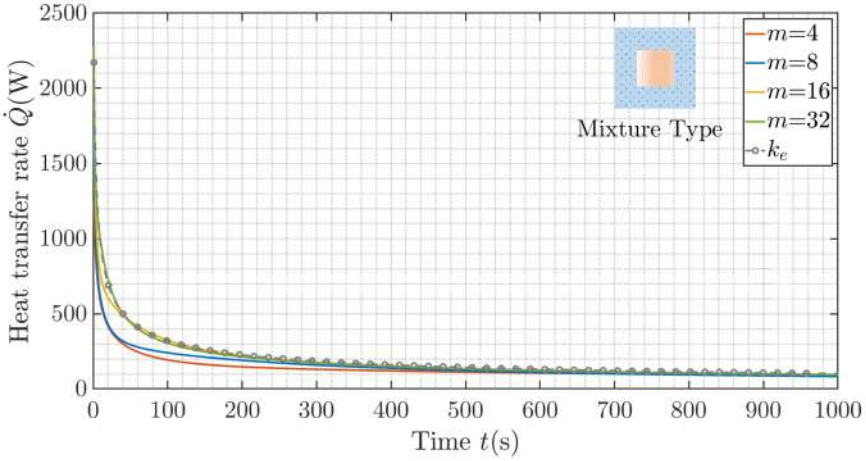

Figure 5.24: Rate of heat transfer through the left boundary of the cavity for Type-4 mixtures in the first 1000 s.

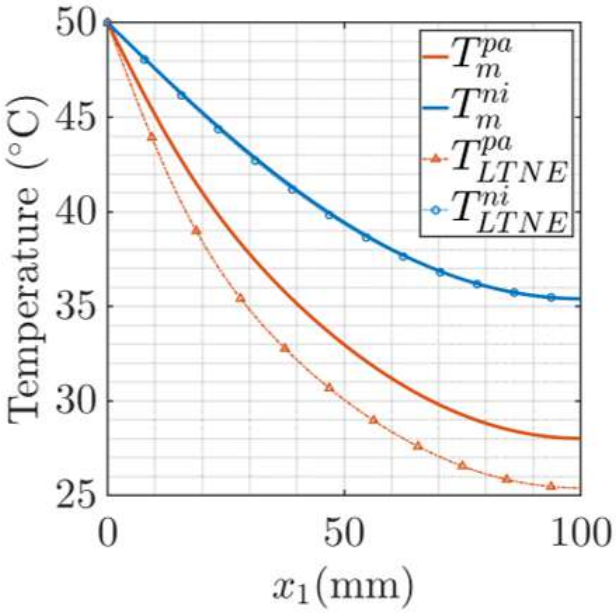

Figure 5.25: Temperatures of nickel and paraffin at t=1000 s for Type-1 mixtures when $m = 4$.

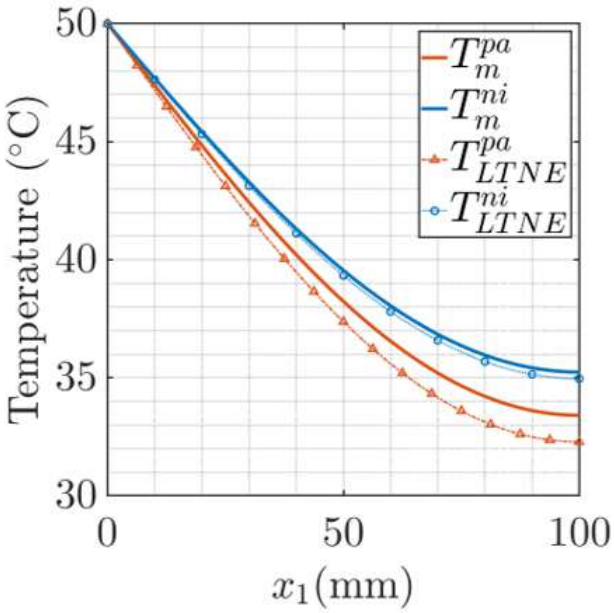

Figure 5.26: Temperatures of nickel and paraffin at t=1000 s for Type-1 mixtures when $m = 8$.

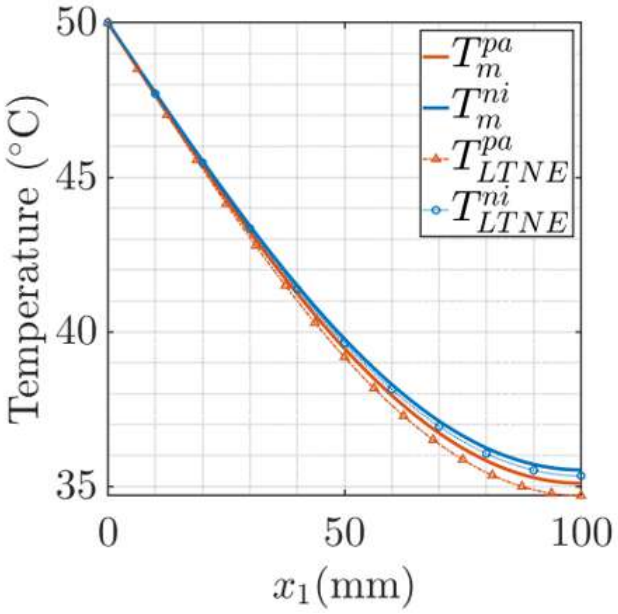

Figure 5.27: Temperatures of nickel and paraffin at t=1000 s for Type-1 mixtures when $m = 16$.

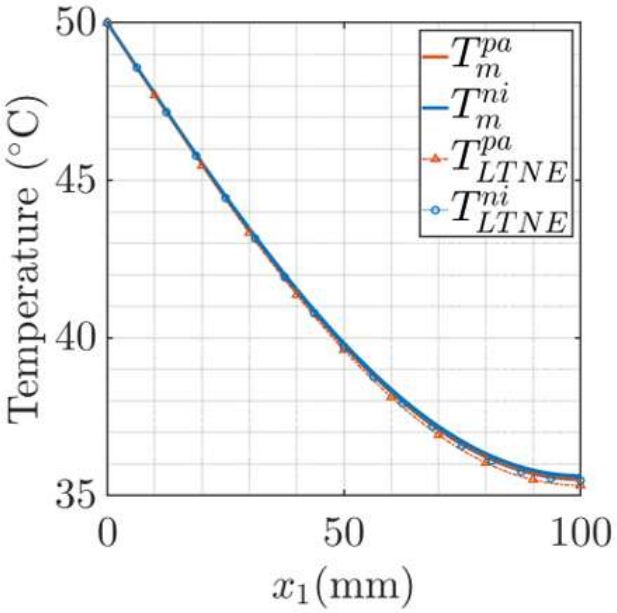

Figure 5.28: Temperatures of nickel and paraffin at t=1000 s for Type-1 mixtures when $m = 32$.

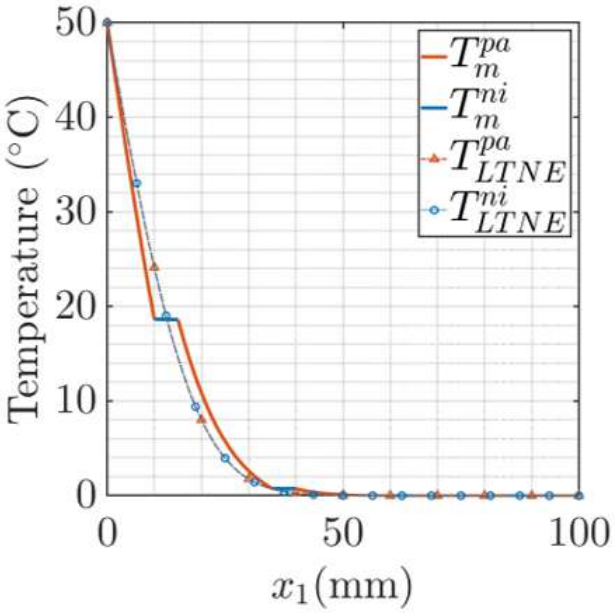

Figure 5.29: Temperatures of nickel and paraffin at t=1000 s for Type-2 mixtures when $m = 4$.

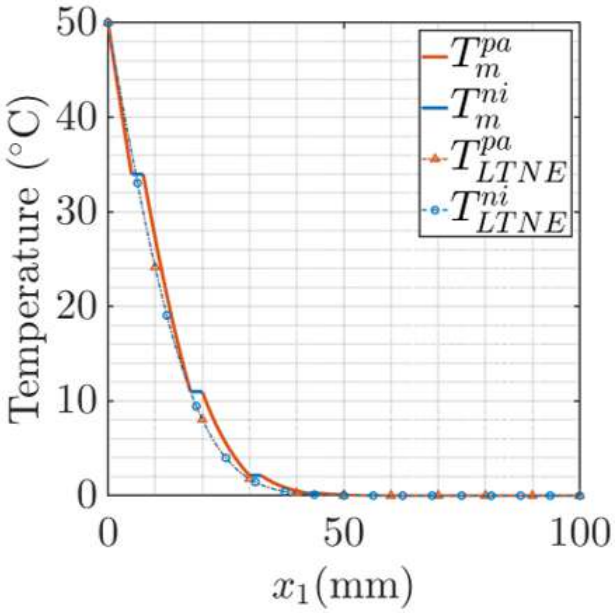

Figure 5.30: Temperatures of nickel and paraffin at t=1000 s for Type-2 mixtures when $m = 8$.

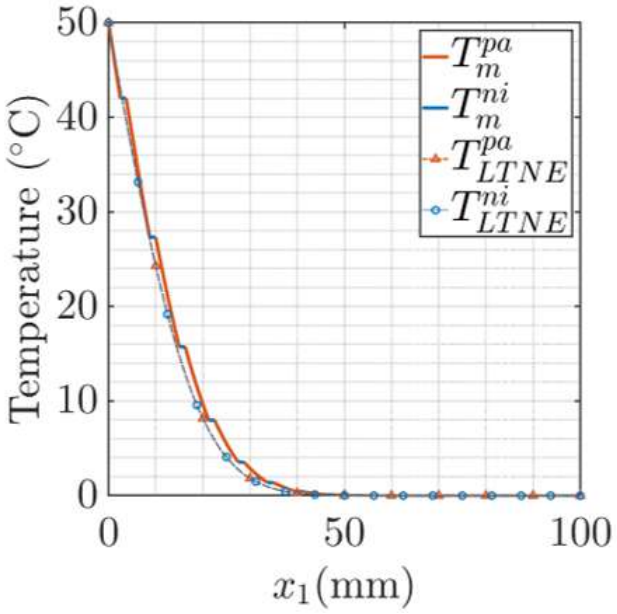

Figure 5.31: Temperatures of nickel and paraffin at t=1000 s for Type-2 mixtures when $m = 16$.

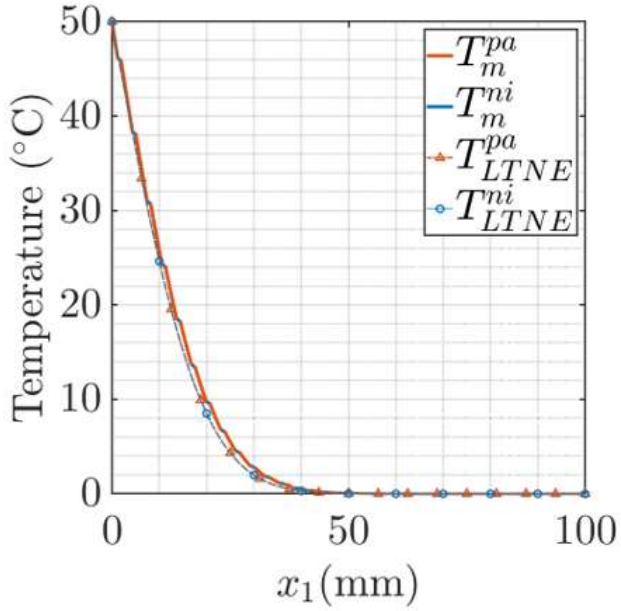

Figure 5.32: Temperatures of nickel and paraffin at t=1000 s for Type-2 mixtures when $m = 32$.

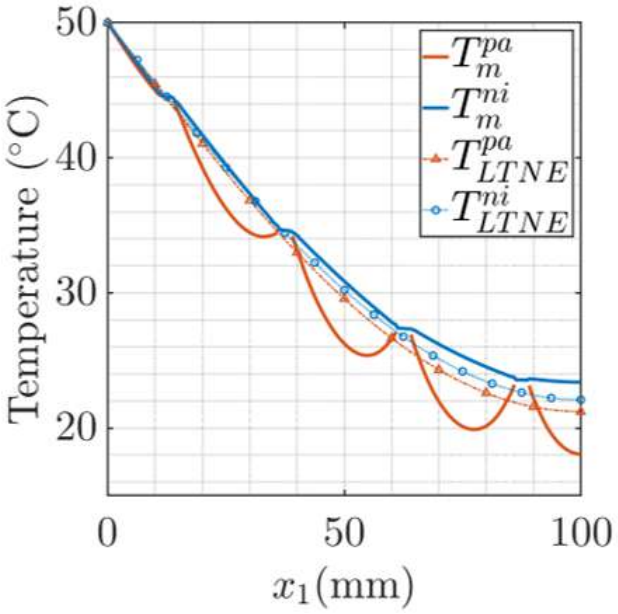

Figure 5.33: Temperatures of nickel and paraffin at t=1000 s for Type-3 mixtures when $m = 4$.

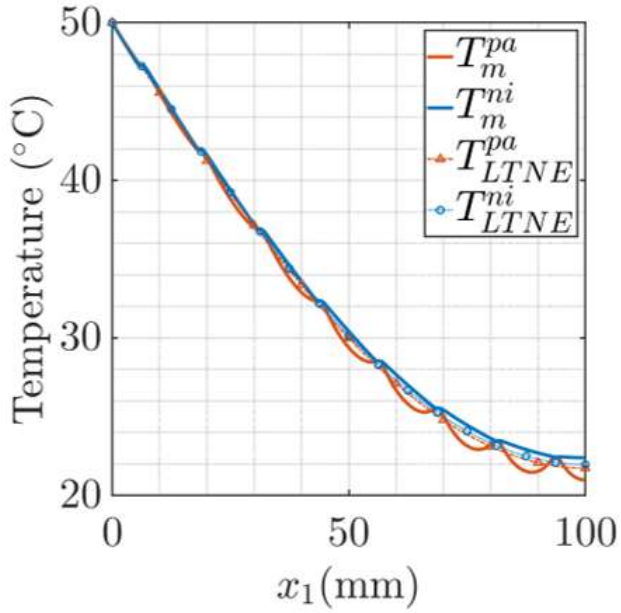

Figure 5.34: Temperatures of nickel and paraffin at t=1000 s for Type-3 mixtures when $m = 8$.

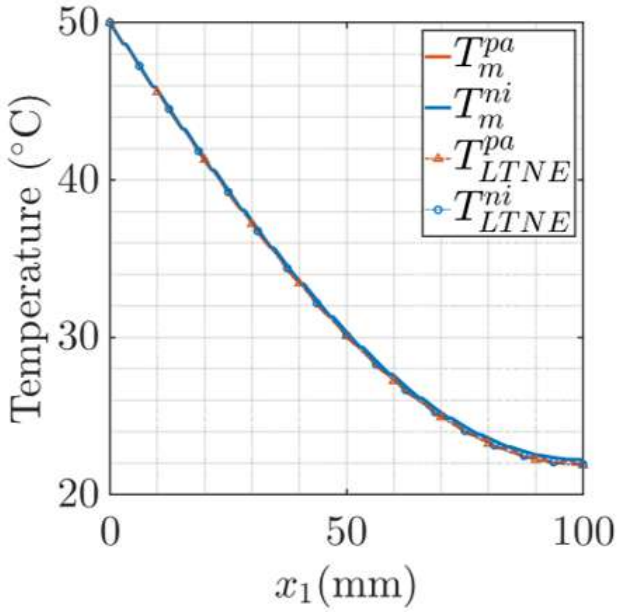

Figure 5.35: Temperatures of nickel and paraffin at t=1000 s for Type-3 mixtures when $m = 16$.

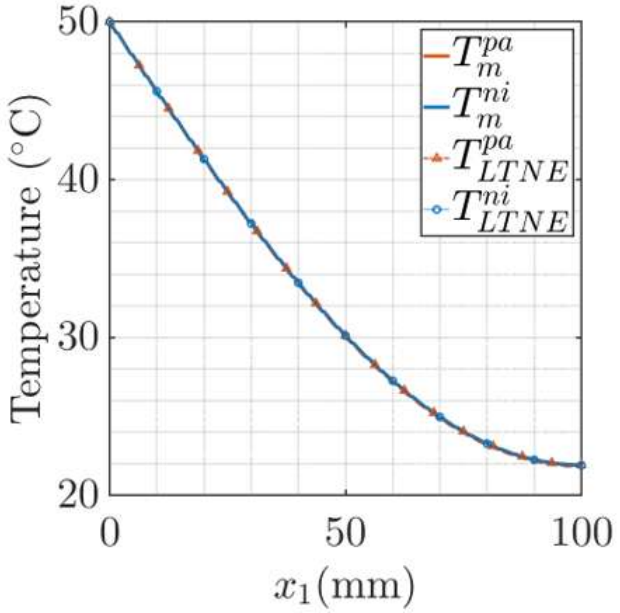

Figure 5.36: Temperatures of nickel and paraffin at t=1000 s for Type-3 mixtures when $m = 32$.

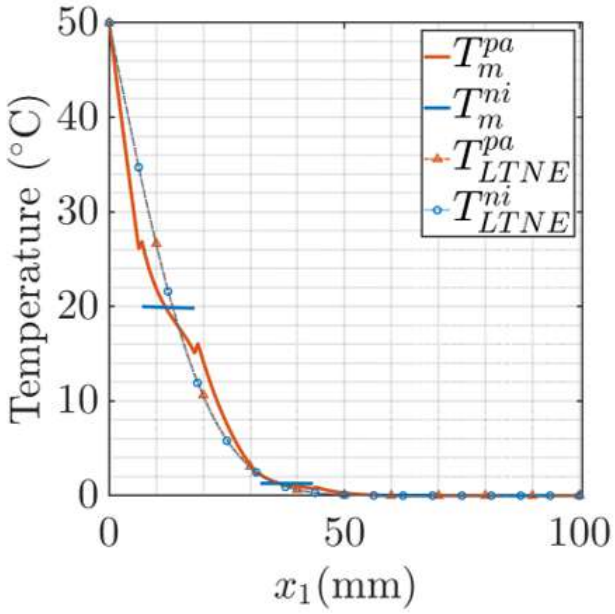

Figure 5.37: Temperatures of nickel and paraffin at t=1000 s for Type-4 mixtures when $m = 4$.

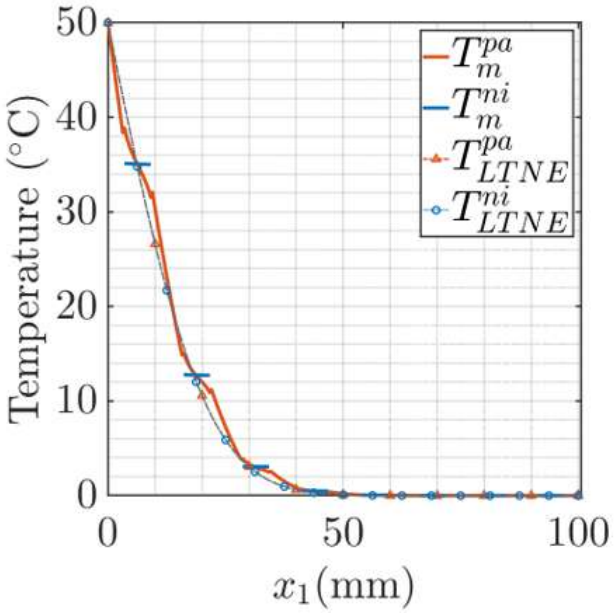

Figure 5.38: Temperatures of nickel and paraffin at t=1000 s for Type-4 mixtures when $m = 8$.

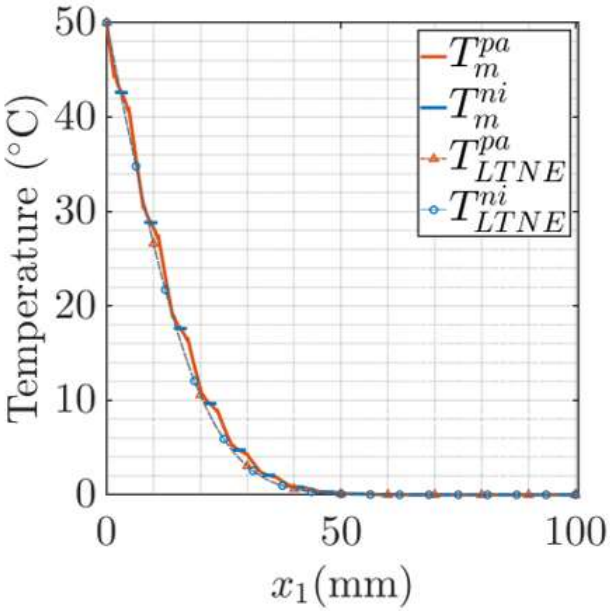

Figure 5.39: Temperatures of nickel and paraffin at t=1000 s for Type-4 mixtures when $m = 16$.

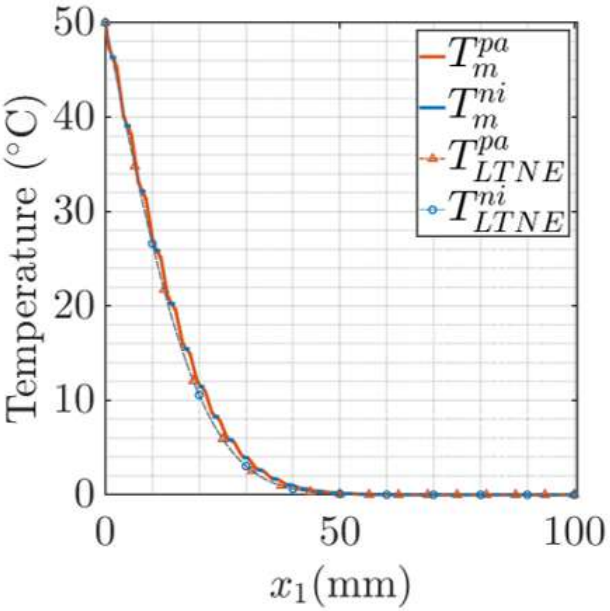

Figure 5.40: Temperatures of nickel and paraffin at t=1000 s for Type-4 mixtures when $m = 32$.

Chapter 6

Conclusion and Future Work

6.1 Summary of Current Work

This research develops a mixture theory model for solving phase change problems of pure PCM and PCM/metal foam composite. For the one-dimensional melting, we give the expression of the liquid velocity driven by the density difference between solid PCM and liquid PCM, which is rarely considered in the present studies. A new interpretation of heat flux terms and internal energy supply terms of each constituent is also presented in this study. Three problems - pure paraffin melting, paraffin/nickel foam composite melting, and paraffin/copper foam composite melting are solved for the one-dimensional problem. The mathematical model regarding each problem is numerically solved by using a finite difference method. Experiments are conducted to validate the theory by comparing the ex-

perimental data to the numerical results. The comparison shows that the mixture theory model is suitable for solving one-dimensional melting of pure PCM and PCM/metal foam composite. The greatest difference between experimental data and numerical results is 2.83 °C observed in the melting of paraffin/copper foam at $x = 20$mm at $t = 6814$s. The importance of the liquid velocity in the model is discussed. Although the scale of u^l is very small, the ignorance of that could lead to a noticeable deviation from the real situation as paraffin transfers from solid to liquid. This deviation is because the model ignoring velocity fails to describe the heat loss through the heating side. However, this conclusion can not be extended to higher order problems. For two-dimensional melting problems, Faden et al. (2021) showed that the density change during PCM melting has little influence on the shape of the melting front. Moreover, for small Stefan numbers, the effect of density change can be neglected. The local thermal non-equilibrium effect is discussed for the paraffin/nickel foam and paraffin/copper foam. The numerical results show that the difference between the paraffin temperature T and metal temperature T^m is apparent only near the top boundary in the first few minutes. Furthermore, the evolution of the mushy zone is analyzed. It is shown that the addition of metal increases the melting speed. The error sources are also discussed in the last section. Generally, this one-dimensional mixture model can also be used for other heat transfer problems involving multiple constituents. However, the solid constituents must be assumed to be rigid, i.e. the solids are not subjected

to any deformation or motion.

For the two-dimensional problem, we give a mixture theory based mathematical model for the phase change problem for pure PCMs. We propose that a melting PCM can be separately modeled for three regions: the liquid region, the solid region and the mushy zone. Like the one-dimensional mixture model, in the two-dimensional model we assume that the velocity field in the mushy zone is solely dependent on the density variation and the flow in the liquid region can not penetrate the boundary of the mushy zone. Thus we can circumvent the problems while using the Darcy's equation, of which the limitations are discussed in Section 2.4. Moreover, if there is local thermal equilibrium, we can simply add another rigid solid constituent to represent the extra additive, and as indicated in the one-dimensional model the addition of non-reactive solids does not increase the order of the governing equation. However, we have not extended the model for 2-dimensional problems involving local thermal non-equilibrium because the Darcy's equation loses its credibility for phase change problems involving local temperature differences in the mixture theory framework (Liu 2016; Ray M Bowen 1980). Thus, a revised Darcy's equation needs to be further investigated for 2-dimensional problems.

We also revise the energy equation in the mixture theory framework for solving heat conduction problems inside a mixture. For the local thermal equilibrium we give a new expression for the effective thermal conductivity, and for the local non-

equilibrium assumption a new energy equation set is proposed together with our definitions of heat flux terms and local heat transfer coefficient. Numerical evaluations are conducted for 4 different types of mixture structures and each structure is solved by both direct method which represents the real situation, and the proposed mixture theory method. By comparing the numerical results, it is suggested that the mixture theory can provide satisfying predictions for the real situations of different mixture structures. If the mixture is well mixed, the boundary heat flow can be evaluated by using the local thermal equilibrium assumption. While if the mixture is not so well mixture, the mixture theory can still provide results with small deviations with the real situations for the constituents with large thermal conductivities by using the local thermal non-equilibrium model. Moreover, the mixture method is numerically friendly because the mixture structures are considered by calculating effective values. However, we should point out the restrictions. First, the constituents are assumed to be static, and as a result, the convective heat transfer and kinematic energy are not considered. If one or more of the constituents are moving, except for adding the convective terms on the left hand side of Eqs. (5.13) and (5.14), the local heat transfer coefficient in Eq. (5.18) need to be revised by considering the motion of the constituents. Second, we assume there is no mass interaction between the constituents, and one to revise the local thermal interaction terms in Eqs. (5.13) and (5.14) and take volumetric fractions as variables if mass interactions between constituents exist. Third, the revised energy equation can not

express the discontinuities of the mixture structures, and thus there would be notable errors while predicting the thermal behaviour of discontinuous constituents when the local heat transfer coefficient h is not large enough.

6.2 Future Work

In the previous study, we have revised the current mixture theory in three aspects: First, the density change during the phase change process of PCMs is considered by introducing a bulk fluid velocity associated with the density variation; second, the heat flux term and local energy interaction term are interpreted; third, the energy equation is revised for both local thermal equilibrium and local thermal non-equilibrium situations, which makes this mixture theory framework more reasonable. Nevertheless, there are still some unsolved problems in the current framework. It is suggested that Darcy's equation would lose its credibility for problems involving local thermal non-equilibrium. As a result, a mixture theory model for PCM composites involving local thermal non-equilibrium is to be developed in the future by deriving a revised Darcy's equation, whic requires the usage of the principle of material frame indifference and the entropy inequality. Also, the solids in the current mixture theory model are assumed to be rigid and not moving, and hence the framework is not applicable to PCM/nanoparticle materials for which the solid is moving along with the liquid. In the future, we will develop a more

general mixture model for PCM composites considering the motion and deformation of the solid constituents. Last, currently we only consider the thermophysical behaviors of PCM and PCM composites while the material behaviors are ignored. In the future we will also study the material properties of the PCMs and investigate phenomenon like cavity formation during the solidification of PCMs. Currently the model is restricted in one-dimensional problems and two-dimensional problems. In the future, we would work on a three-dimensional model for phase change problems, which is expected to cover the lower-dimensional problems.

The future plan for experimental studies would be studying the phase change process of PCM with deformable additives, and nanoparticles. The purpose of the experiments is to validate the mixture theory approach involving deformation and motion of the solid constituents. Except for the experiments for the purpose of validation, we would also work on the development of an optimized metal structure to enhance the heat transfer of PCMs. There are three major problems for the metal foam for the enhancement of heat transfer: first, in Chapter 4 we have shown that the heat transfer performance is mainly dominated by effective volumetric fraction instead of real volumetric fraction, and as a result a part of the metal foam is trivial; second, the metal foam is of a porous structure that would slow down the natural convection of the liquid PCM and hence weaken the heat transfer performance; third, the price of high-porosity metal foams is expensive compared with some carbon materials like graphite. As a result, we want to develop a novel metal

structure for which the direction of metal fibers is made parallel to the heat flux direction to maximize the effect of the metal. Moreover, for the metal foam and our proposed metal structure with the same heat transfer performance, the latter should possess a higher porosity because the unnecessary part of metal is not included in this stricture such that the natural convection is less affected. Last, the price of the new structure is supposed to be more cost-friendly. On one hand, the required amount of metal is less than that of the metal foam for the same heat transfer performance. On the other hand, for the new structure we do not require it is of a porous structure so that the preparation techniques should be much easier.

References

Abhat, A (1983). “Low temperature latent heat thermal energy storage: heat storage materials”. In: *Solar energy* 30.4, pp. 313–332.

Abidi, Awatef, Muhyaddin Rawa, Yacine Khetib, Hatem Faiz Assad Sindi, Mohsen Sharifpur, and Goshtasp Cheraghian (2021). “Simulation of melting and solidification of graphene nanoparticles-PCM inside a dual tube heat exchanger with extended surface”. In: *Journal of Energy Storage* 44, p. 103265.

Akiyama, Tomohiro and Jun-Ichiro Yagi (2000). “Encapsulation of phase change materials for storage of high temperature waste heat”. In: *High temperature materials and processes* 19.3-4, pp. 219–222.

Alshaer, WG, SA Nada, MA Rady, Cedric Le Bot, and Elena Palomo Del Barrio (2015). “Numerical investigations of using carbon foam/PCM/Nano carbon tubes composites in thermal management of electronic equipment”. In: *Energy Conversion and Management* 89, pp. 873–884.

Atkin, Raymond J and RE418619 Craine (1976). “Continuum theories of mixtures: basic theory and historical development”. In: *The Quarterly Journal of Mechanics and Applied Mathematics* 29.2, pp. 209–244.

Bart, Gerardus Cornelius Joseph (1994). “Thermal conduction in non homogeneous and phase change media”. In:

Bedford, A and Do S Drumheller (1983). “Theories of immiscible and structured mixtures”. In: *International Journal of Engineering Science* 21.8, pp. 863–960.

Bennon, WD and FP Incropera (1987). “A continuum model for momentum, heat and species transport in binary solid-liquid phase change systems—I. Model formulation”. In: *International Journal of Heat and Mass Transfer* 30.10, pp. 2161–2170.

Bennon, WD and FP Incropera (1988). “Numerical analysis of binary solid-liquid phase change using a continuum model”. In: *Numerical Heat Transfer, Part A Applications* 13.3, pp. 277–296.

Bhattacharya, Anandaroop, Varaprasad V Calmidi, and Roop L Mahajan (2002). “Thermophysical properties of high porosity metal foams”. In: *International journal of heat and mass transfer* 45.5, pp. 1017–1031.

Bories, Serge (1987). “Natural convection in porous media”. In: *Advances in transport phenomena in porous media*. Springer, pp. 77–141.

Bowen, Ray M (1976). “Theory of mixture”. In: *Continuum physics* 3, pp. 2–129.

Bowen, Ray M (1980). "Incompressible porous media models by use of the theory of mixtures". In: *International Journal of Engineering Science* 18.9, pp. 1129–1148.

Bowen, RM and JC Wiese (1969). "Diffusion in mixtures of elastic materials". In: *International Journal of Engineering Science* 7.7, pp. 689–722.

Calmidi, Varaprasad V and Roop L Mahajan (2000). "Forced convection in high porosity metal foams". In: *J. Heat Transfer* 122.3, pp. 557–565.

Carson, James K, Simon J Lovatt, David J Tanner, and Andrew C Cleland (2005). "Thermal conductivity bounds for isotropic, porous materials". In: *International Journal of Heat and Mass Transfer* 48.11, pp. 2150–2158.

Casey, James (2011). "On the derivation of jump conditions in continuum mechanics". In: *The International Journal of Structural Changes in Solids* 3.2, pp. 61–84.

Change, UN Climate (2019). "Climate action and support trends". In:

Chen, Zhenqian, Dongyan Gao, and Juan Shi (2014). "Experimental and numerical study on melting of phase change materials in metal foams at pore scale". In: *International journal of heat and mass transfer* 72, pp. 646–655.

Choi, S US and Jeffrey A Eastman (1995). *Enhancing thermal conductivity of fluids with nanoparticles*. Tech. rep. Argonne National Lab.(ANL), Argonne, IL (United States).

Copus, Mark, Benjamin Fraser, Roger Reece, Stuart Hands, Dylan Cuskelly, Heber Sugo, Samuel Reed, James Bradley, Alexander Post, and Erich Kisi (2019). "On-sun testing of Miscibility Gap Alloy thermal storage". In: *Solar Energy* 177, pp. 657–664.

Costa, Maria Laura Martins, Rubens Sampaio, and Rogério Martins Saldanha da Gama (1992). "Modelling and simulation of energy transfer in a saturated flow through a porous medium". In: *Applied mathematical modelling* 16.11, pp. 589–597.

Cui, Hongzhi, Waiching Tang, Qinghua Qin, Feng Xing, Wenyu Liao, and Haibo Wen (2017). "Development of structural-functional integrated energy storage concrete with innovative macro-encapsulated PCM by hollow steel ball". In: *Applied energy* 185, pp. 107–118.

Darcy, Henry (1856). *Les fontaines publiques de la ville de Dijon: Exposition et application des principes à suivre et des formules à employer dans les questions de distribution d'eau: Ouvrage terminé par un appendice relatif aux fournitures d'eau de plusieurs villes, au filtrage des eaux et à la fabrication des tuyaux de fonte, de plomb, de tôle et de bitume*. Vol. 2. V. Dalmont.

Dixon, Anthony G and David L Cresswell (1979). "Theoretical prediction of effective heat transfer parameters in packed beds". In: *AIChE Journal* 25.4, pp. 663–676.

Dukhan, Nihad and Sujay Bodke (2010). "An improved PCM heat storage technology utilizing metal foam". In: *2010 12th IEEE intersociety conference on thermal and thermomechanical phenomena in electronic systems*. IEEE, pp. 1–7.

Erastova, Valentina (2012). "Molecular simulation studies of diesel and diesel additives". PhD thesis. Durham University.

Eringen, A Cemal and John D Ingram (1965). "A continuum theory of chemically reacting media—I". In: *International Journal of Engineering Science* 3.2, pp. 197–212.

Esapour, Mehdi, Arash Hamzehnezhad, A Ali Rabienataj Darzi, and Mahmoud Jourabian (2018). "Melting and solidification of PCM embedded in porous metal foam in horizontal multi-tube heat storage system". In: *Energy conversion and management* 171, pp. 398–410.

Faden, Moritz, Andreas König-Haagen, and Dieter Brüggemann (2019). "An optimum enthalpy approach for melting and solidification with volume change". In: *Energies* 12.5, p. 868.

Faden, Moritz, Andreas König-Haagen, Erwin Franquet, and Dieter Brüggemann (2021). "Influence of density change during melting inside a cavity: Theoretical scaling laws and numerical analysis". In: *International Journal of Heat and Mass Transfer* 173, p. 121260.

Farid, Mohammed M, Amar M Khudhair, Siddique Ali K Razack, and Said Al-Hallaj (2004). "A review on phase change energy storage: materials and applications". In: *Energy conversion and management* 45.9-10, pp. 1597–1615.

Fiedler, Thomas, Andreas Öchsner, Irina V Belova, and Graeme E Murch (2008). "Thermal conductivity enhancement of compact heat sinks using cellular metals". In: *Defect and Diffusion Forum*. Vol. 273. Trans Tech Publ, pp. 222–226.

Freeze, R Alan (1979). *J. A. Cherry, Groundwater*.

Frusteri, F, V Leonardi, and G Maggio (2006). "Numerical approach to describe the phase change of an inorganic PCM containing carbon fibres". In: *Applied Thermal Engineering* 26.16, pp. 1883–1892.

Fukahori, Ryo, Takahiro Nomura, Chunyu Zhu, Nan Sheng, Noriyuki Okinaka, and Tomohiro Akiyama (2016). "Macro-encapsulation of metallic phase change material using cylindrical-type ceramic containers for high-temperature thermal energy storage". In: *Applied energy* 170, pp. 324–328.

Gibson, Ronald F, Emmanuel O Ayorinde, and Yuan-Feng Wen (2007). "Vibrations of carbon nanotubes and their composites: a review". In: *Composites science and technology* 67.1, pp. 1–28.

Graham, Michael, Elena Shchukina, Paula Felix De Castro, and Dmitry Shchukin (2016). "Nanocapsules containing salt hydrate phase change materials for thermal energy storage". In: *Journal of Materials Chemistry A* 4.43, pp. 16906–16912.

Green, Albert Edward and Paul Mansour Naghdi (1969). “On basic equations for mixtures”. In: *The Quarterly Journal of Mechanics and Applied Mathematics* 22.4, pp. 427–438.

H Al-Kayiem, Hussain, Saw Chun Lin, and Afolabi Lukmon (2013). “Review on nanomaterials for thermal energy storage technologies”. In: *Nanoscience & Nanotechnology-Asia* 3.1, pp. 60–71.

Hassab, MA, Medhat M Sorour, M Khamis Mansour, and Mostafa M Zaytoun (2017). “Effect of volume expansion on the melting process’s thermal behavior”. In: *Applied Thermal Engineering* 115, pp. 350–362.

Hawlader, MNA, MS Uddin, and Mya Mya Khin (2003). “Microencapsulated PCM thermal-energy storage system”. In: *Applied energy* 74.1-2, pp. 195–202.

Hu, Xusheng and Xiaolu Gong (2019). “Pore-scale numerical simulation of the thermal performance for phase change material embedded in metal foam with cubic periodic cell structure”. In: *Applied Thermal Engineering* 151, pp. 231–239.

Huang, Jin, Tingyu Wang, Panpan Zhu, and Junbin Xiao (2013). “Preparation, characterization, and thermal properties of the microencapsulation of a hydrated salt as phase change energy storage materials”. In: *Thermochimica acta* 557, pp. 1–6.

Huang, Rongzong and Huiying Wu (2015). “Phase interface effects in the total enthalpy-based lattice Boltzmann model for solid–liquid phase change”. In: *Journal of Computational Physics* 294, pp. 346–362.

Jegadheeswaran, S and Sanjay D Pohekar (2009). “Performance enhancement in latent heat thermal storage system: a review”. In: *Renewable and Sustainable energy reviews* 13.9, pp. 2225–2244.

Al-Jethelah, Manar, Syeda Humaira Tasnim, Shohel Mahmud, and Animesh Dutta (2018). “Nano-PCM filled energy storage system for solar-thermal applications”. In: *Renewable energy* 126, pp. 137–155.

Jiao, Kai (2017). “On solutions for the moving boundary problem describing an eroding vascular graft”. PhD thesis. University of Pittsburgh.

Jin, Xing, Xiaodong Xu, Xiaosong Zhang, and Yonggao Yin (2014). “Determination of the PCM melting temperature range using DSC”. In: *Thermochimica acta* 595, pp. 17–21.

Khudhair, Amar M and Mohammed M Farid (2004). “A review on energy conservation in building applications with thermal storage by latent heat using phase change materials”. In: *Energy conversion and management* 45.2, pp. 263–275.

Kumaresan, Vellaisamy, Ramalingam Velraj, and Sarit K Das (2012). “The effect of carbon nanotubes in enhancing the thermal transport properties of PCM during solidification”. In: *Heat and Mass Transfer* 48.8, pp. 1345–1355.

Lane, George A (1983). “Solar heat storage: latent heat materials”. In:

Legay, Mathieu, Nicolas Gondrexon, Stéphane Le Person, Primius Boldo, and André Bontemps (2011). "Enhancement of heat transfer by ultrasound: review and recent advances". In: *International Journal of Chemical Engineering* 2011.

Li, Bao-rang, Hui Tan, Yu Liu, Qi Liu, Gao-qun Zhang, Zhan-feng Deng, Gui-zhi Xu, Yong-quan Guo, and Xiao-ze Du (2019). "Experimental investigations on the thermal stability of Na2CO3–K2CO3 eutectic salt/ceramic composites for high temperature energy storage". In: *Renewable Energy*.

Li, Bin and Xiaoqiang Zhai (2017). "Experimental investigation and theoretical analysis on a mid-temperature solar collector/storage system with composite PCM". In: *Applied Thermal Engineering* 124, pp. 34–43.

Li, TingXian, Ju-Hyuk Lee, RuZhu Wang, and Yong Tae Kang (2014). "Heat transfer characteristics of phase change nanocomposite materials for thermal energy storage application". In: *International Journal of Heat and Mass Transfer* 75, pp. 1–11.

Li, WQ, ZG Qu, YL He, and WQ Tao (2012). "Experimental and numerical studies on melting phase change heat transfer in open-cell metallic foams filled with paraffin". In: *Applied Thermal Engineering* 37, pp. 1–9.

Lin, Yaxue, Yuting Jia, Guruprasad Alva, and Guiyin Fang (2018). "Review on thermal conductivity enhancement, thermal properties and applications of phase change materials in thermal energy storage". In: *Renewable and sustainable energy reviews* 82, pp. 2730–2742.

Liu, I-Shih (2014). "A solid–fluid mixture theory of porous media". In: *International Journal of Engineering Science* 84, pp. 133–146.

Liu, I-Shih (2016). "A mixture theory of porous media and some problems of poroelasticity". In: *Continuous Media with Microstructure 2*. Springer, pp. 267–285.

Lu, Shilei, Tianshuai Zhang, and Yafei Chen (2018). "Study on the performance of heat storage and heat release of water storage tank with PCMs". In: *Energy and Buildings* 158, pp. 1770–1780.

Mahdavi, Mahboobe, Saeed Tiari, and Vivek Pawar (2018). "Heat Transfer Analysis of a Low-Temperature Heat Pipe-Assisted Latent Heat Thermal Energy Storage System With Nano-Enhanced PCM". In: *ASME International Mechanical Engineering Congress and Exposition*. Vol. 52088. American Society of Mechanical Engineers, V06BT08A051.

Mahdi, Jasim M, Sina Lohrasbi, Davood D Ganji, and Emmanuel C Nsofor (2018). "Accelerated melting of PCM in energy storage systems via novel configuration of fins in the triplex-tube heat exchanger". In: *International Journal of Heat and Mass Transfer* 124, pp. 663–676.

McNaughton, JL, Günther Höhne, W Hemminger, H-J Flammersheim, and H-J Flammersheim (2003). *Differential scanning calorimetry*. Springer Science & Business Media.

Mehling, Harald and Luisa F Cabeza (2008). *Heat and cold storage with PCM*. Vol. 308. Springer.

Mesalhy, Osama, Khalid Lafdi, Ahmed Elgafy, and Keith Bowman (2005). "Numerical study for enhancing the thermal conductivity of phase change material (PCM) storage using high thermal conductivity porous matrix". In: *Energy Conversion and Management* 46.6, pp. 847–867.

Naghdbishi, Ali, Mohammad Eftekhari Yazdi, and Ghasem Akbari (2020). "Experimental investigation of the effect of multi-wall carbon nanotube–Water/glycol based nanofluids on a PVT system integrated with PCM-covered collector". In: *Applied Thermal Engineering* 178, p. 115556.

Nield, DA (1991). "Estimation of the stagnant thermal conductivity of saturated porous media". In: *Int. J. Heat Mass Transfer* 34, pp. 1575–1576.

Nield, Donald A, Adrian Bejan, et al. (2006). *Convection in porous media*. Vol. 3. Springer.

Noël, John A, Samer Kahwaji, Louis Desgrosseilliers, Dominic Groulx, and Mary Anne White (2016). "Phase change materials". In: *Storing Energy*. Elsevier, pp. 249–272.

Oh, YK, SH Park, and YI Cho (2002). "A study of the effect of ultrasonic vibrations on phase-change heat transfer". In: *International Journal of Heat and Mass Transfer* 45.23, pp. 4631–4641.

Onder, E and N Sarier (2015). *Thermal regulation finishes for textiles functional finishes for textiles improving comfort performance and protection (pp. 17–98)*.

Preziosi, L and A Farina (2002). "On Darcy's law for growing porous media". In: *International Journal of Non-Linear Mechanics* 37.3, pp. 485–491.

Qiao, Y, PØ Andersen, S Evje, and DC Standnes (2018). "A mixture theory approach to model co-and counter-current two-phase flow in porous media accounting for viscous coupling". In: *Advances in water resources* 112, pp. 170–188.

Rabin, Y, I Bar-Niv, E Korin, and B Mikic (1995). "Integrated solar collector storage system based on a salt-hydrate phase-change material". In: *Solar Energy* 55.6, pp. 435–444.

Rajagopal, Kumbakonam R (2007). "On a hierarchy of approximate models for flows of incompressible fluids through porous solids". In: *Mathematical Models and Methods in Applied Sciences* 17.02, pp. 215–252.

Rajagopal, Kumbakonam R and Luoyi Tao (1995). *Mechanics of mixtures*. Vol. 35. World scientific.

Rao, ZH and GQ Zhang (2011). "Thermal properties of paraffin wax-based composites containing graphite". In: *Energy Sources, Part A: Recovery, Utilization, and Environmental Effects* 33.7, pp. 587–593.

Rathod, Manish K and Jyotirmay Banerjee (2013). “Thermal stability of phase change materials used in latent heat energy storage systems: a review”. In: *Renewable and sustainable energy reviews* 18, pp. 246–258.

Rathore, Pushpendra Kumar Singh and Shailendra Kumar Shukla (2019). “Potential of macroencapsulated pcm for thermal energy storage in buildings: A comprehensive review”. In: *Construction and Building Materials* 225, pp. 723–744.

Regin, A Felix, SC Solanki, and JS Saini (2008). “Heat transfer characteristics of thermal energy storage system using PCM capsules: a review”. In: *Renewable and Sustainable Energy Reviews* 12.9, pp. 2438–2458.

Ren, Yajie, Huaqing Xie, and An Cai (2005). “Effective thermal conductivity of nanofluids containing spherical nanoparticles”. In: *Journal of Physics D: Applied Physics* 38.21, p. 3958.

Sandnes, B and J Rekstad (2006). “Supercooling salt hydrates: Stored enthalpy as a function of temperature”. In: *Solar Energy* 80.5, pp. 616–625.

Sandnes, Bjørnar (2003). “Exergy efficient production, storage and distribution of solar energy”. In: *Department of Physics. Oslo, Norway, University of Oslo, PhD*.

Sarı, Ahmet (2003). “Thermal characteristics of a eutectic mixture of myristic and palmitic acids as phase change material for heating applications”. In: *Applied Thermal Engineering* 23.8, pp. 1005–1017.

Sarı, Ahmet and Ali Karaipekli (2009). “Preparation, thermal properties and thermal reliability of palmitic acid/expanded graphite composite as form-stable PCM for thermal energy storage”. In: *Solar Energy Materials and Solar Cells* 93.5, pp. 571–576.

Shaikh, Shadab, Khalid Lafdi, and Kevin Hallinan (2008). “Carbon nanoadditives to enhance latent energy storage of phase change materials”. In: *Journal of applied physics* 103.9, p. 094302.

Sharma, Atul, V Veer Tyagi, CR Chen, and Dharam Buddhi (2009). “Review on thermal energy storage with phase change materials and applications”. In: *Renewable and Sustainable energy reviews* 13.2, pp. 318–345.

Sheikholeslami, M, Rizwan-ul Haq, Ahmad Shafee, Zhixiong Li, Yassir G Elaraki, and I Tlili (2019). “Heat transfer simulation of heat storage unit with nanoparticles and fins through a heat exchanger”. In: *International Journal of Heat and Mass Transfer* 135, pp. 470–478.

Sparrow, EM and JA Broadbent (1982). “Inward melting in a vertical tube which allows free expansion of the phase-change medium”. In:

Srivatsa, PVSS, Rajesh Baby, and C Balaji (2014). “Numerical investigation of PCM based heat sinks with embedded metal foam/crossed plate fins”. In: *Numerical Heat Transfer, Part A: Applications* 66.10, pp. 1131–1153.

Sun, Xiaoqin, Quan Zhang, Mario A Medina, and Kyoung Ok Lee (2016). “Experimental observations on the heat transfer enhancement caused by natural

convection during melting of solid–liquid phase change materials (PCMs)". In: *Applied energy* 162, pp. 1453–1461.

Telkes, Maria (1952). "Nucleation of supersaturated inorganic salt solutions". In: *Industrial & Engineering Chemistry* 44.6, pp. 1308–1310.

Tian, Yuan and CY Zhao (2011). "A numerical investigation of heat transfer in phase change materials (PCMs) embedded in porous metals". In: *Energy* 36.9, pp. 5539–5546.

Truesdell, Clifford and Richard Toupin (1960). "The classical field theories". In: *Principles of classical mechanics and field theory/Prinzipien der Klassischen Mechanik und Feldtheorie*. Springer, pp. 226–858.

Ukrainczyk, Neven, Stanislav Kurajica, and Juraj Šipušić (2010). "Thermophysical comparison of five commercial paraffin waxes as latent heat storage materials". In: *Chemical and biochemical engineering quarterly* 24.2, pp. 129–137.

Verma, Sudeep and Anupam Dewan (2017). "Assessment of Characteristics of Phase Change Region during Solidification of a Binary Alloy in Different Flow Regimes". In: *Materials Today: Proceedings* 4.9, pp. 9445–9449.

Vicente, Romeu and Tiago Silva (2014). "Brick masonry walls with PCM macrocapsules: an experimental approach". In: *Applied Thermal Engineering* 67.1-2, pp. 24–34.

Voller, VR (1985). “Implicit finite—difference solutions of the enthalpy formulation of Stefan problems”. In: *IMA journal of numerical analysis* 5.2, pp. 201–214.

Voller, VR, N Markatos, and M Cross (1985). “TECHNIQUES FOR ACCOUNTING FOR THE MOVING INTERFACE IN CONVECTION/DIFFUSION PHASE CHANGE.” In: *Unknown Host Publication Title*. Pineridge Press, pp. 595–609.

Wakao, N and S Kaguei (1982). “Topics in chemical engineering”. In: *Heat and mass transfer in packed beds* 1.

Wang, Lijiu and Duo Meng (2010). “Fatty acid eutectic/polymethyl methacrylate composite as form-stable phase change material for thermal energy storage”. In: *Applied Energy* 87.8, pp. 2660–2665.

Weber, Heinrich and Bernhard Riemann (1919). *Die partiellen differential-Gleichungen der mathematischen Physik: nach Riemann's Vorlesungen*. Vol. 2. F. Vieweg.

Wu, Weixiong, Guoqing Zhang, Xiufang Ke, Xiaoqing Yang, Ziyuan Wang, and Chenzhen Liu (2015). “Preparation and thermal conductivity enhancement of composite phase change materials for electronic thermal management”. In: *Energy conversion and management* 101, pp. 278–284.

Xia, X, H Y Zhang, and Y C Deng (Aug. 2016). “Numerical analysis of phase change materials for thermal control of power battery of high power dissipations”. In: *IOP Conference Series: Earth and Environmental Science* 40,

p. 012046. DOI: 10.1088/1755-1315/40/1/012046. URL: https://doi.org/10.1088/1755-1315/40/1/012046.

Yagi, J and T Akiyama (1995). "Storage of thermal energy for effective use of waste heat from industries". In: *Journal of Materials Processing Technology* 48.1-4, pp. 793–804.

Yang, Shuo, RS Simmonds, EJ Birch, et al. (2014). "Physicochemical characterization and thermal properties of lipids from R. opacus PD630." In: *Food and Public Health* 4.3, pp. 87–92.

Yang, Xiaohu, Pan Wei, Xin Cui, Liwen Jin, and Ya-Ling He (2019). "Thermal response of annuli filled with metal foam for thermal energy storage: an experimental study". In: *Applied Energy* 250, pp. 1457–1467.

Zalba, Belen, Jose Ma Marın, Luisa F Cabeza, and Harald Mehling (2003). "Review on thermal energy storage with phase change: materials, heat transfer analysis and applications". In: *Applied thermal engineering* 23.3, pp. 251–283.

Zeng, JL, LX Sun, F Xu, ZC Tan, ZH Zhang, J Zhang, and T Zhang (2007). "Study of a PCM based energy storage system containing Ag nanoparticles". In: *Journal of Thermal Analysis and Calorimetry* 87.2, pp. 371–375.

Zhang, Muxing, Changling Wang, Ailian Luo, Zhenghao Liu, and Xiaosong Zhang (2020). "Molecular dynamics simulation on thermophysics of paraffin/EVA/graphene nanocomposites as phase change materials". In: *Applied Thermal Engineering* 166, p. 114639.

Zhang, Peng, Zhaonan Meng, Hua Zhu, Yanling Wang, and Shiping Peng (2015). "Experimental and numerical study of heat transfer characteristics of a paraffin/metal foam composite PCM". In: *Energy Procedia* 75, pp. 3091–3097.

Zikanov, Oleg (2019). *Essential computational fluid dynamics*. John Wiley & Sons.

Zou, Deqiu, Xianfeng Ma, Xiaoshi Liu, Pengjun Zheng, and Yunping Hu (2018). "Thermal performance enhancement of composite phase change materials (PCM) using graphene and carbon nanotubes as additives for the potential application in lithium-ion power battery". In: *International Journal of Heat and Mass Transfer* 120, pp. 33–41.

Appendices

Appendix I: Optimized time steps and grid sizes

The optimized time steps and grid sizes obtained by grid sensitivity tests for section 5.1.3 are shown in the following table. In the numerical calculation, for the two constituents: nickel and paraffin, we use different time steps while the grid sizes are the same. The table shows the time steps that used for the paraffin, and the time steps for nickel can be obtained by dividing the time steps shown in the table by 200.

Table: Optimized time steps and grid sizes for section 5.1.3.

Mixture type	m	Δx (m)	Δt (s)
Type-1	4	6.25e-4	7.81e-1
	8	3.13e-4	1.95e-1
	16	1.56e-4	4.88e-2
	32	7.81e-5	1.22e-2
Type-2	4	6.25e-4	7.81e-1
	8	3.13e-4	1.95e-1
	16	1.56e-4	4.88e-2
	32	7.81e-5	1.22e-2
Type-3	4	3.13e-4	1.95e-1
	8	1.56e-4	4.88e-2
	16	7.81e-5	1.22e-2
	32	3.91e-5	3.10e-3
Type-3	4	6.99e-4	9.76e-1
	8	3.49e-4	2.44e-1
	16	1.75e-4	6.10e-2
	32	8.73e-5	1.53e-2

Appendix II: Finite Difference Equation at Interfaces

There are two types interfaces between 2 materials in our numerical calculation as shown in the following two figures. The finite difference equation for the straight interface is

$$\begin{aligned}\frac{1}{2}\Delta x\Delta y(\rho_1 Cp_1+\rho_2 Cp_2)\frac{T_{i,j}^{n+1}-T_{i,j}^{n}}{\Delta t} &= \Delta y k_1\frac{T_{i,j-1}^{n}-T_{i,j}^{n}}{\Delta x}+\Delta y k_2\frac{T_{i,j+1}^{n}-T_{i,j}^{n}}{\Delta x}\\ &+\frac{1}{2}\Delta x k_1\frac{T_{i-1,j}^{n}-T_{i,j}^{n}}{\Delta y}\\ &+\frac{1}{2}\Delta x k_2\frac{T_{i-1,j}^{n}-T_{i,j}^{n}}{\Delta y}\\ &+\frac{1}{2}\Delta x k_1\frac{T_{i+1,j}^{n}-T_{i,j}^{n}}{\Delta y}\\ &+\frac{1}{2}\Delta x k_2\frac{T_{i+1,j}^{n}-T_{i,j}^{n}}{\Delta y}\end{aligned}$$

The finite difference equation for the straight interface is

$$\begin{aligned}\Delta x\Delta y(\frac{3}{4}\rho_1 Cp_1+\frac{1}{4}\rho_2 Cp_2)\frac{T_{i,j}^{n+1}-T_{i,j}^{n}}{\Delta t} &= \Delta x k_1\frac{T_{i-1,j}^{n}-T_{i,j}^{n}}{\Delta y}+\Delta y k_1\frac{T_{i,j-1}^{n}-T_{i,j}^{n}}{\Delta x}\\ &+\frac{1}{2}\Delta x k_1\frac{T_{i+1,j}^{n}-T_{i,j}^{n}}{\Delta y}\\ &+\frac{1}{2}\Delta x k_2\frac{T_{i+1,j}^{n}-T_{i,j}^{n}}{\Delta y}\\ &+\frac{1}{2}\Delta y k_2\frac{T_{i,j+1}^{n}-T_{i,j}^{n}}{\Delta x}\\ &+\frac{1}{2}\Delta y k_1\frac{T_{i,j+1}^{n}-T_{i,j}^{n}}{\Delta x}\end{aligned}$$

where the numbers 1 and 2 represent the two materials, and i, j are the grid numbers. For the insulated boundary involving the interfaces between the two materials, fictitious points are to be established and then the above two equations can still be applicable.

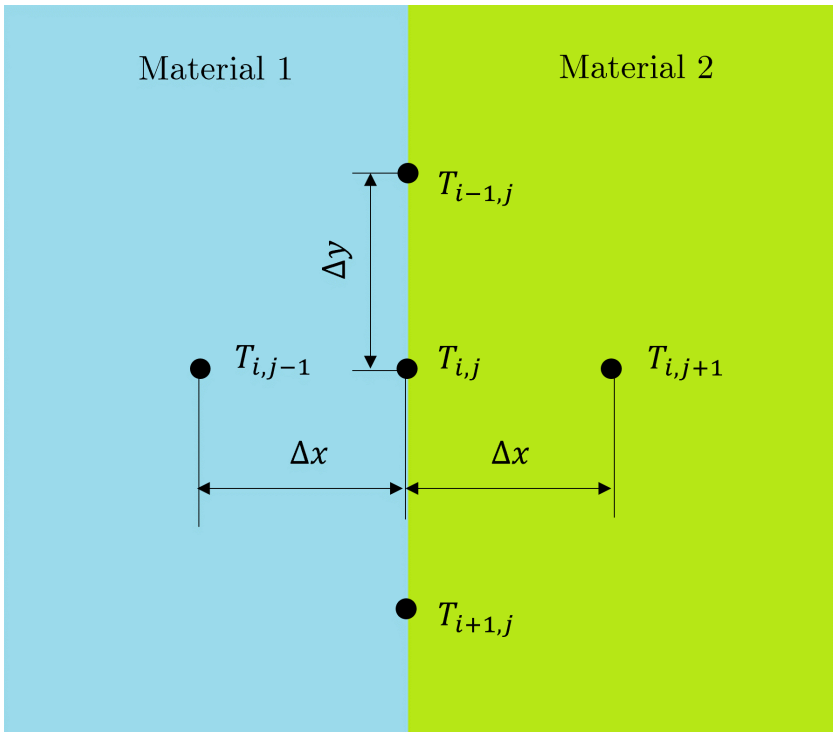

Figure: Straight interface between two materials.

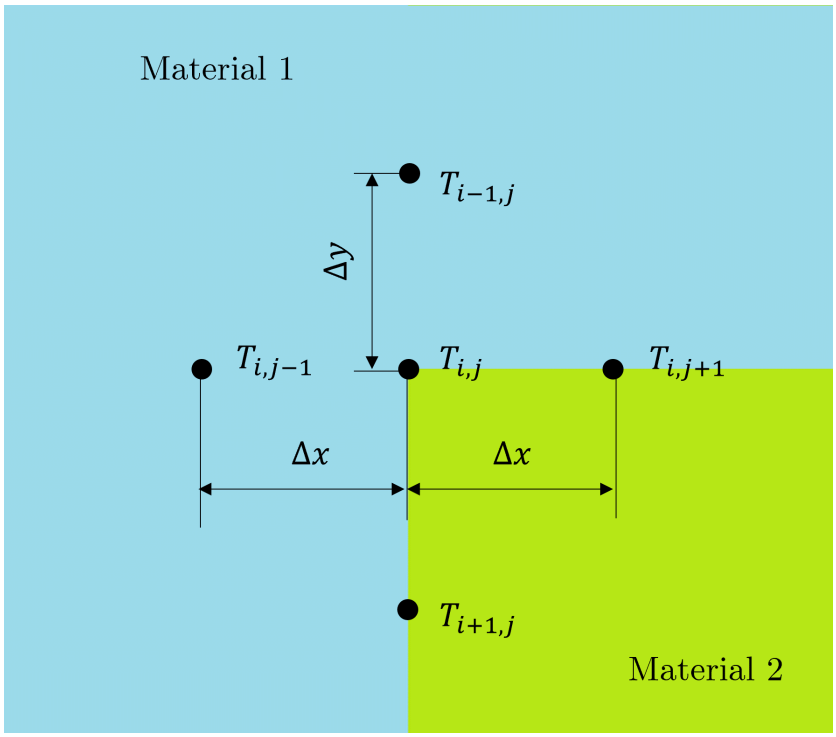

Figure: Corner interface between two materials.